# TECHNISCHE UNIVERSITÄT MÜNCHEN

Institut für Wasserchemie und Chemische Balneologie

Lehrstuhl für Analytische Chemie


# Label-Free Applications of SERS for Bacteria Analysis


**Haibo Zhou**



Vollständiger Abdruck der von der Fakultät für Chemie der Technischen Universität München zur Erlangung des akademischen Grades eines

**Doktors der Naturwissenschaften (Dr. rer. nat.)**

genehmigten Dissertation.

| | |
|---|---|
| Vorsitzender: | Univ.-Prof. Dr. M. Groll |
| Prüfer der Dissertation: | 1. Univ.-Prof. Dr. R. Nießner |
| | 2. Priv.-Doz. Dr. C. Haisch |

Die Dissertation wurde am 24.10.2014 bei der Technischen Universität München eingereicht und durch die Fakultät für Chemie am 18.11.2014 angenommen

# ACKNOWLEDGEMENTS

This thesis is based on research conducted between November 2011 and October 2014 at Lehrstuhl für Analytische Chemie, Institut für Wasserchemie und Chemische Balneologie, Technische Universität München. This thesis would not have been completed without following person's kind help and their academic knowledge.

I would like to give my special thanks to Prof. Dr. Reinhard Nießner for the chance to finish my PhD work under his friendly supervision, and also thank for giving me the trust necessary to accomplish my thesis. Furthermore, I get a lot of ideas of scientific research from his profound knowledge.

I would like to express my warmly gratitude to PD Dr. Christoph Haisch for the interesting research topic and invaluable encouragement and support throughout my work. I am impressed by his rigorous scientific attitude, profound knowledge and enthusiasm in research. In addition, I would like to thank him for his patience towards my poor written English. Thanks to extensive corrections work my publications, otherwise my paper can not be published so quickly.

Furthermore, I would like to thank Dr. Natalia P. Ivleva for her patient instruction on the Raman instruments and revision of my publications. Also to be thanked is Prof. Dr. Dietmar Knopp, who gave me a lot of enthusiastic help. I also want to thank my cooperation team - Prof. Dr. Sören Schubert and Dr. Andreas Wieser from Max von Pettenkofer, Institut für Hygiene und Medizinische Mikrobiologie, Ludwig-Maximilians-University, who supported me with a lot of knowledge and ideas on microbiology.

I thank M. Hanzlik and Christine Sternkopf for the measurement of TEM images and ICP/MS. And I thank Susanna Mahler for the preparation of microarrary and Sebastian Wiesemann and Roland Hoppe for the fabrication of microfluidic devices. I also thank Prof. Claudimir Lucio do Lago from University of São Paulo, Brazil. We had a span of good cooperation time (two months) in designing the microfluidic devices at the institute.

Furthermore, I would like to thank all other colleagues in the institute for the inspiring working atmosphere and their constant help, both scientific and non-scientific. In particular, I would like to mention the following persons: Kathrin Schwarzmeier, Christoph Berger, Nicoleta E. Mircescu, Danting Yang, Lu Pei, Xu Wang, Maria Knauer, Maria Hübner, Christian Metz, Clemens Thaler, Henrike Bladt and Xiangjiang Liu.

Very special thanks to China Scholarship Council's financial support for three years. With this scholarship, I spent an interesting time in Germany. I also would like to thank my master's supervisor, Prof. Zhongping Zhang at University of Science and Technology of China (USTC), Hefei, China. He is the first person who guided me into the scientific world.

At the end, I would like to express my deepest gratitude to my family: my parents, brother and grandmother. Thanks for their unconditional support and confidence along my entire studies. Although my grandmother passed away in 2012, she will live in my heart forever.

# PUBLICATIONS

Parts of this thesis have been published in following scientific journals:

**Haibo Zhou**, Danting Yang, Natalia P. Ivleva, Nicoleta E. Mircescu, Reinhard Niessner, and Christoph Haisch*. SERS Detection of Bacteria in Water by in Situ Coating with Ag Nanoparticles. ***Anal. Chem.*** 2014, 86, 1525-1533.

Danting Yang, **Haibo Zhou**, Yibin Ying*, Reinhard Niessner, Christoph Haisch*. Surface-enhanced Raman scattering for quantitative detection of ethyl carbamate in alcoholic beverages. ***Anal. Bioanal. Chem.*** 2013, 405, 9419-9425.

Nicoleta E. Mircescu, **Haibo Zhou**, Nicolae Leopold, Vasile Chiş, Natalia P. Ivleva, Reinhard Niessner, Andreas Wieser, Christoph Haisch*. Towards a receptor-free immobilization and SERS detection of urinary tract infections causative pathogens. ***Anal. Bioanal. Chem.*** 2014, 406, 3051-3058.

Danting Yang, Nicoleta E. Mircescu, **Haibo Zhou**, Nicolae Leopold, Vasile Chiş, Mircea Oltean, Yibin Ying* and Christoph Haisch*. DFT study and quantitative detection by surface-enhanced Raman scattering (SERS) of ethyl carbamate. ***J. Raman. Spectrosc.*** 2013, 44, 1491-1496.

# ABSTRACT

The biosensing for the detection of bacteria has been widely explored with the use of various sensing materials and techniques. It is still a challenge to achieve sensitive and selective but simple, rapid, and inexpensive detection of bacteria. In the first part, we report on surface-enhanced Raman scattering (SERS) for living bacteria detection in drinking water by employing a synthesis of silver nanoparticles coating the cell wall of bacteria (Bacteria@AgNPs). We found that the Raman signal intensity of bacteria after AgNPs synthesis mainly depends on the zeta potential of the cell wall. The enhancement of the Raman signal of bacteria using this strategy is about 30 times higher than in the case of simply mixed colloid-bacterial suspension (Bacteria-AgNPs). The total assay time required is only 10 min and the total reactants' volume needed in order to analyze bacteria in a real environment is as low as 1 mL. Only one droplet of 3 μL sample is necessary for each SERS measurement. Furthermore, we were able to use this novel strategy to discriminate three strains of *E. coli* and one strain of *S. epidermidis* by hierarchy cluster analysis (HCA). Finally, we can detect bacteria down to $2.5 \times 10^2$ cell/mL on a hydrophobic glass slide by SERS mapping.

In the second part of this thesis, we present a label-free SERS detection of bacteria on microarray at single cell level. We combined our novel Bacteria@AgNPs method with the microarray strategy. This straight-forward, efficient strategy allows the sensitive detection of bacteria on microarray platforms. The Raman signal of bacteria using this strategy is about 10 times higher than in previously reported microarray results, based on simple mixing of bacteria and AgNPs. The optimum SERS enhancement of such Bacteria@AgNPs nanostructures could be reached at 633 nm laser excitation, most likely due to the plasmonic interaction of aggregated AgNPs. Sensitivity and simplicity of the strategy for the identification and quantification of single bacteria on a microarray are discussed. The application of the novel Bacteria@AgNPs nanostructures for microarray readout provides a valuable tool for bacteria detection in environment monitoring,

medical diagnosis and food safety.

In the third part of this thesis, we prepared live and dead bacteria Bacteria@AgNPs nanostructures by our in situ synthesis method. We found that only the live Bacteria@AgNPs give strong SERS signals of bacteria, however, the dead Bacteria@AgNPs almost have no SERS signals. We designed detailed experiments to confirm that this phenomenon was ascribed to the membrane charge of the bacteria. We further successfully demonstrate the utility of SERS for calculating different percentage of dead bacteria in aqueous environment. Finally, we successfully counted live and dead bacteria with the novel method by SERS mapping technique.

Thus, our novel detection method offers prominent advantages, such as reduced assay times, simple handling, low reactant volumes, small amount of sample, and higher sensitivity and selectivity compared to previously reported label free methods. This novel strategy may be extended to open an avenue for developing various SERS-based biosensors.

# Contents

# 1 Theoretical Background

# 1.1 Introduction

Accurate and sensitive detection of microorganisms in water and food, such as *Escherichia coli* (*E. coli*), *Legionella Pneumophila*, *Salmonella typhimurium*, and other waterborne and foodborne pathogens, is critical for food safety and human health care.[1,2] The main reason is that many serious and even fatal diseases are caused by these bacterial infections or contaminations.[3] For example, stomach ulcers can be caused by *helicobacter pylori*. Sexually-transmitted diseases and meningitis can be caused by anthrax (*Bacillus anthracis*). Furthermore, global bioterrorism attacks make these conditions even worse because of the intention to spread bacterial agents within the target communities. Since the US 9/11 terrorist attack, such situation has attracted great attention by governments in the whole world. "Bioterrorist attack" is defined as "deliberate release of viruses, bacteria, or other agents used to cause illness or death in people, animals, or plants (agroterrorism)".[4] Terrorists are inclined to use biological agents because they are difficult to detect and do not cause illness immediately.[5] On the other hand, some microorganisms, like *E. coli* and hydrogen sulfide producing bacteria, are used as indicator bacteria of water contamination. The reason for the analysis of such indicator bacteria is that there exists no online method for the simultaneous detection of multiple pathogenic bacteria in water. According to EU regulations, the absence of indicator bacteria in 250 mL water sample is the requirement for drinking water quality in closed containments.[13] Thus, fast detection and characterization of microorganisms has attracted huge worldwide attention.

# 1.2 Bacterial structure and function

## 1.2.1 The bacteria cell

Bacteria are microscopic organisms with each bacterium being a single autonomous cell. Bacteria constitute a large domain of prokaryotic microorganisms. Microbial cells are very different from those of plants and animals in that microorganisms are

independent entities that carry out their life processes independently. By contrast, plant and animals cells can not live alone in nature and instead exist only as parts of multicellular structures, such as the organ systems of animals or the leaves of plants. In general, the size of bacteria is a few micrometers, and the shapes of bacteria vary from spheres to rods and spirals. Meanwhile, there are many other shapes of bacteria, such as spirochete, budding and appendage, or filamentous (Figure 1.1). Bacteria inhabit soil, water, acidic hot springs, radioactive waste, and even the deep portions of Earth's crust. Bacteria also live in plants, food, animals, and even survive in space. Although the microorganisms are the smallest forms of life, higher organisms (humans, plants, and animals) could not sustain in the absence of microorganisms. Because their recycling of key nutrients and degradation of organic matters are intimately tied to microbial activities. It may even be stated: no other life forms are as important as microorganisms for the support and maintenance of life on earth.

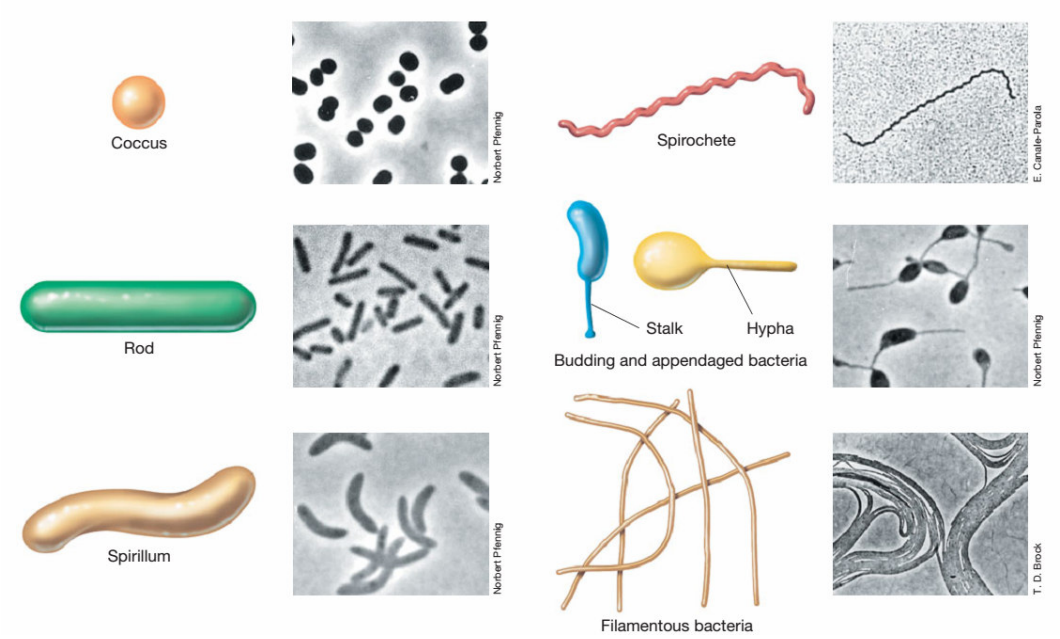


**Figure 1.1** Major bacteria morphologies. Next to each drawing is a phase-contrast photomicrograph showing an example of that morphology. Microorganisms are cocci, Thiocapsa roseopersicina (diameter of a single cell = 1.5 µm); rod, Desulfuromonas acetoxidans (diameter = 1 µm); spirilli, Rhodospirillum rubrum (diameter =1 µm); spirochete, Spirochaeta stenostrepta (diameter = 0.25 µm); budding and appendaged, Rhodomicrobium vannielii (diameter = 1.2 µm); filamentous, Chloroflexus aurantiacus (diameter = 0.8 µm). Reprinted from ref.[6]

Bacteria can be classified into Gram-positive and Gram-negative strains. Their cell wall components differ and can be identified by the visual staining procedure using crystal violet (CV). This method was first developed by Hans Christian Gram in 1884.[7] The Gram stain is one of the most popularly used methods for the detection and classification of bacteria in the last century. The strategy is routinely used for clinical diagnostic purposes as well as environmental samples. The procedure is based on staining bacteria with CV, which binds to the peptidoglycan layer of Gram-positive and Gram-negative bacteria. Then, an insoluble compound is formed by adding iodine solution (CV–I). Gram-positive bacteria have a thick peptidoglycan layer (10 - 100 nm), whereas Gram-negative bacteria only have a thin peptidoglycan layer covered by lipopolysaccharides (LPS) and lipoproteins (2 - 3 nm). When a decolourizer such as acetone or alcohol is added, it interacts with the lipids of cell membrane. The Gram-negative bacteria lose their outer LPS membrane, and the inner peptidoglycan layer is left exposed. Thus the CV-I complexes are washed from the Gram-negative bacteria along with the outer membrane. In contrast, the Gram-positive bacteria become dehydrated from the ethanol treatment. The large CV-I complexes become trapped in the thick layer of peptidoglycan. After that, the Gram-negative bacteria lose their purple colour (pink-red), while the Gram-positive bacteria remain purple. Despite the robustness and simplicity of the staining procedure, it often requires intensive sample pretreatment and user-dependent skilled techniques. Strategies for rapid, sensitive, low cost, and automated detection are highly in demand, especially for the diagnosis of infectious pathogens.

In this thesis, we used three kinds of bacteria as model microorganisms, one is Gram-negative, *Escherichia coli*, and the other two are Gram-positive, *Staphylococcus epidermidis* and *Corynebacterium*.

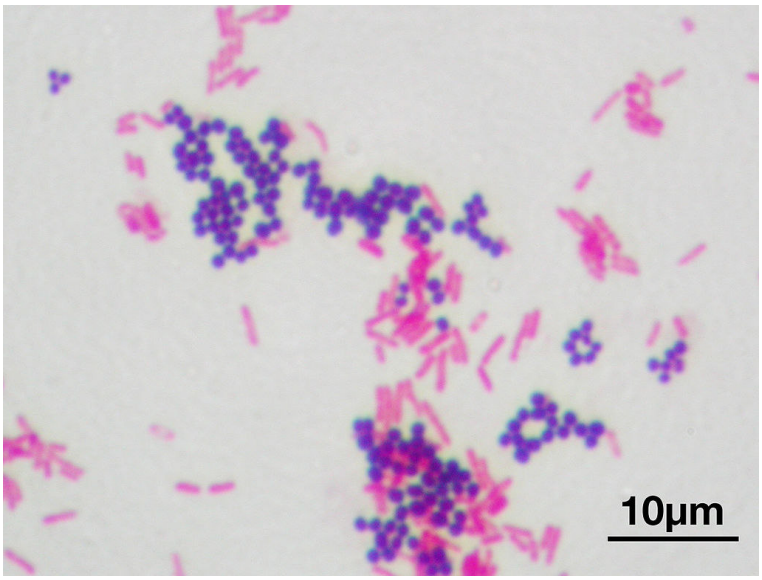


**Figure 1.2** A Gram stain of mixed *Staphylococcus aureus* (*S. aureus ATCC 25923*, Gram-positive cocci, in purple) and *Escherichia coli* (*E. coli ATCC 11775*, Gram-negative bacilli, in red). Reprinted from ref.[8]

## Escherichia coli

*Escherichia coli* (*E. coli*) belong to the family of enterobacteriaceae and are rod-shaped Gram-negative bacteria with a length of 2 - 6 µm and a diameter of 1.1 - 1.5 µm.[6] Most of *E. coli* strains are harmless, but some can produce toxins and cause perilous diseases (e.g. *E. coli* O157:H7 may lead to hemorrhagic diarrhea and kidney failure). Normally, the harmless ones can produce vitamin $K_2$ for benefiting their host. Owing to easy and inexpensive *E. coli* culture in routine, *E. coli* has been the most widely studied model microorganisms in the field of environmental chemistry, biological chemistry and microbiology for almost one century. That is also the reason why we choose *E. coli* as our research object in this thesis. Furthermore, *E. coli* grow fast, it only take 20 minutes (min) to reproduce one generation under favourable conditions (appropriate concentrations of saline and pH values). Figure 1.3 shows the typical growth curve for the bacteria population in ideal culture conditions (suitable temperature, sufficient oxygen and culture medium). The growth curve describes an entire growth cycle, including lag phase, exponential phase, stationary phase, and death phase. General speaking, we harvested the *E. coli* at the end of exponential phase, i.e. usually after 16 hours (h), because the bacteria

are typically in their healthiest state in this period, and hence are most desirable for studies of their enzymes or other cell components (i.e. cell wall integrity). *E. coli* are normally found in animal and human intestines. Cheese, meat and milk can be contaminated by *E. coli* through the host animal and even harvested foodstuff, which has been treated with fertilizer, can be contaminated.

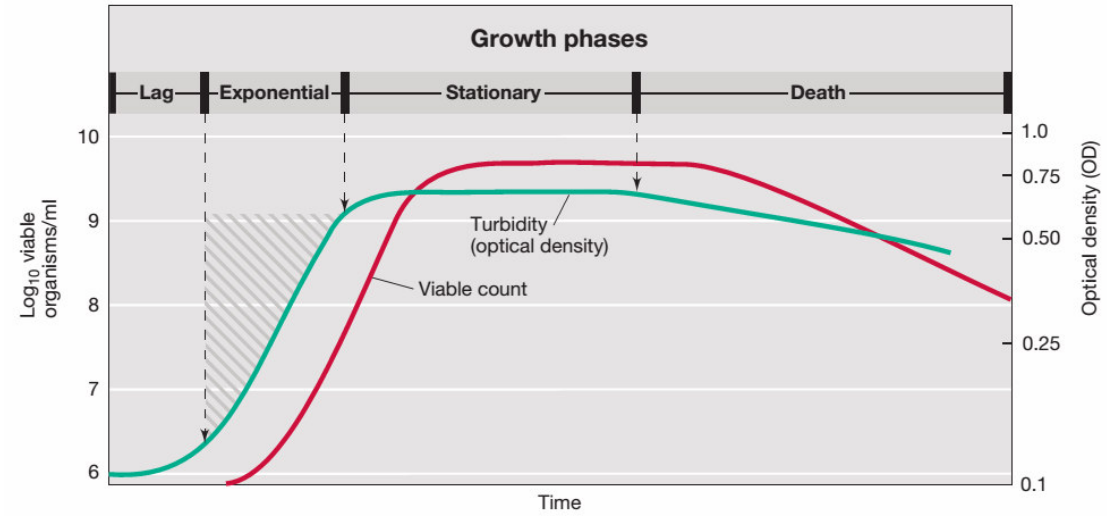


**Figure 1.3** Typical growth curves for a bacterial population. A viable count measures the cells in the culture that are capable of reproducing. Optical density (turbidity), a quantitative measure of light scattering by a liquid culture, increases with the increase in cell number. Reprinted from ref.[6]

## Staphylococcus epidermidis

*Staphylococcus epidermidis* (*S. epidermidis*) is a Gram-positive bacteria and is grape-shaped with a diameter of 0.5 to 1.5 µm. *S. epidermidis* is one of over 40 species belonging to the family of the genus Staphylococcus. It always appears on the human skin. It can also be found in the mucous membranes and in animals. *S. epidermidis* is not usually pathogenic; patients can prevent infection by their immune systems. However, infections can occur e.g. with contaminated implants, which pose a great threat to hospital patients. For example, a disease called endocaritis occurs most often in patients with defective heart valves.

### Corynebacterium

*Corynebacterium* is also a Gram-positive bacterium and is rod-shaped with a length of 2 - 6 µm and diameter of 0.5 µm. It is widely distributed in nature and it is mostly innocuous. Some are useful in industrial settings such as *corynebacterium glutamicum (C. glutamicum)*. Others can cause human disease, such as *corynebacterium diphtheriae (C. diphtheriae)*, which is the pathogen responsible for diphtheria. It is an acute and contagious infection characterized by pseudomembranes of dead epithelial cells, white blood cells, red blood cells, and fibrin that form around the tonsils and back of the throat. Several species cause disease in animals, most notably *corynebacterium pseudotuberculosis (C. pseudotuberculosis*), which causes the disease caseous lymphadenitis and some are also pathogenic in humans.

## 1.2.2 The cell wall

Since the effects and methods discussed in this thesis are mostly addressing the cell wall of bacteria, a deeper understanding of the structures, the properties, and the functions of cell wall is crucial.

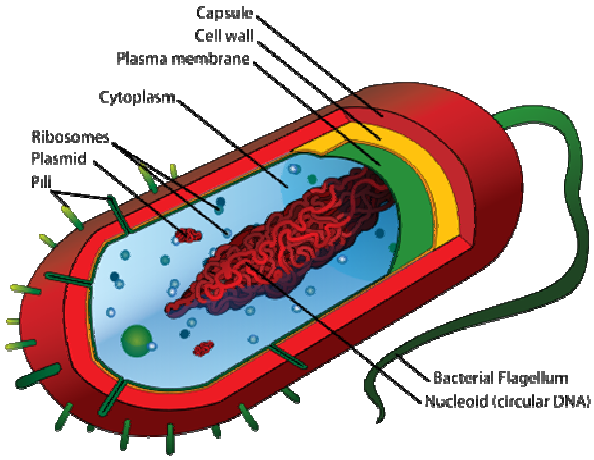


**Figure 1.4** Typical cell structure of a Gram-positive prokaryote bacteria.[9]

The cell wall is the outmost structure of prokaryote. Figure 1.4 shows the typical structure of prokaryotic cells. In most bacteria, the cell wall provides the structural integrity of the cell. The activities of transport systems in the membrane produce a

significant osmotic pressure of up to 2 bars in a typical bacterial cell. To withstand such pressures and prevent cell rupture, the cell wall is formed. Moreover, the cell wall also maintains shape and rigidity of the cell.

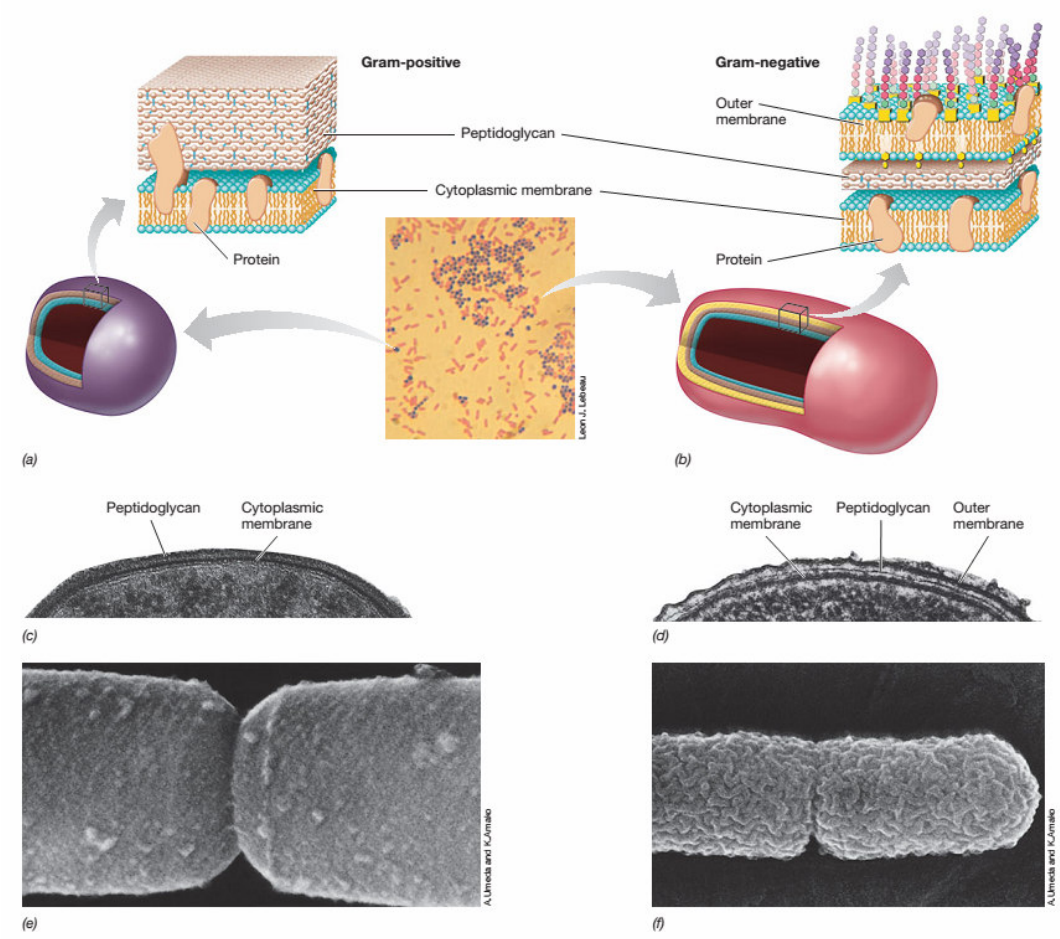


**Figure 1.5** Cell wall of Gram-positive and Gram-negative bacteria. (a, b) Schematic diagrams of Gram-positive and Gram-negative cell walls. The Gram stain photo in the center shows cells of *S. aureus* (purple, Gram-positive) and *E. coli* (pink, Gram-negative). (c, d) Transmission electron micrographs (TEMs) showing the cell walls. (e, f) Scanning electron micrographs (SEMs) of bacteria. Note differences in surface texture. Each cell in the TEMs is about 1 μm wide. Reprinted from ref.[6]

In general, bacterial cell walls consist of proteins, RNA, DNA, phospholipids, lipopolysaccharides, peptidoglycans, glycogens and other components. The cell wall is usually 10 - 100 nm thick, and plays an important role in cell division. The main component in all bacterial cell wall is peptidoglycan. As mentioned before, the bacteria can be divided into Gram-positive and Gram-negative based on the Gram staining method. However, the reason which directly causes the different Gram stain reaction is the difference of cell wall structures. The structures of Gram-positive and Gram-negative are

shown in Figure 1.5. Obviously, the amount of peptidoglycan in Gram-positive bacterial cell walls is higher than that in Gram-negative bacterial cell walls. As much as 90% of the wall is peptidoglycan in Gram-positive bacterial cell walls, whereas this value is only about 10% in Gram-negative bacterial cell walls. The Gram-negative cell wall consists of at least two layers (peptidoglycan and outer membrane), whereas the Gram-positive cell wall only consists of a single layer of peptidoglycan. Almost no other molecular layers exist except the teichoic acid which is embedded in some kinds of bacterial cell wall. Although most Gram-positive bacteria have only a single layer of peptidoglycan, stronger cell wall structures can be formed by cross-linked glycan strands. This is the reason why Gram-positive bacteria have a more rigid cell wall than Gram-negative bacteria.

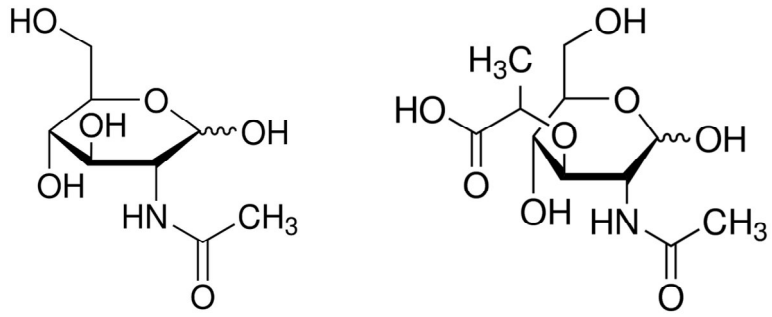


**N-acetylglucosamine** **N-Acetylmuramic acid**

**Figure 1.6** The chemical structures of N-acetylglucosamine and N-acetylmuramic acid.

So, what is the peptidoglycan? Peptidoglycan is a polysaccharide, which composes of two sugar derivatives: N-acetylglucosamine and N-acetylmuramic acid. Their chemical structures are shown in Figure 1.6. Furthermore, a few amino acids, such as L-alanine, D-alanine, D-glutamic acid, and either lysine or diaminopimelic acid (DPA) are included. Calcium-dipicolinate (Ca-DPA) is a biomarker for bacillus spores, thus there are many publications related to the detection of highly pathogenic *B. anthracis* based on the concentrations of Ca-DPA.[10] All of these components are cross-linked to form a repeating structures-glycan tetrapeptide (Figure 1.7). The cross-links are archived through glycosidic bonds formation in the X direction and peptide bonds in the Y direction (Figure 1.7B). The rigidity of bacteria depends on the extents of cross-linking. The more extensive the cross-linking is, the greater is the rigidity. Although the peptidoglycan is

very strong, it can be destroyed by special agents such as enzyme lysozyme and some antibiotics (i.e. penicillin and ampicillin). The destruction mechanisms are different. Lysozyme cleaves the N-acetylmuramic acid in peptidoglycan (Figure 1.7A) and causes cell lysis. Antibiotics prevent peptidoglycan biosynthesis and eventually cause osmotic lysis.

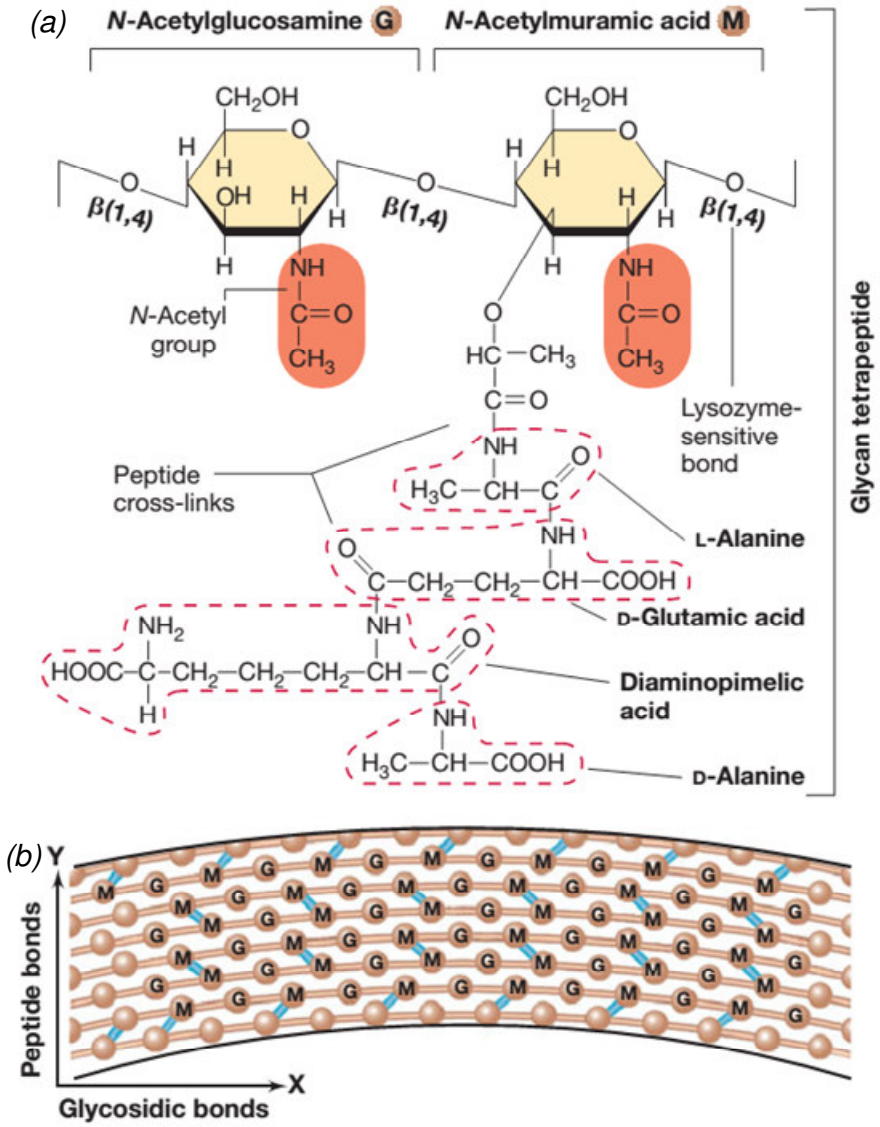


**Figure 1.7** Structure of the peptidoglycan. (a) Structures of the glycan tetrapeptide. The structure given is that found in E. coli and most of other Gram-negative bacteria. (b) Schematic overall structure of peptidoglycan. Reprinted from ref.[6]

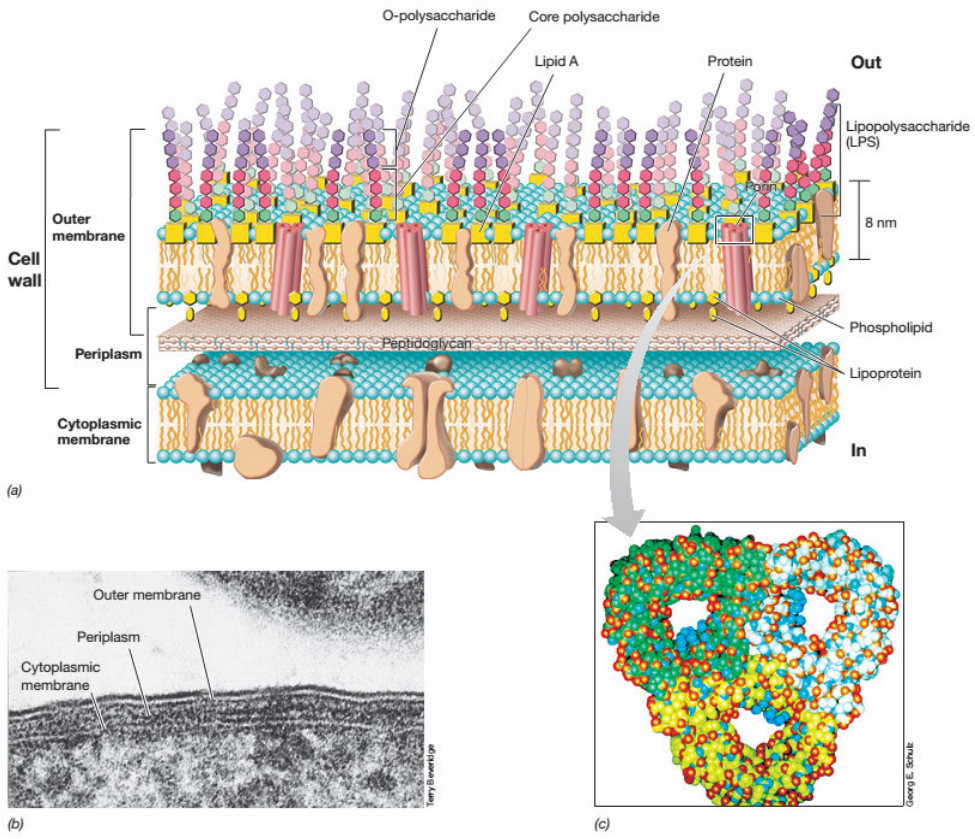


**Figure 1.8** The structure of Gram-negative cell wall. (a) Cartoon of the lipopolysaccharides (LPS), lipid A, phospholipid, porins, and lipoprotein in the outer membrane. (b) TEM of a cell of *E. coli* showing the cytoplasmic membrane and cell wall. (c) Molecular model of porin proteins. Reprinted from ref.[6]

Because *E. coli* was taken as the model microorganism in my doctoral research, I will particularly discuss the Gram-negative cell wall structure in the following. There is an outer membrane outside of the peptidoglycan. The main component of this outer membrane are lipopolysaccharides (LPS). It is a complex of lipids and polysaccharides which are linked. The part of polysaccharide has two components, the core polysaccharide and the O-polysaccharide. The lipid in the LPS, called lipid A, is not a typical glycerol lipid. The polysaccharide always has six primer sugars. On these sugar-core structures, side chains are present which bear species-specific epitopes. The main function of these sugar structures is to protect the bacteria from destruction by the immune response. In *E. coli*, the LPS consists of highly branched sugars, linked to a glycosamine containing lipid, and often determines the somatic antigen specificity.[11] The detailed structure of Gram-negative bacteria is shown in Figure 1.8. From this graph, we

can see that there are also proteins, porins, phospholipids and lipoproteins in the outer membrane. LPS occupies almost half of the outer membrane. By contrast, lipoprotein only exists in the inner part of outer membrane along with phospholipid. It likes an anchor to fix outer membrane on the peptidoglycan. The porins embedded in the outer membrane act as channels for the transfer of small molecules (i.e. ions and water). The diameter of the channel in porins is about 1 nm, which can make very small solutes traverse.

Although the main function of outer membrane is to maintain the bacterial integrity, the LPS layer on the outer membrane is the direct factor to cause diseases of animals, humans and plants, especially the lipid A. For example, diarrhea in humans is caused by the endotoxins, released by the LPS of Salmonnela.

The presence of either teichoic acid in Gram-positive bacteria or the outer membrane LPS in Gram-negative bacteria makes the bacteria negatively charged. The negative charge comes from the large number of carboxyl. This charge is a key factor for the sensitive and selective detection of bacteria by surface-enhanced Raman scattering (SERS) as discussed in this thesis.[12]

Bacteria can secrete various substances such as polysaccharides upon metabolic activity. These polysaccharide chains produce a sticky gel surrounding the bacteria, which provides a protecting function. In addition, the polysaccharide chains are useful due to their adhesion properties and prevent the cells from dehydration.

## 1.3 Conventional method for bacteria detection

In the last century, scientists have developed a lot of methodologies to detect infectious and toxigenic bacteria. These methodologies are based on different characteristics of bacteria, such as optical, electronic, magnetic and other properties. Several methods, including plating and culturing, microscopy, flow cytometry, enzyme-linked immunosorbent assay (ELISA), and polymerase chain reactions (PCR) have been

widely used for bacteria detection. The most relevant methods are discussed in the following.

## 1.3.1 Plate count

This is the most common and oldest method for the detection of bacteria. The method is based on following principle: each viable bacterium can grow and divide to yield one colony. Thus, colony numbers reflect the initial bacteria concentration. It was first established in 1905 using the MacConkey's agar.[14] Typically, a Petri dish containing a growth medium (agar plus nutrients) is used to culture microorganisms (Figure 1.9). Different growth media are used for different bacterial species and purposes. If an antibiotic is added into the growth media, bacteria with the corresponding antibiotic resistance can be selectively grown. Individual bacteria put on the plate will grow into individual colonies. Thus, the plate count method can be used either to determine the concentration of microorganisms or to separate individual bacteria species from a mixture of different microorganisms. Most bacteria species can be detected by culture methods. Although culturing and plating methods are sensitive and selective, they are exceedingly time-consuming (up to several weeks) for they rely on several enrichment steps. In recent times, attempts have been made to develop automated cultural methods. Examples are the Omnilog™ and Micrologᵀᴹ (Biolog, CA) systems which can identify over 2000 species of microorganisms.[15]

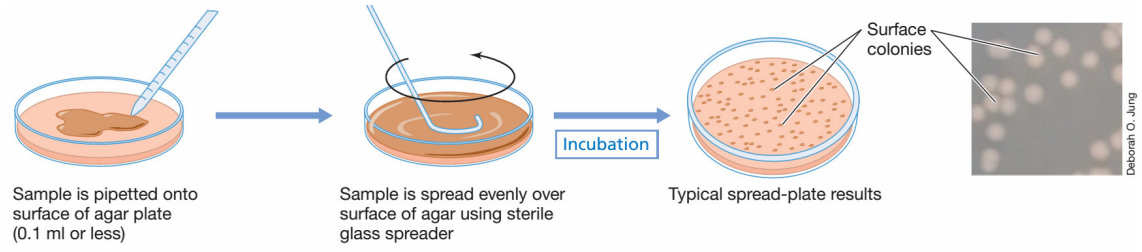


**Figure 1.9** Schema of plate count. Reprinted from ref.[6]

## 1.3.2 Microscopy

Nowadays, using common microscopy method to detect bacteria need combination with fluorescence or Raman techniques. For example, if bacteria are stained with 4',6-diamidino-2-phenylindole (DAPI), the viable bacteria can emit blue fluorescence ($\lambda_{max}$ = 461 nm) under ultraviolet light excitation. The structure of DAPI is shown in Figure 1.10d. DAPI can easily penetrate through intact cell membrane and then strongly bind to deoxyribonucleic acid (DNA). DAPI can be used to detect bacteria in various environments, such as water, food, soil and human. Such strategy is widely used in food industry, clinical diagnosis and biology. There are many other fluorescent dyes as staining agents, such as green fluorescent protein (GFP) and acridine orange. Therefore, we can employ muti-fluorescent staining agents to discriminate different bacteria at one time.

Recently, confocal microscopy has become an important technique allowing subcellular organelle's levels of bacteria to be detected, owing to its high spatial resolution and three-dimensional (3D) imaging capabilities. Laser Raman microscopy spectroscopy and confocal scanning laser microscopy (CSLM) have been widely used in bacteria detection (Figure 1.10e). CSLM combines the advantages of laser source's accuracy and fluorescent microscope's spatiality, which can generate a 3D image and allow the viewer to profile different depth of the specimens. It is possible to improve the 0.2-μm spatial resolution of the bacteria using CSLM. It is better to improve the sensitivity compared with normal optical microscopy.

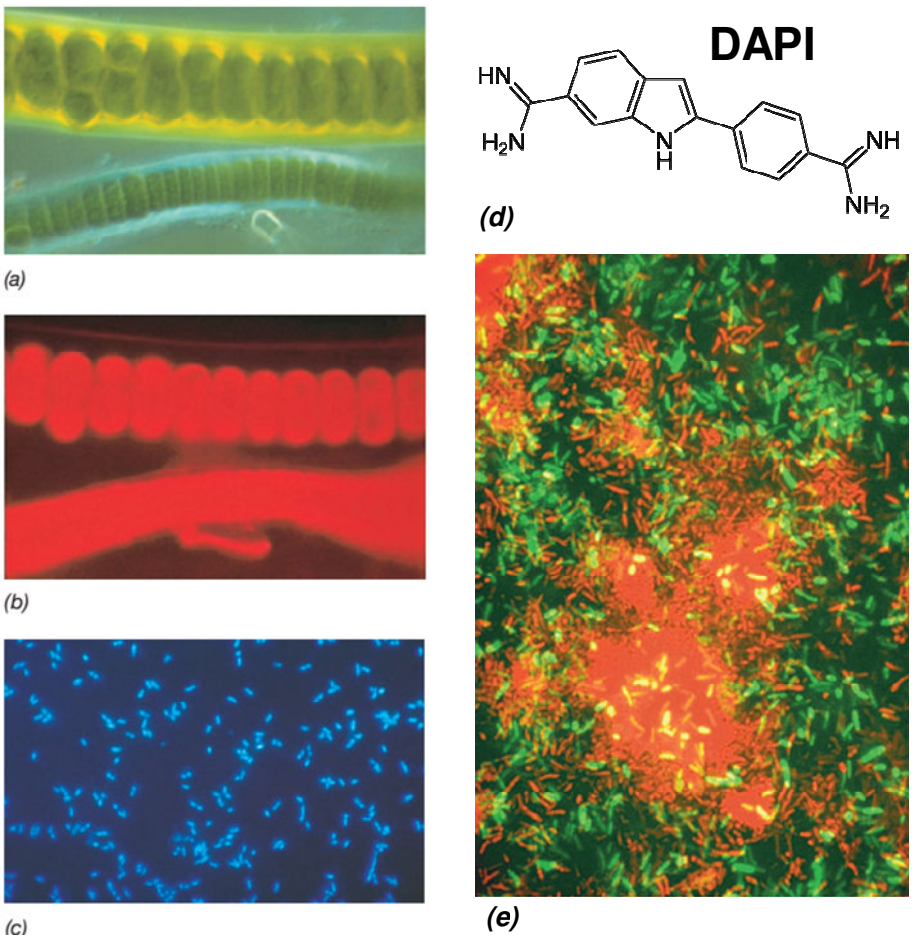


**Figure 1.10** Fluorescence microscopic technologies. (a, b) *Cyanobacteria*. The same cells are observed by bright-field microscopy in part a and by fluorescence microscopy in part b. The cells fluoresce red because they contain chlorophyll a and other pigments. (c) Fluorescence photomicrograph of cells of *E. coli* made fluorescent by staining with the fluorescent dye DAPI. (d) The structure of DAPI. (e) Confocal image of a microbial biofilm community cultivated in the laboratory. Reprinted from ref.[6]

We can see only 0.2-μm cell structures through the improved light microscope, we need to use electron microscopy (i.e. SEM and TEM) to clearly see down to nm cell structures. The resolution of a TEM is much greater than that of the light microscope. The resolving power of a high-quality TEM can reach about 0.2 nm. With such powerful enlargement ability, even single protein and DNA can be visualized (Figure 1.5 and 1.8). We can clearly see the sub-structures of bacteria via electron microscope, such as cell wall, cytoplasmic membrane, protein, flagellum and DNA. If only the external features of microorganisms are to be observed, one can image the bacteria using SEM or atomic force microscopy (AFM). Figure 1.11 shows TEM, SEM and AFM images of bacteria.

The researcher can choose the corresponding technique based on their purpose. In order to see nanoparticles (NPs) coating the cell wall of bacteria, I choose the highest resolving TEM technique as my main research tool.

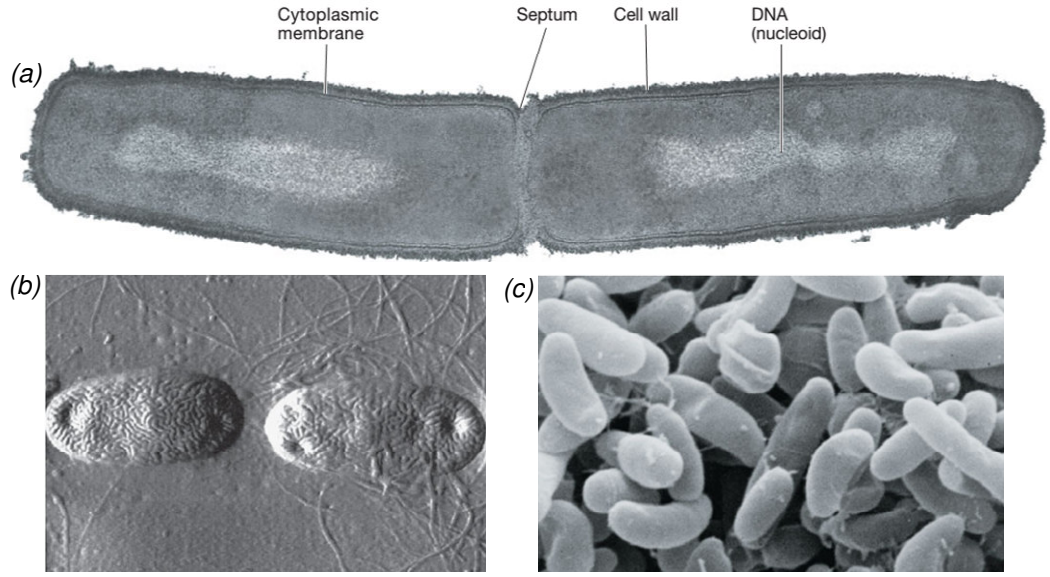


**Figure 1.11** Electron micrographs of microorganisms. (a) TEM image of a dividing bacterial cell. (b) AFM image of bacterial cell. (c) SEM image of bacterial cell. Reprinted from ref.[6]

Microscopy is a fast and easy way to estimate the number of microorganisms. However, it has several disadvantages. For light microscopy: (1) it is hard to differentiate live and dead bacteria without the special staining fluorescent dyes. (2) It is difficult to count low concentrations of bacteria (i.e. below $10^6$ cell/mL) without preconcentration. (3) Some fragments of bacteria may be miscounted for real bacteria cells. (4) Some kinds of bacteria are too small to be seen. (5) Except above mentioned, the microscopic technique can not precisely count the huge cell number. Although microscopy analyzing a great number of bacteria can be realized via automated software, most of microscopic analyses still rely on the practiced eye of the investigator. Electron microscopy requires expensive instruments and often requires intensive sample preparation by skilled technical personnel. Thus, there is a great demand in developing cheaper, more precise and functional technique to detect microorganisms.

### 1.3.3 Flow cytometry

Flow cytometry is a laser-based, biophysical technology employed in cell counting, biomarker detection and protein engineering, by suspending cells in a stream of liquid and passing them by a light scatter and/or fluorescence detection apparatus. Both the number and the size of bacteria can be determined. It allows the analysis of thousands of particles per second. A major advantage of flow cytometry is the capacity to combine multiple parameters in analyzing a microbiological sample or finding a specific population. The first fluorescence-based flow cytometry instrument was developed at the University of Münster, Germany, in 1968 by Wolfgang Göhde.[16] In the beginning, both living and dead bacteria will be counted together by this preliminary equipment, which means it can not discriminate living and dead cells. Recent developments applied on this apparatus can overcome the potential disadvantages. Detection only of living bacteria is obtained by using a combination of antibody and viability markers. Pinder and his co-workers used chemchrome as a fluorogenic marker for the detection of viable bacteria by flow cytometry.[17] This marker was used in combination with fluorescently labelled monoclonal antibodies against *Staphylococcus typhimurium (S. typhimurium)*. This novel protocol is sensitive only to living *S. typhimurium* and can reduce errors due to the intrinsic fluorescence and non-specific binding. The detection time for 100 cells, with the presence of large numbers of non-target or dead microorganisms, is 30 min. Furthermore, flow cytometry is a powerful technique in the medical field for counting and differentiating cells and other cell typesets from clinical samples (Figure 1.12). In this thesis, we use flow cytometry to determine the original concentrations of bacteria. Up to the present date, no reports have discussed this approach in terms of label-free detection of bacteria. The reported literature relies on labeling with fluorochrome, which diminishes their effectiveness owing to the fact that the application of labeling reagents requires large reactant volumes, additional preparation steps and more time. Thus, development of a label-free method for distinction of living and dead bacteria is greatly demanded. This is also one of the main tasks that need to be solved in my thesis.

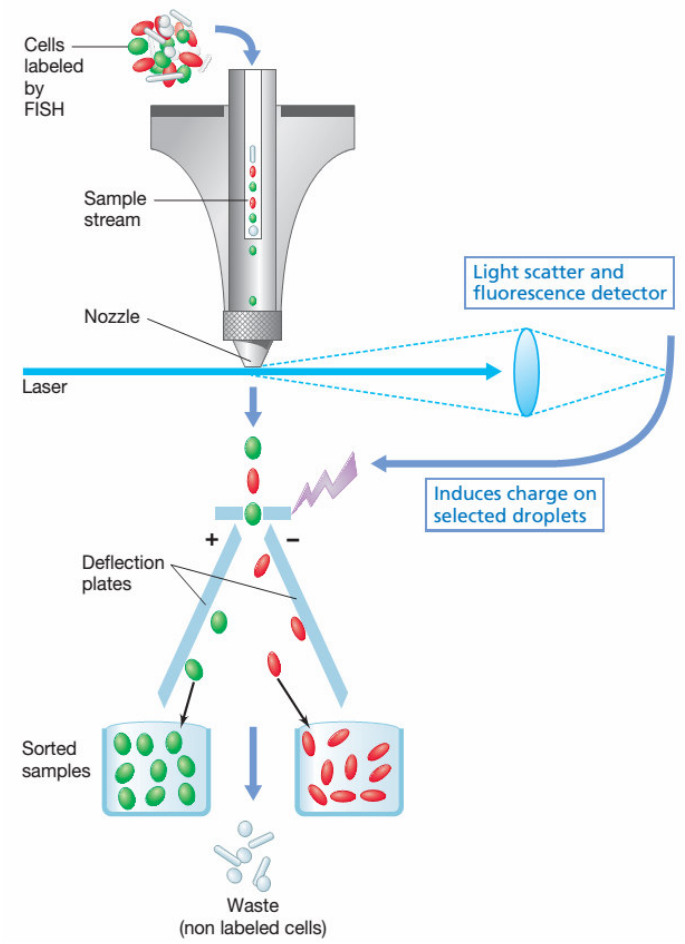


**Figure 1.12** The principle of flow cytometry in cell sorting. Reprinted from ref.[18]

## 1.3.4 Enzyme-linked immunosorbent assay (ELISA)

ELISA is a well-known format of "wet-lab" type analytical assay that uses a solid-phase enzyme immunoassay to detect bacteria in liquid samples. This technique involves the use of antibodies to which enzymes have been covalently bound. Normally, ELISA includes the following steps (indirect ELISA): 1) the antigens (bacteria) should be attached to a microtiter plate, which has strong adherence to the bacteria. The microtiter plate is usually made from polystyrene. 2) A specific antibody is applied on the surface, so it can bind to the bacteria. This antibody always links to an enzyme. 3) Addition of a substance containing the enzyme's substrate. The typical enzymes used include peroxidase, alkaline phosphatase, and β-galactosidase. The subsequent reaction produces a detectable signal, such as a colour change in the substrate, fluorescence, or chemiluminescence. Between each step, the plate typically is washed with a mild

detergent solution to remove any proteins or antibodies that are not bound specifically. Depending on the detection mechanism, the ELISA can be divided into three types: direct ELISA-sandwich ELISA (Figure 1.13a), indirect ELISA (Figure 1.13b), and competitive ELISA (Figure 1.13c). The major difference of indirect ELISA is the use of a secondary antibody, which binds to the primary antibody. As we know, e.g. indirect ELISAs are widely used to detect antibodies to human immunodeficiency virus (HIV) in human body.

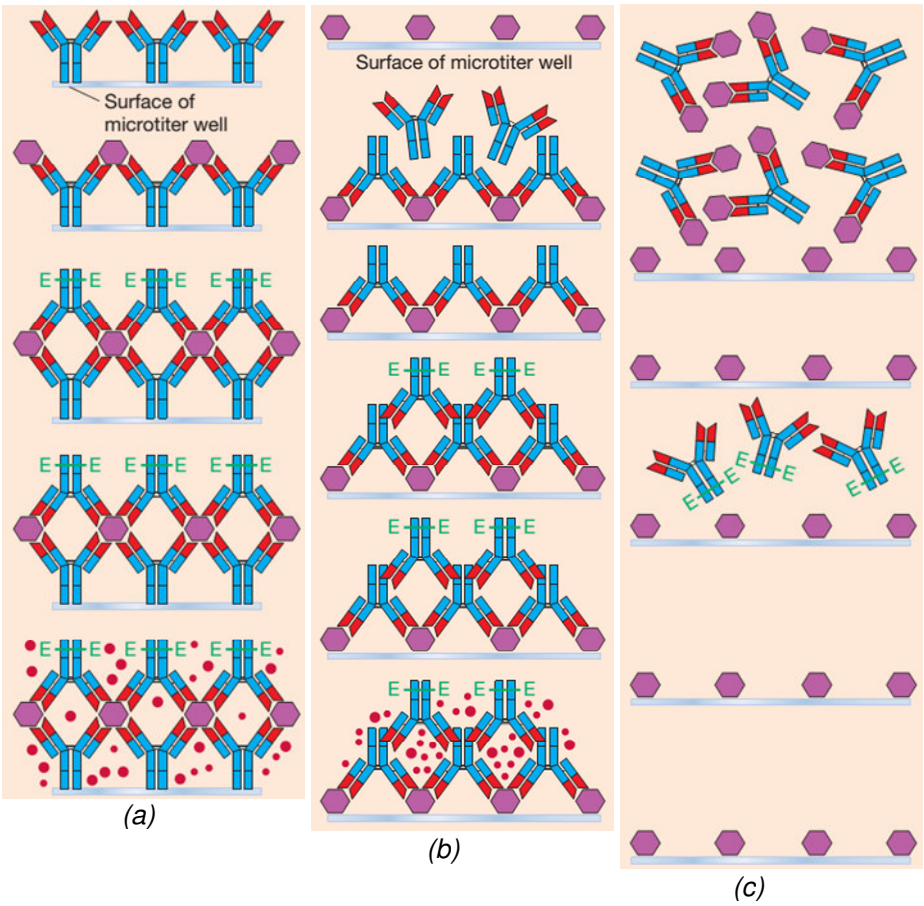


**Figure 1.13** The principles of ELISA. (a) Direct ELISA - Sandwich ELISA. (b) Indirect ELISA. (c) Competitive ELISA. Reprinted from ref.[6]

A major disadvantage of the indirect ELISA is that the antigen immobilization has not enough specificity, when a complicated sample (waste water or human serum) is applied. Many of the substances in the sample may attach to the surface of microtiter plate well. However, the sandwich and the direct ELISA can solve such problem by using a capture antibody, which has specific capture ability to grab the target analyte from the complex samples. The competitive ELISA is usually used to detect bacteria, drugs and

other compounds of interest in clinical diagnosis. The intensity of color is inversely proportional to the amount of antigen in the patient samples, which is opposite to direct/indirect ELISA's results. In general, competitive ELISA is more sensitive than either direct or indirect ELISA.

### 1.3.5 Polymerase chain reaction (PCR)

Of all the methods described, PCR-based methods have made the biggest impact in terms of the number of papers published. This is because it can dramatically reduce the analysis times and labour costs. PCR is a molecular biology technology to amplify a single or a few copies of a piece of DNA or RNA by several orders of magnitude, generating thousands to millions of copies of a particular DNA/RNA sequence. PCR can be used to detect a wide range of microorganisms in environment, food industry and human disease. The major advantage of PCR for bacteria detection is that a single cell can be detected in about an hour compared with conventional methods that may need days or even several weeks. However, a disadvantage is that the amount of DNA/RNA sequence is hard to know for a given microorganism.

Typically, PCR involves the three major steps of denaturing, annealing, and elongation. The denaturing step is the first regular cycling and the temperature is 94 - 98 °C for 20 - 30 seconds (Figure 1.14). The aim of this step is disrupting the hydrogen bonds between complementary bases of DNA/RNA, generating single-stranded DNA/RNA molecules. Following denaturing, the mixture is quickly cooled to 50 - 65 °C for 20 - 40 seconds, where the primers anneal to the single-strand DNA/RNA template. The polymerase binds to the primer-template hybrid and DNA/RNA begins formation. Finally, the elongation is achieved by polymerization at 72 °C (the optimum temperature of the enzyme). At this step, the DNA/RNA polymerase synthesizes a new DNA/RNA strand that is complementary to the DNA/RNA template strand. The elongation time depends both on the DNA/RNA polymerase used and the length of the DNA/RNA fragment to be amplified. Under optimum conditions, the amount of DNA/RNA is

doubled at each elongation step, leading to exponential amplification of the target's DNA/RNA fragment. Normally, DNA polymerase includes the *Escherichia coli* Pol III, Taq polymerase and Pfu polymerase, their optimum activity temperature is different. The scientists can choose the best polymerase for their specific DNA/RNA.

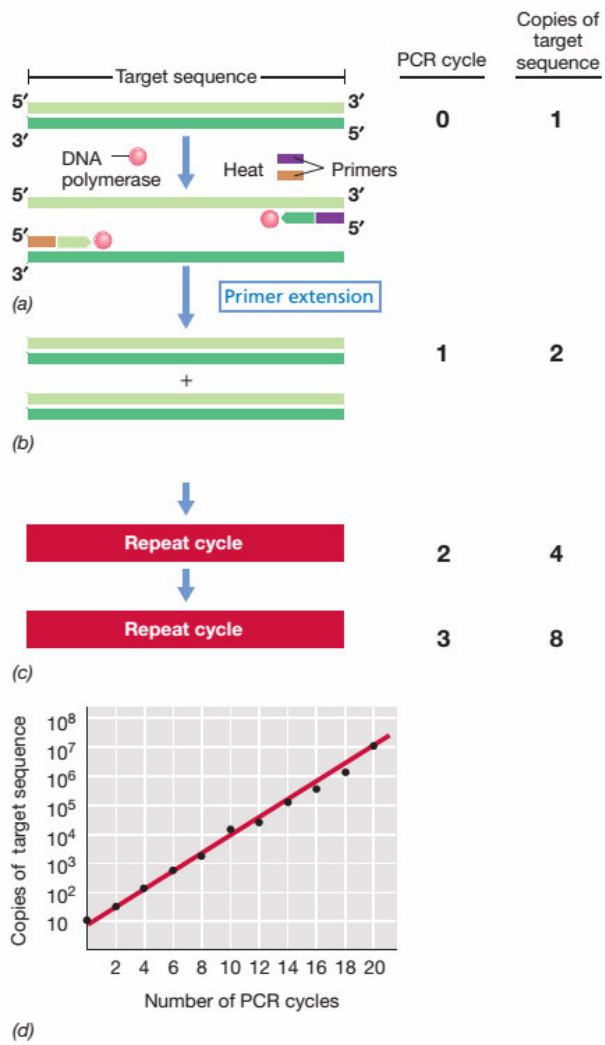


**Figure 1.14** The polymerase chain reaction (PCR).The PCR amplifies specific DNA sequences. (a) Target DNA is heated to separate the strands, and a large excess of two oligonucleotide primers, one complementary to each strand, is added along with DNA polymerase. (b) Following primer annealing, primer extension yields a copy of the original double-stranded DNA. (c) Two additional PCR cycles yield four and eight copies, respectively, of the original DNA sequence. (d) Effect of running 20 PCR cycles on a DNA preparation originally containing ten copies of a target gene. Note that the plot is semilogarithmic. Reprinted from ref.[6]

For bacteria detection, PCR amplification of a target gene sequence in bacteria, followed by hybridization with DNA/RNA polymerase, provides the sensitivity and

specificity required in food and environment monitoring. However, there is a major disadvantage in the subject of bacteria detection by PCR, that is, this rapid strategy allows DNA/RNA from dead microorganisms to be also detected, and such procedure can not be applied in distinction of living and dead bacteria. So, the viability of bacteria is an issue that has to be considered. This major problem also exists in the ELISA method. However, this issue is especially important in clinical diagnosis where false-positive results have to be carefully excluded. Thus, there has always been a strong driving force to develop a novel strategy to rapid and accurate distinct living and dead bacteria.

### 1.3.6 Microarray

Although above mentioned methodologies have a lot of advantages for detection of bacteria, such as fast, reliable, high selective and specific, they can not provide high-throughput and multianalyte detection principle. In the past decade, high-throughput screening methods using immunoassays on microarray technologies have been applied as miniaturized analytical tools in modern biology and biochemistry.[19] The first functional microarray was developed in 1991 by Fodor et al. as a light-directed, spatially addressable parallel chemical analysis.[20] In general, microarray systems should use fluorescence and chemiluminescence as detection of bacteria or other biomolecules principles.

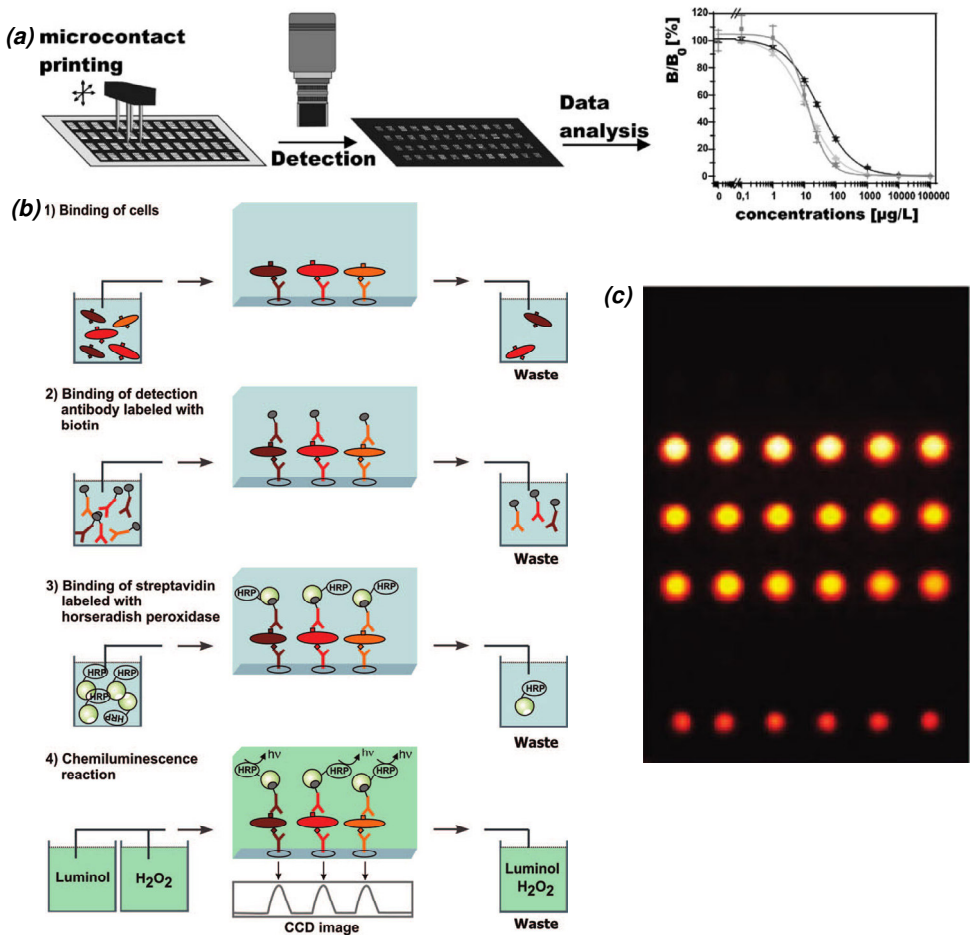


**Figure 1.15** The principle of microarray. (a) Schematic diagram of producing microarray. (b) Strategy of multiplexed analysis by use of a chemiluminescence microarray with a automated sample and reagent supply. (c) Image of chemiluminescence signals for the detection of bacterial cells on microarray. Reprinted from ref.[19,21,22]

In our institute, a lot of research work was done on chemiluminescence microarray for sensitive and selective detection of pathogens.[19,21,22] The first flow-through chemiluminescence microarray was developed and characterized for the rapid and simultaneous detection of *E. coli* O157:H7, *Salmonella typhimurium*, and *Legionella pneumophila* in water samples using a semiautomated readout system (Figure 1.15). The chemiluminescence was generated by a streptavidin-horseradish peroxidase (HRP) catalyzed reaction of luminol and hydrogen peroxide. Then the chemiluminescence reaction was recorded by a sensitive charge coupled device (CCD) camera. The device (microarray chip reader, MCR 3) is shown in Figure 1.16. Microarray technology represents a high-potential tool for solving multianalyte problems in single experiment in

the analytical and bioanalytical field.[23] In addition, the immunoassay technique applied on the microarray system offers the possibility to selectively capture specific antigens, such as bacteria and viruses.[22] Thus, a highly sensitive, selective, multianalysis, and high-throughput bacteria assay is highly demanded.

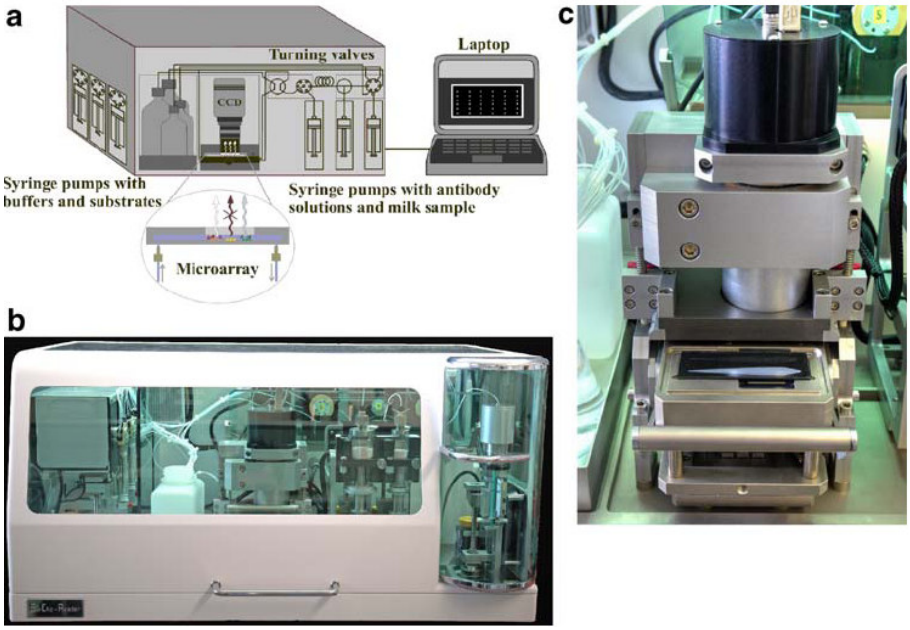


**Figure 1.16** (a) Schematic drawing of the MCR 3. (b) Image of the chemiluminescence microarray chip reader (MCR 3; Institute of Hydrochemistry, TU Munich). (c) The microarray loading unit and the inserted flow-through microarray chip.[19]

# 1.4 Raman spectroscopic characterization of bacteria

Raman spectroscopy (RS) is a nondestructive spectroscopic analytical technique which is based on the effect of inelastic light scattering by molecules.[24] RS has several advantages compared to infrared spectroscopy (IR): 1) a very small amount of sample is needed; 2) water is a weak Raman scatterer, almost has no Raman signals, allowing for the in situ detection of analytes in aqueous environment. 3) RS is "cleaner" than mid-IR spectra. Raman bands are narrower, and overtone and combination bands are generally weak; 4) The standard spectral range reaches well below 400 $cm^{-1}$, making the technique ideal for both organic and inorganic species; 5) RS can be used to measure symmetric bands which are weak in the IR spectral range(e.g. -S-S-, -C-S-, -C=C-). Furthermore, RS can provide "whole-organism fingerprints" for the characterization and identification of

different biological systems (e.g., bacteria, yeast, and pollen) with spatial resolution of optical microscopy. All biologically relevant substances such as polysaccharides, amino acids, nucleic acid, lipids and proteins display distinct spectral features.[25]

However, RS lacks sensitivity for the characterization of microorganisms, since the typical quantum efficiency of the normal Raman effect is in the order of $10^{-6}$ - $10^{-8}$. Thus, in order to obtain high signal-to-noise Raman spectra of bacteria, more collection time and higher laser power are needed. This will have another side-effect: the high laser power can burn the samples, the known D and G bands of soot will appear.[26] The soot occurs in many carbon-containing systems, such as microorganisms. This is due to the fact that the soot has a very large Raman cross-section, whose spectrum can quickly become dominant and obscure all other contributions. Thus, we can not get the Raman spectra of bacteria under such circumstances. In order to overcome such problems, one needs to use low laser power to get high signal-to-noise Raman spectra of bacteria. Such needs can be realized by another Raman technique, surface-enhanced Raman scattering (SERS).

## 1.5 Surface-enhanced Raman scattering (SERS)

Since the discovery in the 1970s that Raman signals are enhanced at rough silver electrode surface,[27-29] SERS has become a subject of interest for the detection of chemical,[30] biological species,[31] as the molecular imaging, and monitoring at microorganisms,[32] cell,[33] tissue[34] even in vivo.[35] This is because of its high sensitivity, intrinsic selectivity due to the spectroscopic fingerprint, simple and fast preparation, and nondestructive data acquisition in aqueous environment. In particular, the detection and identification of microorganism by SERS has attracted interest recently, motivated by the potential application on single microorganism.[2,36,37] The enhancement is generally attributed to the electromagnetic field in the proximity of nanostructured metal surfaces.[30] The Raman effect can be dramatically enhanced if a molecule is attached to or in the immediate proximity to noble metallic (Au, Ag and Cu) surfaces. These noble metals are

used in different formats, e.g. as metal colloids,[38,39] plates,[40] rods,[41-43] prisms[44] and stars.[45,46] Moreover, there are recently caused large efforts for the fabrication of various SERS active substrates such as nanoparticles dimers,[47] nanogaps,[48,49] nanowire/nanorod arrays,[50,51] and periodic 2D nanostructures.[52,53] These novel SERS active substrates can provide a enhancement factor in the range of $10^3$ - $10^6$ and, under certain conditions, even up to $10^{14}$ (allowing to detect single molecules),[54,55] for different chemical species.

Generally speaking, three possible effects contribute to the total enhancement factor.[56,57] 1) the electromagnetic enhancement effect, or surface plasmon resonance, is supported to contribute most of the enhancement effect and takes place on the ~10-nm scale of SERS substrates. 2) Chemical enhancement or charge transfer is assumed to involve transfer of electrons between the absorbed molecule and the conduction band of the metal and take place at sites of atomic-scale roughness on the metal surface. 3) Resonance enhancement or resonances within the molecule itself can provide 2 - 3 orders of magnitude of additional enhancement and take place when the analyte has a chromophore that coupled to the localized surface plasmon of plasmonically active nanostructures.[52,58-62] These three components are often treated as independently contributing to the overall effect, with the implication that by properly choosing the experimental parameters, one or more can be ignored.

However, the varying experimental conditions can influence the relative degree of each enhancement effect and the total enhancement factor. In general, higher enhancement can often be obtained by combining two or more resonances. Each resonance contributes a part of effect on the appearance of the resulting Raman spectrum, and it is necessary to invoke one or more of these resonances to completely describe a particular experiment. However, it is hard to completely describe all observations of the SERS phenomenon with consideration of all three of these contributions.

## 1.5.1 Electromagnetic enhancement

There are typically three electromagnetic enhancement theories: surface mirror field theory, lightning effects and localized surface plasmon resonance. It is generally considered that electromagnetic enhancement theories originates from the enhancement of the local electromagnetic field on metal surface, an effect which is called localized surface plasmon resonance (LSPR). Here, we just discuss the LSPR (Figure 1.17).

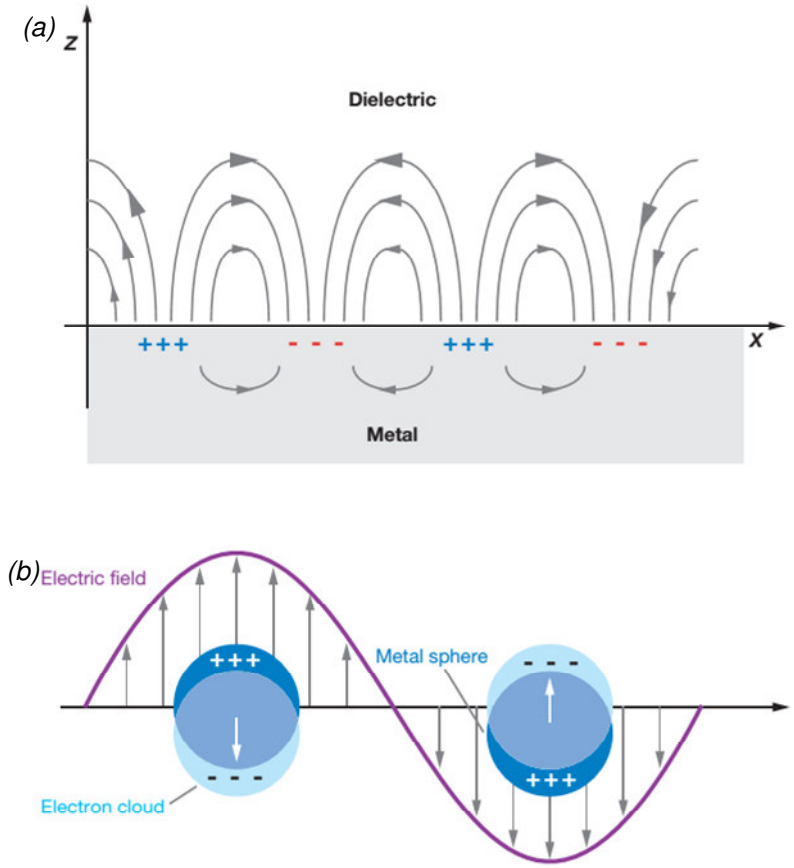


**Figure 1.17** Schematic diagrams illustrating (a) a surface plasmon polariton (or propagating plasmon) and (b) a localized surface plasmon (LSPR). Reprinted from ref.[61]

As mentioned above, the LSPR is a common characteristic of metals. When laser light illuminates the surface of rough metals, a local amplification electromagnetic field will be generated on the metal surfaces. Once molecules are positioned in the local amplification electromagnetic field, the scattering cross of molecules section will be greatly amplified, thereby molecular giant enhanced Raman scattering spectrum can be obtained. The relation between the Raman intensity, $I$, and the local EM strength, $E$, is

usually approximated as $I \propto |E|^4$.[63,64] We can find that only small increment on $E$, the Raman intensity $I$ of molecules will be greatly enhanced. The relation between local EM strength, $E$, and the interspaced distance, $D$, is usually described as $E \propto (1/D)^{12}$.[57,65] Thus, if the distance between the molecules and surface of metal increases a little, $E$ will be dramatically reduced, resulting in a significant reduction of SERS signals.

However, only a few kinds of precious metals can produce LSPR under laser irradiation. Only the LSPR of nanoscaled Ag, Au and Cu can be matched with the usual Raman laser (e.g., 532 nm, 633 nm, and 780 nm) through the classical electromagnetic theory calculation. In addition, the surface roughness of the metal,[66,67] particle size,[68] morphology,[69] and arrangement[70] have a great effect on LSPR. Furthermore, the LSPR changes with different types of lasers.[63]

According to the electromagnetic enhancement mechanism, to achieve the maximum SERS enhancement the following conditions are to meet. 1) molecules should be positioned on the metal surface; 2) the diameter of metallic particles should be smaller than the wavelength of the laser; 3) the frequency of laser should be matched to the LSPR of the metal. In addition, it can be seen from the electromagnetic enhancement mechanism, that the Raman spectra depends on the distance from the metal surface and they are independent from the structure of the molecule. This can not explain why different molecules have different SERS spectra on the same metal substrate, even isomers have different SERS spectra on the same metal substrate.[71]

## 1.5.2 Chemical enhancement

The above mentioned questions can not be solved by the electromagnetic enhancement mechanism. The chemical enhancement mechanism is presented to explain the phenomenon which can not be interpreted by physical enhancement mechanism (EM enhancement). Chemical enhancement mainly studies the interaction between the molecules and metal surface, including the absorption orientation feature of molecules and the charge transfer between molecules and SERS substrates. Chemical enhancement

mechanism includes two models: atomic absorption model and the charge transfer model. The latter is widely accepted by scientists.

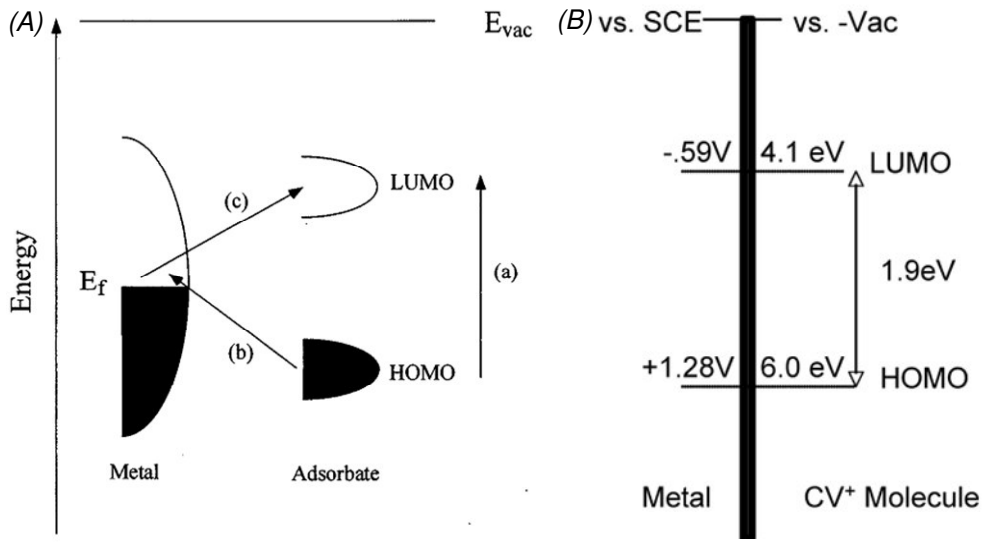


**Figure 1.18** Chemical enhancement. (A) Energy level diagram for a "molecule-metal system" showing also possible resonant Raman processes involving molecular states (path (a)) and molecular and metallic states (paths (b), (c)). (B) Exemplification of charge transfer system obtained from electrochemistry. Reprinted from ref.[64,72]

Charge transfer (CT) model[60,73] is that: when the molecules are absorbed to the metal surface, the adsorbed molecules can produce some special compounds on the surface of the metal atoms by proper chemical bonds, resulting in a new excited state. Thus a new absorption peak can be formed. Two kinds of charge transfer transitions can occur under appropriate laser excitation. As shown in Figure 1.18, the adsorbed molecules of the highest occupied molecular orbital (HOMO) and the lowest unoccupied molecular orbital (LUMO) are symmetrically distributed in the metal Fermi level sides. The free electrons in the metal can be resonantly transited from the metal Fermi level to the LUMO (process c), or charge transfer from the adsorption molecular HOMO to the surface of the metal. Resonance will occur through this charge transfer, and the polarization ratio of adsorbed molecules will be greatly changed, so as to enhance the SERS effect. For example, the electrochemical HOMO-LUMO gap of crystal violet cation is 1.9 eV, which is almost identical to the lowest optical singlet π-π* transition. Thus, if a 633-nm (2 eV) laser line is used as excitation source and the Fermi energy of the metal is around -4.1 eV, then

both a molecule-to-metal CT transition and the π-π* molecular resonance will occur (Figure 1.18).[72]

The key of charge transfer model is that the adsorbed molecules can react with atoms on the surface of metals, thus a new chemical bond is formed. This kind of model can explain the following phenomenon: 1) when the distance between molecules and metal increases, the SERS effect will drop to zero immediately with the disappearance of the chemical bond. 2) Different molecules adsorbed on the same SERS substrate display different SERS spectra, even under the same laser irradiation, because the molecular energy level is different. Not all of the molecules absorbed on the metal surface can be enhanced, only those which are in the surface active site of metal can be enhanced. However, the active site on the SERS substrate is rare. The active sites account for just about 63 in 1,000,000 of the total, but contribute about 24% to the overall SERS intensity.[52] Furthermore, the difference between SERS spectra and normal Raman spectra, such as the largely shifted peaks, the change of peak shape and intensity, or appearance of new peaks, can be interpreted by chemical enhancement mechanism.

### 1.5.3 Resonance enhancement

When a molecule, which is accessible to resonance Raman (e.g. a chromophore), adsorbs on the surface of rough Ag, Au, and Cu etc, the Raman signals of molecules show an additional $10^4$ - $10^6$ enhancement except to the electromagnetic enhancement. This phenomenon is known as surface-enhanced resonance Raman scattering (SERRS).[74] SERRS is a technique that combines the electromagnetic enhancement and resonance enhancement. The most typical example in this regard is focused on the detection of single molecule-fluorescent dyes, such as rhodamine 6G[54] and crystal violent.[55] SERRS successfully solves the problem that many Raman inactive molecules (e.g. pesticides, explosives, etc.) can not be detected by SERS even under high concentrations. These molecules can not be detected by SERS because the electromagnetic enhancement is not high enough to enhance such Raman inactive molecules. SERRS effect requires that the

target molecules have a visible chromophore (or create a supramolecular chromophore generated in a host-guest binding system) and the absorption of the visible chromophore matches with the laser excitation. The resonance enhancement can provide 2 - 3 orders of magnitude of additional enhancement relative to surface enhancement alone.[30,74,75] The chromophore coupled to the localized surface plasmon of plasmonically active nanostructures lead to spectral, resonant, and surface enhancements.[63,76] This effect allows the ultrahigh Raman scattering of the bacterial components by multiple enhancement techniques.

The most well-known group in subject of SERRS is the group of Duncan Graham from the University of Strathclyde, UK. They successfully detected explosives (TNT, RDX),[77,78] protease activity,[79] DNA and RNA,[80] prostate-specific antigen,[81] oligonucleotides,[82] human tumor necrosis factor[83] etc. via SERRS technique. The basic idea is based on following procedure: the target analyte is usually a Raman inactive substance, usually undetectable by SERS. However, the Raman inactive molecules can be changed to Raman active molecules through a special chemical reaction, which can connect a chromophore on the Raman inactive molecules. Normally, the absorption of resultant Raman active analytes is located near the laser wavelength. Thus, the analytes will be in resonance with the laser line, so as to achieve the purpose of sensitive detecting analytes. For example, owing to the fact that TNT is a Raman inactive molecule, it is difficult to detect it by SERS. TNT was first reduced to an azo dye in 2002.[77] One of the nitro groups in TNT was changed into an amino group. Such molecule further reacted with the chromophore molecule, to generate chromophore azo compounds. The absorption of the azo compounds is in the visible region, which will be in resonance with the laser line to achieve the purpose of detection TNT by SERRS.

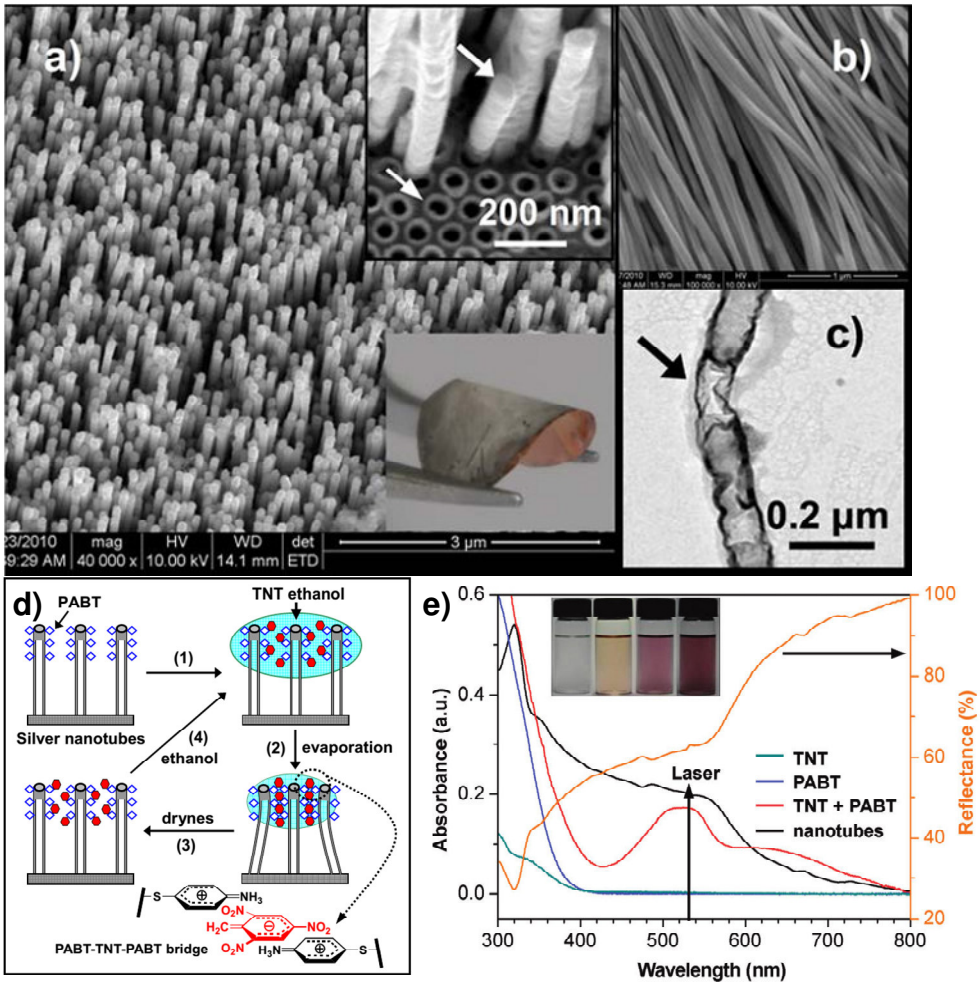


**Figure 1.19** Trinitrotoluene (TNT) explosive lights up ultrahigh Raman scattering of nonresonant molecule on a top-closed silver nanotube Array. (a) SEM image of a top-closed silver nanotube array (b) SEM image of the individual nanotubes liberated completely from an alumina template. (c) TEM image of silver nanotubes. (d) Mechanism for TNT-Induced Resonance Raman Enhancement of PABT on the Top-Closed Silver Nanotube Array. (e) UV-vis absorption spectra of TNT, PABT, TNT-PABT complex, and top-closed silver nanotube array. The inset images show the colors with the addition of 0, 40, 120, and 200μL of 0.01 M PABT into 4 mL of 0.1 mM TNT solution, respectively. Reprinted from ref.[30]

In my previous work,[30] it was designed a novel strategy to ultrasensitive and highly selective detection of TNT explosives by formation of a charge transfer TNT-PABT (p-aminobenzenethiol) suprachromophore complex on a top-closed flexible silver nanotube array. Raman hot spots can spontaneously form in a reversible way by the self-approaching of flexible nanotubes driven through the capillary force of solvent evaporation. Meanwhile, the PABT-TNT-PABT bridges between self-approaching silver nanotubes possibly form by the specific complexing and zwitterion interactions, and the

resultant chromophores can absorb the visible light that matches with the incident laser and the localized surface plasmon of a silver nanotube array. The enhancement effect is repeatedly renewable by the reconstruction of molecular bridges and can selectively detect TNT with a detection limit of $1.5 \times 10^{-17}$ mol/L (M) (Figure 1.19).

# 1.6 Detection of bacteria based on label-free SERS

Up to now, most of bacterial SERS sensors developed are based on two principal approaches (Figure 1.20). One is indirect detection of bacteria through the Raman signals of labeled molecules, such as dyes and thiol compounds, which are connected to SERS-active particles (SERS tags).[84] This method is similar to fluorescence technique. Normally, SERS tags are made by coating a SERS-active particle (AgNPs or AuNPs) with a Raman-active molecule (Raman reporter) that has a strong and unique Raman spectral fingerprint and then encapsulate it in silica. Then the SERS tags are attached to the surface of bacteria or transferred inside the bacteria by immuno-diagnostic assays.[85] The other approach is a label-free method, which is based on the direct recording of the Raman signals specific to bacteria by using the enhancement of the cell components fingerprint.[86] Label-based techniques do not exploit the high selectivity in bacteria distinction and require for larger reactant volumes and additional preparation steps, which greatly diminishes their efficiency.[87,88]

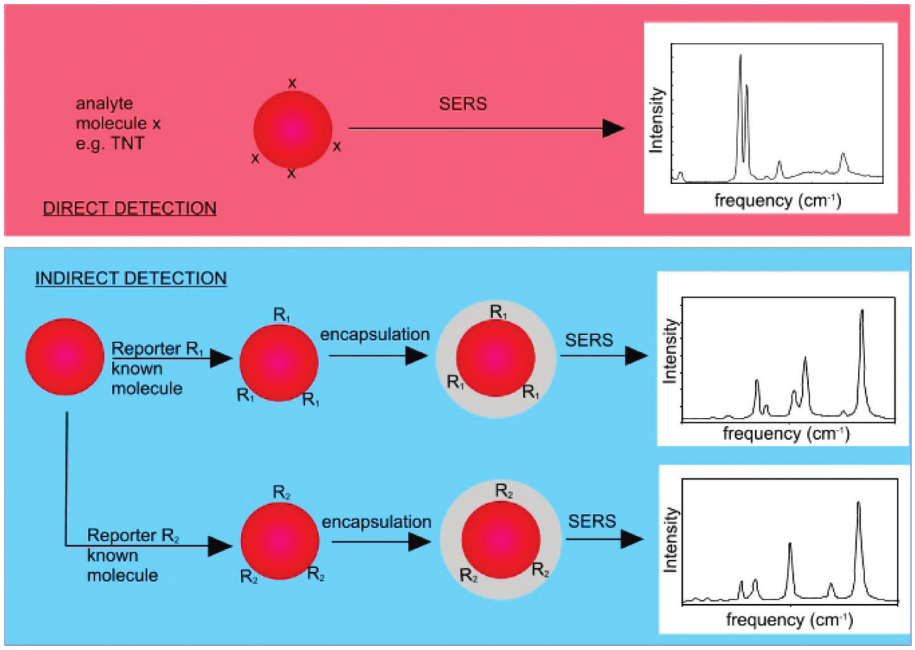


**Figure 1.20** Illustration demonstrating methods used for direct detection via SERS-label-free method (top panel) and preparation of labels for SERS-based indirect detection-label method (bottom panel). Reprinted from ref.[89]

In recent label-free bacterial SERS experiments, mostly suspensions of either colloidal gold (AuNPs) or silver nanoparticles (AgNPs) of various shapes, or particle aggregates, induced by inorganic salt, were employed to generate the SERS effect, by mixing with the bacterial cells.[90-93] While mixing is a common approach for SERS detection of bacteria (owing to its easier and faster procedure), the generated mixture is not always homogeneous.[91,94] There are no specific interactions between the bacteria and NPs. Additionally, the capping reagent employed for stabilizing the NPs prohibits intimate contact with bacteria. The inefficient interaction of NPs with the bacterial cell wall resulted in a limited reproducibility of bacterial SERS spectra. This limitation can be overcome either by increasing the NP concentration[90,95] or by the "convective assembly" method,[96] but these methods often have poor reproducibility due to the difficulty posed by efficient, precise control of the NP aggregation process on the bacteria. Thus, the main goal is that the NPs could come into contact with the bacteria surface at as many points and close as possible.[90]

Recently, an electrostatic attraction force strategy for efficient, precise self-assembly NPs on bacteria has been developed.[36,97,98] It is based on the fact that bacteria wall is

negatively charged for the presence of either teichoic acid in Gram-positive bacteria,[97] or the outer membrane lipopolysaccharides in Gram-negative bacteria.[99] The positive charged poly (L-lysine) coated AuNPs,[98] cetyltrimethylammonium bromide (CTAB)-terminated nanorods[97] and poly (allylamine hydrochloride) (PAH)/AuNPs/PAH layer by layer (LbL) structures[36] allow the highly efficient and precise deposition of NPs onto the bacterial cell wall through electrostatic interaction. However, all these methods have either a complicated procedure or fail to provide reliable results for real samples, no actual SERS experiments are realized; furthermore, they probably have the potential to create interfering SERS signals of the capping reagents.[36]

Therefore, there has always been a strong drive to develop a rapid, simple, and efficient method to deposit NPs on the bacterial cell wall for SERS application. Until now, Efrima's group has developed a method to directly produce NPs in the presence of the bacteria.[26,93,100,101] They can direct the production of the NPs to either intimate contact at external (cell wall) or interior components of bacteria.[26] Although this procedure ensures an intimate contact of the colloids with the cell, the authors obtained very similar spectra for different species of silver-coated bacteria, which makes the method unsuitable for bacteria discriminating. Furthermore, they do not deeply discuss the formation mechanism and the direct influence of this synthesis methodology. A literature survey shows that there is only one additional paper from another group concerning in situ preparation of NPs on the surface of bacteria for SERS application.[37] So, in addition to a more straightforward and efficient synthesis of NPs on the surface of bacteria for SERS application in real-world samples, a more clear interaction mechanism of the NPs with bacteria should also be addressed.

In this thesis, we report on an in situ synthesis of AgNPs coating on the cell wall of bacteria for SERS-based label-free analysis of bacteria in drinking water. With such novel coating method, first, we can detect and discriminate different kinds of bacteria, including Gram-positive and Gram-negative bacteria. Second, detection of bacteria on a microarray

at single cell level was successfully achieved by SERS. Third, we can discriminate single live and dead bacterium and counting live and dead bacteria by SERS mapping.

# 2 Experiment Section

# 2.1 Chemicals and other Materials

## 2.1.1 Chemicals

The following chemicals and solvents were used without further purification if not otherwise stated.

3-glycidoxypropyltrimethoxysilane (GOPTS, Sigma-Aldrich, Taufkirchen, Germany)

Ammonia ($NH_4OH$, 25%, Sigma-Aldrich, Taufkirchen, Germany)

Casein (Sigma-Aldrich, Taufkirchen, Germany)

Dimethylaminopyridine (DMAP, Sigma-Aldrich, Taufkirchen, Germany)

Dimethylformamide (DMF, Sigma-Aldrich, Taufkirchen, Germany)

Di(N-succinimidyl)-carbonate (DSC, Sigma-Aldrich, Taufkirchen, Germany)

Ethanol ($C_2H_5OH$, Sigma-Aldrich, Taufkirchen, Germany)

Hydrochloric acid (HCl, 37%, Sigma-Aldrich, Taufkirchen, Germany)

Hydroxylamine hydrochloride ($NH_2OH \cdot HCl$, Sigma-Aldrich, Taufkirchen, Germany)

Methanol ($CH_3OH$, Sigma-Aldrich, Taufkirchen, Germany)

Pluronic F 127 (Sigma-Aldrich, Taufkirchen, Germany)

Silver nitrate ($AgNO_3$, Sigma-Aldrich, Taufkirchen, Germany)

Sulfuric acid ($H_2SO_4$, 98%, Sigma-Aldrich, Taufkirchen, Germany)

Sodium azide ($NaN_3$, Sigma-Aldrich, Taufkirchen, Germany)

Sodium carbonate ($Na_2CO_3$, Sigma-Aldrich, Taufkirchen, Germany)

Sodium choride (NaCl, Sigma-Aldrich, Taufkirchen, Germany)

Sodium hydroxide (NaOH, Sigma-Aldrich, Taufkirchen, Germany)

Sodium hydrogen carbonate ($NaHCO_3$, Sigma-Aldrich, Taufkirchen, Germany)

Trehalose (Sigma-Aldrich, Taufkirchen, Germany)

Triethylamine (Sigma-Aldrich, Taufkirchen, Germany)

Trimethoxy(propyl)silane ($CH_3CH_2CH_2Si(OCH_3)_3$, Sigma-Aldrich, Taufkirchen, Germany)

## 2.1.2 Biochemicals

*E. coli DSM 498/1116/5695* shock frozen strains and were purchased from DSM nutritional products (Grenzach, Germany).

*Staphylococcus epidermidis 61741 (S. epidermidis)* was supported by Max-von-Pettenkofer-Institute, Ludwig-Maximilians-University.

Anti-*E. coli* antibodies (pAB rabbit, Biotin Conj. Cat#1007) were ordered from KPL Inc. (Gaithersburg, MD-USA).

## 2.1.3 Materials

Activation of glass slides, cleaning steps and hydrophobic procedure were performed in plastic containers from Carl Roth.

Cuvette (UV-vis) Rotilabo®, PMMA, 10 mm, 280 - 800 nm (Carl Roth GmbH Karlsruhe, Germany).

Diamino-PEG 2000 Da (Jeff-Amine) was a gift from Huntsman Holland (Rozenburg, The Netherlands).

Glass slides (26 mm × 76 mm × 1 mm) were purchased from Carl Roth (Karlsruhe, Germany).

Hellmanex solution was purchased from Hellma (Muellheim, Germany).

Microtiter plate BD-Falcon™ 384 well, PP, low binding, flat bottom (VWR International Darmstadt, Germany).

Milli-Q water (18.2 MΩ cm) was produced using Millipore water purification

system.

Stealth solid pin SNS 9 (ArrayIt BioRad Laboratories GmbH, Munich, Germany).

Syringes 10 mL steril PP/PE (Carl Roth GmbH, Karlsruhe, Germany).

### 2.1.4 Buffers

**Phosphate buffered saline (PBS buffer, pH 7.6, 1L, 200 mM)**

3.40 g (25 mM) $KH_2PO_4$

30.50 g (175 mM) $K_2HPO_4$

21.25 g (362.5 mM) NaCl

were dissolved in 1 L Milli-Q water.

The other concentrations of PBS buffers (0.1, 1, 10, 80, 100 mM) were diluted from this bulk PBS buffer (200 mM).

**Carbonate buffer (pH 9.6, 1L)**

0.20 g (31 mmol) $NaN_3$

1.59 g (15 mmol) $Na_2CO_3$

2.93 g (35 mmol) $NaHCO_3$

were dissolved in 1 L Milli-Q water.

## 2.2 Instruments

Autoclave, Laboklav 55MV-FA (SHP Steriltechnik, Magdeburg).

Centrifuge Universal 320R (Hettich, Tuttlingen, Germany)

Flow-cytometer Cell LabQuanta$^{TM}$ SC Flow Cytometer (Beckman Coulter, Krefeld, Germany)

ICP-MS (Perkin-Elmer SCIEX ELAN 6100, PerkinElmer Inc.)

Incubator (Binder, Tuttlingen, Germany)

Incubator B 290 (Heraeus, Hanau, Germany)

Microplate shaker EAS 2⁄4 (SLT Labinstruments, Crailsheim, Germany)

pH meter SG2 (Mettler-Toledo, Giessen, Germany)

Pipets Eppendorf Research Plus (100 - 1000 µL, 10 - 100 µL, 0.5 - 10 µL) and Multipette (2 - 5 mL) (Eppendorf, Hamburg, Germany)

Raman microscope (LabRAM HR, HORIBA Scientific, Japan)

Scales Mettler PB3000 Delta Range (Mettler-Toledo, Giessen, Germany)

Scales Sartorius (Sartorius, Göttingen, Germany)

Spotter (BioOdyssey Calligrapher Mini Arrayer BioOdyssey Munich, Germany)

TEM JEM 2010 (LaB6 cathode, JEOL GmbH Munich, Germany)

Ultrapure water purification system (Milli-Q plus 185 Millipore Schwalbach, Germany)

Ultrasonic bath Sonorex RK 102 (Bandelin, Berlin, Germany)

UV-vis spectrometer, Photometer Specord 250 plus (Analytik Jena, Jena, Germany)

Vortexer, Top Mix FB15024 (Fisher Scientific, Pittsburg, USA)

Zeta potential, Zetasizer Nano ZS (Malvern Instrument Ltd. Worcestershire, UK)

# 2.3 List of Experiments

## 2.3.1 Microorganisms preparation

Shock-frozen *E. coli DSM 498/1116/5695* cells were cultivated in LB medium (Lennox) (100 mL in 250 mL flasks) in gyratory shaker at 100 rpm and 37 °C for 16 h. 10 mL of bacteria were harvested and washed twice in $H_2O$ (“Bacteria($H_2O$)”) or PBS (“Bacteria(PBS)”) by centrifugation at 4500 rpm and 4 °C. Then the bacteria were stored in refrigerator at 4 °C for further use. Preparation of *S. epidermidis* 61741 was obtained from the strain collection of the Max-von-Pettenkofer-Institute, Ludwig-Maximilians-

University. Prior to analysis, all cell suspensions were diluted in PBS or $H_2O$ to reach the desired concentrations. The stock cell concentration of *E. coli* was determined by flow-cytometry using SYTO9.

## 2.3.2 Zeta potential measurement

The zeta potential of *E. coli DSM 1116* in water and PBS was measured by dynamic light scattering with Zetasizer Nano ZS (Malvern Instrument Ltd. Worcestershire, UK), equipped with a glass electrophoresis cell. The concentrations of *E. coli DSM 1116* were $1 \times 10^8$ cell/mL; no pH adjustment was carried out. These parameters were consistent for all the following reported measurements.

## 2.3.3 Glass slides hydrophobic treatment

**Cleaning**

The normal glass slides were put in a chip reservoir containing 2 % Hellmanex solution and left 1 h in ultrasonic bath to rinse. Subsequently, the chips were put on a shaker overnight (15 h) at room temperature followed by an additional hour in ultrasonic bath. The treated slides were thoroughly washed five times in 200 mL Milli-Q water and dried under nitrogen flow. The prepared glass slides were dipped in 200 mL of methanol/hydrochloric acid solution (1:1) and left shaking for 1 h at room temperature. A washing step in water followed, where the chips were rinsed five times in 200 mL Milli-Q water. Subsequently, they were submerged in concentrated sulfuric acid and left shaking for 1 h at room temperature. An additional washing step in water followed and the slides were again dried under a nitrogen flow.[21]

**Hydrophobic treatment**

The cleaned slides were put in a chip reservoir containing 150 mL methanol and 150 mL water mixed solution under magnetic stirring, then 2 mL trimethoxy(propyl)silane was added dropwise, then following by addition of 3 mL 25% ammonia. The solution was

stirred overnight. Finally, the chips were thoroughly washed five times in 300 mL absolute ethanol and the slides were again dried under nitrogen flow.[111]

## 2.3.4 Microarray preparation

The microarray preparation consists of two separate steps, the chip coating and the subsequent antibody spotting on the chip.

**Chip coating**

The microarray chip was prepared following a coating procedure developed by Wolter et al. on glass slides.[21] Glass slides are chemically and physically stable and exhibit negligible background signals for optical measurements. The produced amino-modified glass surfaces are highly homogeneous and have a high binding efficiency. Activation is achieved by a two-step procedure. Step one consists of the substitution reaction of an alcohol by a silane. Silanization is carried out on a glass slide activated with acid by the organosilane GOPTS. The second step consists of the nucleophilic ring-opening reaction of oxacyclo propane. A poly(ethylene glycol) (PEG)-diamine is then reacted with the surface. The configuration at the steric center is maintained as it does not take part in the reaction. As a silanized surface often possesses hydrophobic properties, this final step consisting of PEG functionalization is important. After the immobilization of haptens on the amino-PEG modified surface, remaining active amino sites are deactivated by casein to prevent unspecific binding.

*Substrate pretreatment.* Conventional glass slides were first carved on one edge with a diamond carver (*Proxxon NG 2/S*) in order to recognize on which side a coating had been carried out. Then the glass slides were put in a chip reservoir containing 2 % Hellmanex solution and left 1 h in ultrasonic bath to rinse. Subsequently, the chips were put on a shaker overnight (15 h) at room temperature followed by an additional hour in ultrasonic bath. The treated slides were thoroughly washed five times in 200 mL Milli-Q water and dried under nitrogen flow. The prepared glass slides were dipped in 200 mL of methanol/hydrochloric acid solution (1:1) and left shaking for 1 h at room temperature. A

washing step in water followed where the chips were rinsed five times in 200 mL demineralized water. Subsequently, they were dipped in concentrated sulfuric acid and left shaking for 1 h at room temperature. An additional washing step in water followed and the slides were again dried under nitrogen flow. Hereafter, the carved side of the chips were lied facing down in a petri-dish.

*Silanization.* At room temperature, 600 µL GOPTS was added to each slide and covered with a second slide with the carved side facing upwards forming a sandwich. After one hour the chips were separated carefully by hand and covered in 200 mL ethanol in which the slides were left for 1 h to rinse in an ultrasonic bath. The ethanol was exchanged with 200 mL methanol and the set of slides were left a following hour in ultrasonic bath. Finally, the rinsing step in ethanol was repeated followed by a drying under nitrogen flow.

*PEG layer preparation.* 10 g diamino-PEG was molten in a beaker at 98 °C. 600 µL was pipetted over the silanized side of the glass chips which again were covered with other silanized glass chips as sandwiches. The PEG-ylation was carried out 15 h at 98 °C in closed petri-dishes. Still hot slides were dipped in 200 mL Milli-Q water and left in an ultrasonic bath for 15 min and additionally rinsed with fresh Milli-Q water. A final drying step in nitrogen flow was carried out. The chips were stored at room temperature in a desiccator under inert atmosphere.

**Antibody immobilization**

The method for antibody immobilization also follows a procedure presented earlier.[22] Briefly, prior to the antibody immobilization, N-hydroxysuccinimide (NHS) activation was carried out on the amino PEG-ylated glass chips (4 h). A total of 600 µL of a solution of 80 mg (0.31 mmol) of DSC, 4 mg (0.03 mmol) of DMAP, 1.6 mL of absolute DMF, and 125 µL of triethylamine were added to two PEG-ylated chips using a sandwich technique. The activated chips were cleaned in MeOH two times for 10 min in an ultrasonic bath. Subsequently, the chips were dried under $N_2$ atmosphere. In order to

prevent denaturation of the spotted antibodies, a solution of Pluronic F 127 and 10% trehalose in PBS was prepared as an antibody stabilizer. This solution keeps the spots hydrated throughout the entire incubation time of 15 h. Also, an uneven spreading of the spots was prevented with the aid of 0.005% Pluronic F 127 which acts as strong protein structure stabilizer. The individual spotting solution, containing 1.0 g/L anti-E. coli antibodies, was pipetted into cavities of a 384-well microtiter plate. Antibody solution was spotted by a contact spotter (BioOdyssey Calligrapher miniarrayer, Bio-Rad, Munich, Germany). A solid pin (SNS 9, TeleChem Stealth, Perkin Elmer GmbH, Germany) was used to create a spot of 1 nL sample volume with a diameter of ~400 µm. The spotting procedure was carried out at 50% humidity and 15 °C plate temperature. After incubation at 20 °C for 15 h in Petri-dishes containing 200 µL of $H_2O$, the chip surface surrounding the spots was inactivated in 2% casein in PBS by vortexing for 1 min 45 sec and left shaking at room temperature (RT) in 2% casein in PBS for 5 h. The chips were finally cleaned in water and PBS. Storage of the chips is possible for several weeks in PBS containing 0.1% $NaN_3$ at 4 °C without degradation.

## 2.3.5 Conventional silver nanoparticle preparation

As a reference, standard silver nanoparticles (AgNPs) were synthesized as used in earlier experiments.[86,113,115] The preparation follows a modified procedure of Leopold and Lendl.[123,124] Briefly, 17 mg (0.1mmol) $AgNO_3$ were dissolved in Milli-Q water (10 mL). 100 mL of 11.6 mg (0.17 mmol) $NH_2OH{\cdot}HCl$ solution containing 3.3 mL NaOH (0.1 M) was prepared and divided in 9 mL batches in centrifuge tubes. To the reducing agent, 1 mL of $AgNO_3$ was added in a flow rate of 0.67 mL $s^{-1}$ without stirring. Finally, the centrifuge tube was inverted once to complete the mixing. The size distribution of silver colloid suspension was tested using a UV-vis spectrometer and TEM (procedure details are described later). The yellow/greenish colloid sols were stored in the dark at 4 °C.

## 2.3.6 Bacteria-AgNPs preparation

Before any further processing, a volume of 1 mL of the sample was centrifuged at 4500 rmp for 10 min and the supernatant was discarded. Further sample treatment varies depending on the kind of SERS colloids used and is discussed in the following.

**In suspension**

A 1 mL sample liquid was centrifuged at 4500 rpm, the supernatant was discarded, was further added to 1 mL of prepared AgNPs and then vortexed to ensure homogeneity. Subsequently, we pipetted 10 µL of 1 M NaCl into the prepared mixture as agglomerating agent. The final concentration of NaCl was 0.01 M. The resulting hybrid bacterial suspension is designated as Bacteria-AgNPs.[12]

**On microarray**

For microarray-analysis, the centrifugate was resuspended in 1 mL PBS then incubated for 1 h on the antibody-spotted glass chip. In order to eliminate unspecifically bound microorganisms, the chip was thoroughly washed in PBS. The chip was then placed in a polycarbonate tray which was filled with AgNPs containing 0.03 M NaCl.[86]

## 2.3.7 Bacteria@AgNPs preparation

**In suspension**

Again, 1-mL sample liquid was centrifuged at 4500 rpm and the supernatant was discarded. 100 µL 10 mM $AgNO_3$ solution were added, the mixture was vortexed and then, an interaction time of 5 min was allowed. Subsequently, 900 µL $NH_2OH{\cdot}HCl$ solution were pipetted into the prepared mixture and the mixture was again vigorously vortexed. Finally, we stored the suspension in the dark at 4 °C until they were analyzed. The resulting hybrid bacterial suspension is designated as Bacteria@AgNPs. In detail, the water-washed *E. coli* are called Bacteria($H_2O$)@AgNPs, and the different concentrations of PBS-washed *E. coli* are called Bacteria(PBS)@AgNPs. The same procedure was used for *S. epidermidis*.[12]

**On microarray**

As for the microarray analysis by the simple mixing approach, the sample preparation for the Bacteria@AgNPs consisted of two steps. First, the sample, again resuspended in PBS buffer, was incubated for 1 h on the coated glass chip and then the chip was washed first with PBS and then with water. Then, 1.0 mL 10 mM $AgNO_3$ solution was added, incubated for another 30 min inside a polycarbonate tray. After that, 9 mL $NH_2OH \cdot HCl$ solution was added to the $AgNO_3$ solution and the tray was shaken for 5 min. The procedure is shown in Figure 2.1.

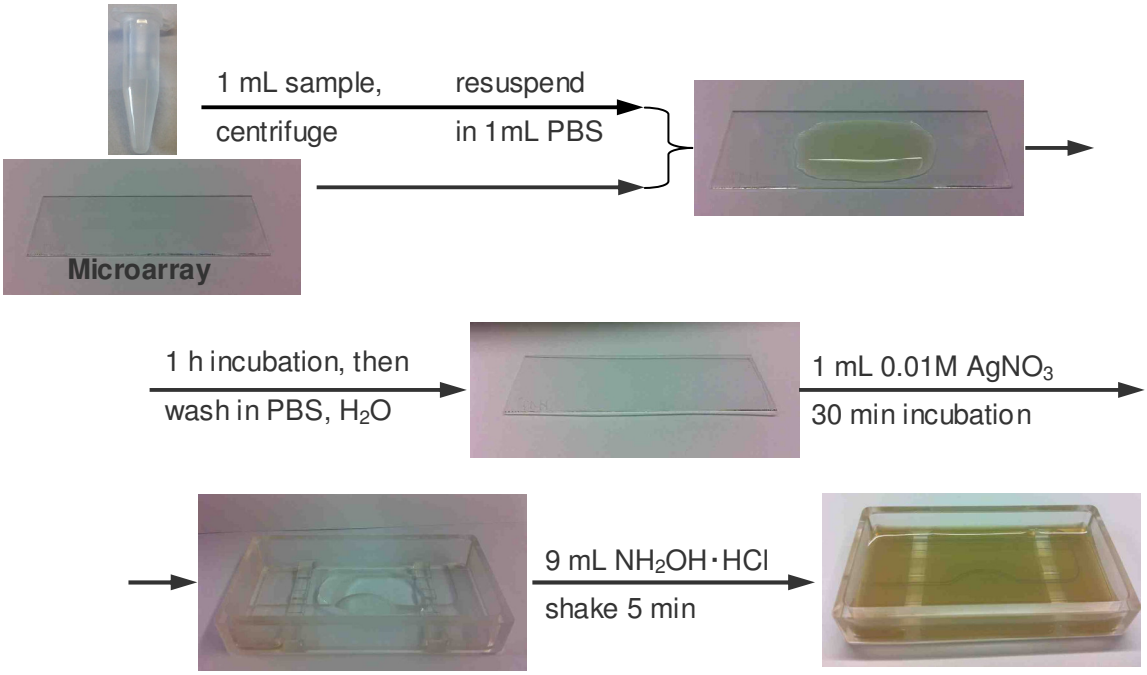


**Figure 2.1** Experimental procedures for the in situ synthesis of Bacteria@AgNPs for SERS detection of bacteria on a microarray.

# 2.4 SERS measurements

## 2.4.1 SERS detection of bacteria in suspension

3 μL sample suspension, already treated with the different colloid preparations, was pipetted onto the normal glass slides. The recording of the Raman spectra was started right after this sample preparation, using the 633-nm line of a He-Ne with 14 mW power at the sample and a 10× objective. The Raman spectra were continuously (one spectrum

every 40 s) collected with the auto repeat function until the droplet was dried. If not explicitly stated, the exposure time was 1 s and and the accumulation number was 10, respectively, and the confocal slit width was 100 μm, detecting a spectra region of 50 to 3000 $cm^{-1}$.

## 2.4.2 SERS mapping on glass slides

A droplet of 3-μL sample suspension was added on the hydrophobic glass slides, and then dried at room temperature. If not explicitly stated, all SERS mapping data were obtained by using the 633-nm He-Ne laser line with 1.4 mW power and a 50× objective. The exposure time was 1 s and the accumulation number was 5, and the slit width was 100 μm, detecting a spectra region of 50 to 2000 $cm^{-1}$. The mapping area is 40 μm × 40 μm with step size of 2 μm. 441 Raman spectra were collected for each map.

## 2.4.3 SERS detection of bacteria on microarray

SERS spectra were obtained with a Raman microscope (LabRAM HR, HORIBA Scientific, Japan) with three different laser sources (532 nm 30 mW max. power at sample; 633 nm, 14 mW; 785 nm, 55 mW) and a 10× objective. If not explicitly stated, the exposure time was 1 s and the accumulation number was 10, the slit width was 100 μm, and the recorded spectral region is 50 to 3000 $cm^{-1}$. Each sample was measured at least three times. Wavelength calibration was performed by measuring a silicon wafer surface through a 50× objective, evaluating the first-order phonon band of Si at 520.7 $cm^{-1}$.

# 3 Results and Discussion

# 3.1 SERS detection of bacteria in water

## 3.1.1 Dynamic SERS

For the analysis, a new SERS detection method was used. It is called dynamic surface-enhancement Raman spectroscopy and has been demonstrated to enhance the signals of analytes in comparison to the traditional methods by several orders of magnitude.[102,103] The approach is straightforward and reliable: right after dropping 3 μL of Bacteria@AgNPs solution on the glass slides, Raman spectra are recorded continuously at an interval of 40 s until the droplet is dried. In the course of the droplet drying, the SERS signal of the bacteria gradually increases, with the 17$^{th}$ spectrum (after ~ 680 s) reproducibly yielding the highest intensity. Afterwards, the signal suddenly decreases and fluorescent background appears after the water evaporation was completed. The results are shown in Figure 3.1.

A tentative explanation of this phenomenon could be that the interparticle distance of Bacteria@AgNPs becomes reduced due to the capillary force during solvent vaporization. During the initial drying, which leads to droplet shrinking, a great number of hot spots are generated by the decreasing interparticle distance of Bacteria@AgNPs, which drives the initially separated Bacteria@AgNPs nanostructures to self-assembly into clusters. However, cluster growth is limited by the increasing electrostatic repulsion of the cluster. The equilibrium short-range attraction and long-range Coulomb repulsion determines a finite aggregation number.[102] At the final stage, when the droplet is dried, the hot spots disappear; probably due to the formation of very big clusters. The Raman results obtained by using this approach are highly reproducible and reliable. The reproducibility of this dynamic SERS approach for bacteria characterization, based on the evaluation of the seventeenth spectrum, is demonstrated by the analysis five different sample batches of $1\times10^8$ cell/mL *E. coli DSM 1116* (water-washed, see Figure 3.2).

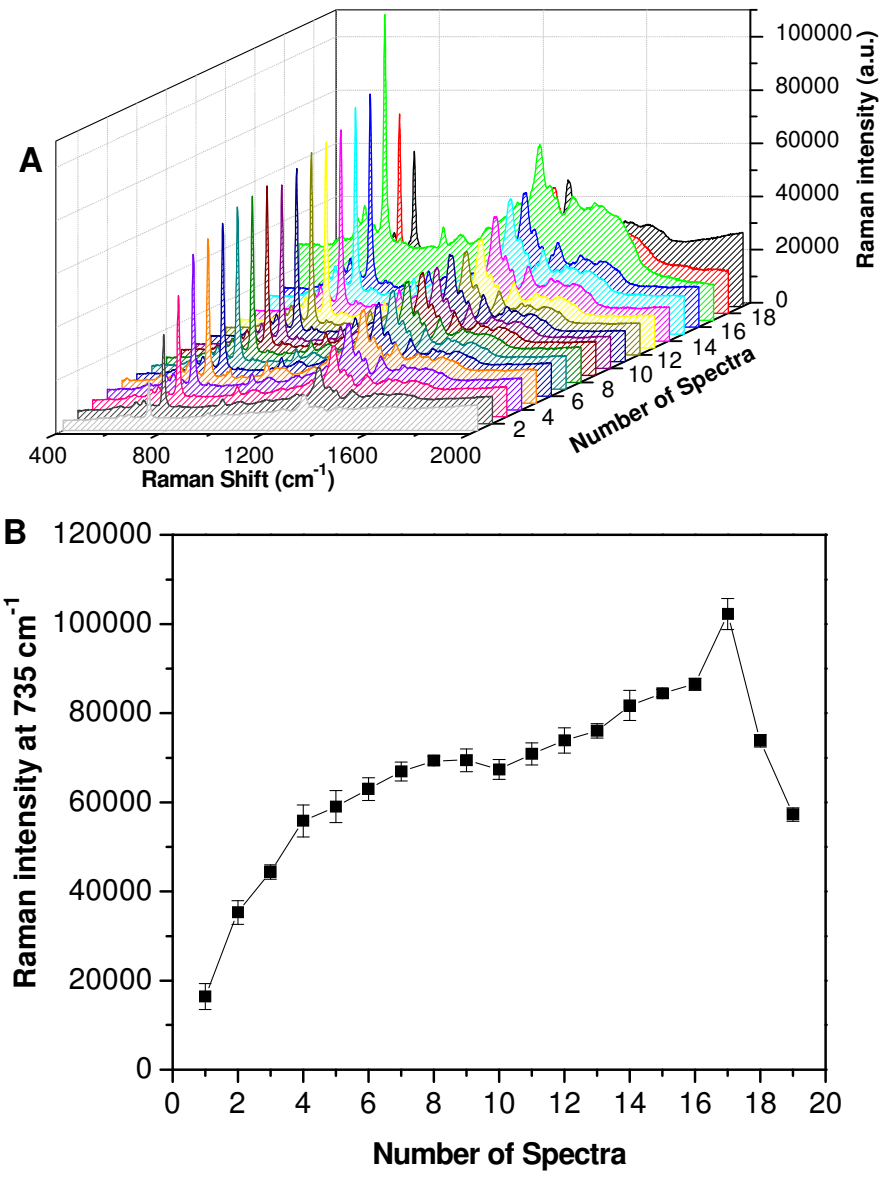


**Figure 3.1** (A) Example of time-resolved SERS spectra of $1 \times 10^8$ cell/mL Bacteria($H_2O$)@AgNPs at the interval of 40 s after dropping 3 µL on the normal glass slides, called dynamic surface-enhanced Raman scattering. (B) Temporary evolution of corresponding Raman intensity at 735 $cm^{-1}$ based on three measurement times.

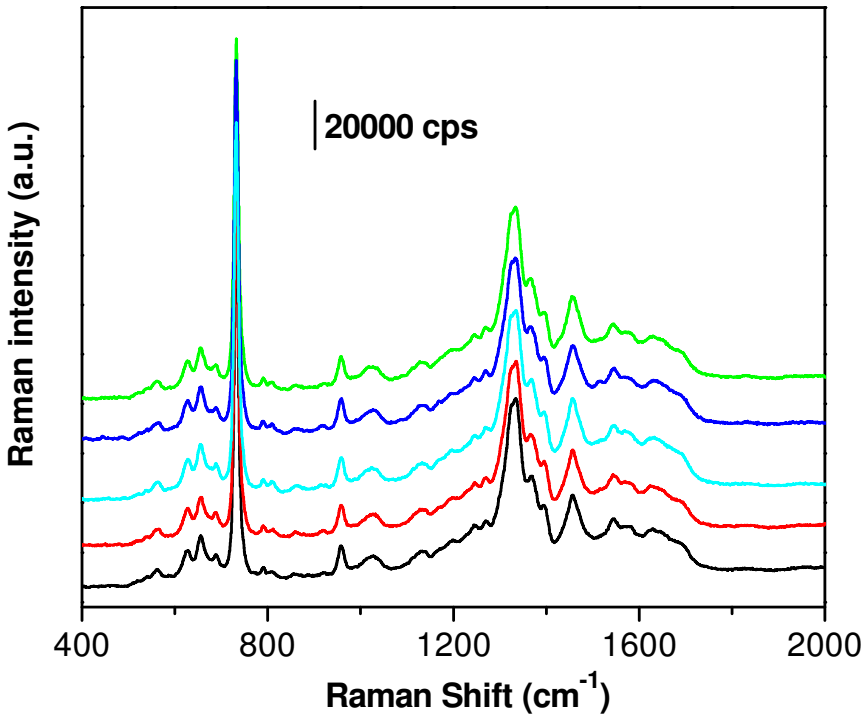


**Figure 3.2** SERS spectra of 1 × $10^8$ cell/mL *E. coli DSM 1116* in water from 5 different batches of samples, measured by dynamic surface-enhanced Raman scattering.

## 3.1.2 Colloid assessment

Figure 3.3 illustrates the *in situ* formation of AgNPs coating on the cell wall of bacteria. The resulting complexes are then detected by SERS. The bacteria cell wall is negatively charged due to the presence of either teichoic acid in Gram-positive bacteria[97] or the outer membrane lipopolysaccharides in Gram-negative bacteria.[99] Hence, the silver ions strongly adhere to the bacterial cell wall by electrostatic interaction. Silver ions can also be attached to various electron-rich binding sites of nitrogen, sulfur, or carboxylate on the cell wall of bacteria via coordination force.[100] Finally, the addition of hydroxylamine hydrochloride leads to the formation of colloid deposits on the surface of bacteria (Bacteria@AgNPs). From the TEM images, it can clearly be seen that the AgNPs are successfully synthesized around the bacterial cell wall (see Figure 3.8).

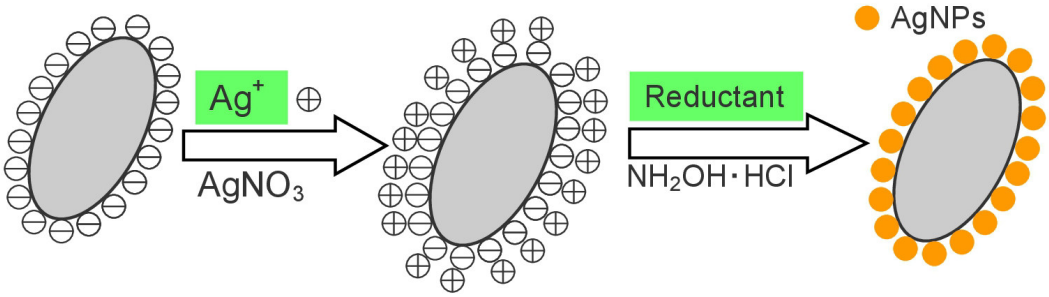


**Figure 3.3** Schema of the *in situ* synthesize of nanoparticles on the bacterial surface. The silver ions adsorbed to the bacteria cell wall by electrostatic attraction generate AgNPs on the surface of bacteria immediately after the addition of the reducing reagent.

The negative charge of the bacteria surface can be affected by a number of parameters, such as pH-value, ionic strength, and the concentration of surfactants in the suspending medium.[104-108] To assess the surface negative charge of bacteria, the bacteria were washed with different concentrations of PBS buffer; *E. coli DSM 1116* was selected as model bacteria. Firstly, we prepared different concentration of PBS solution, e.g., 0, 0.1, 1.0, 10, 80, 100 mM. Secondly, we used these prepared PBS solution to wash $1 \times 10^8$ cell/mL *E. coli DSM 1116* twice. Finally, we used these washed bacteria to measure the corresponding zeta potential (see Figure 3.4) and to prepared different Bacteria(PBS)@AgNPs samples, and finally measure the corresponding Raman spectra. As shown in Figure 3.5A and 3.5B, when the concentrations of PBS increased, the zeta potential of the cell walls became less negative, which is consistent with previous reports.[104] Correspondingly, the SERS signals of the bacteria decreased with higher PBS concentrations.

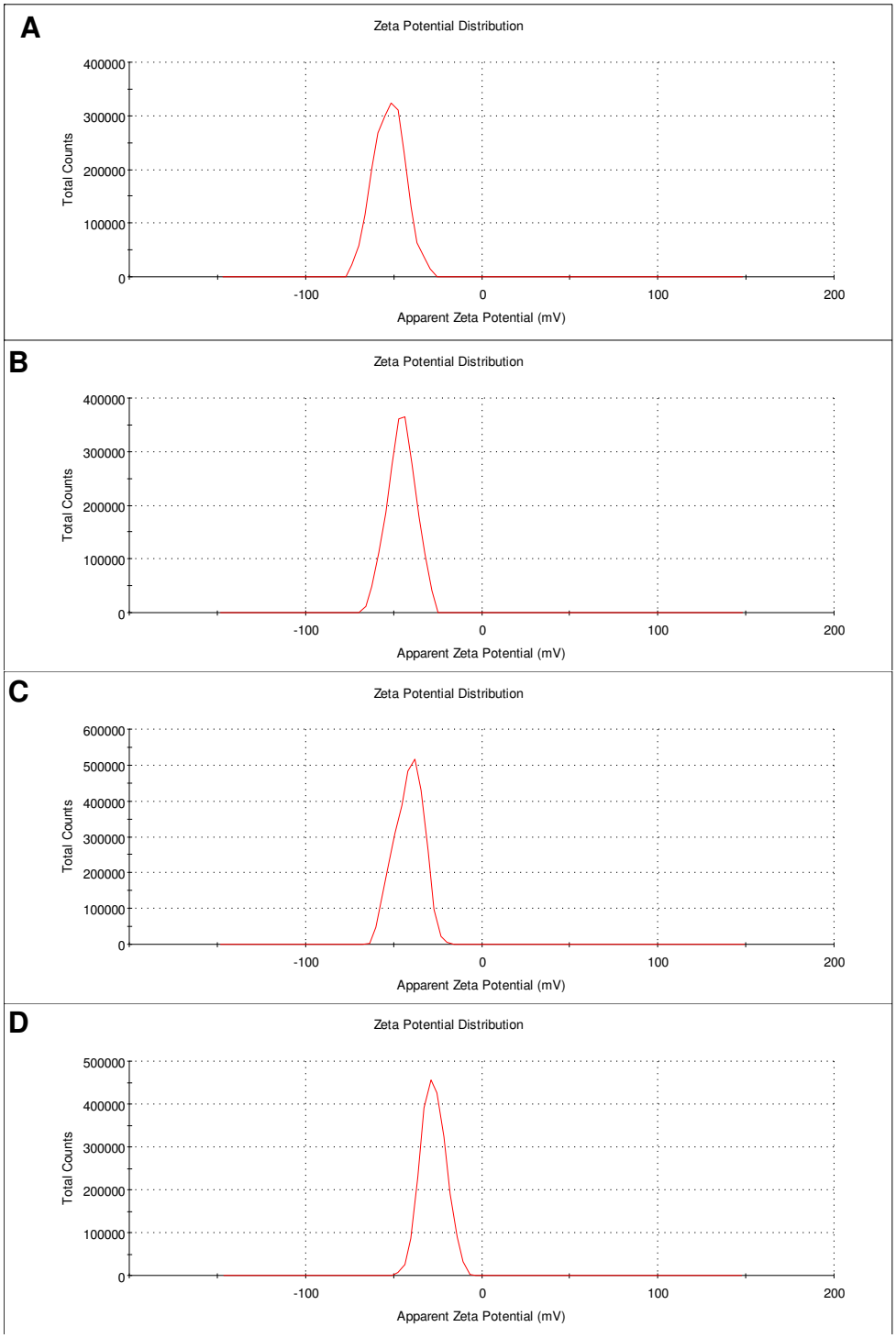


**Figure 3.4** Zeta potential of bacteria washed by 0 (A), 0.1 (B), 1.0 (C) and 10 mM (D) PBS, respectively.

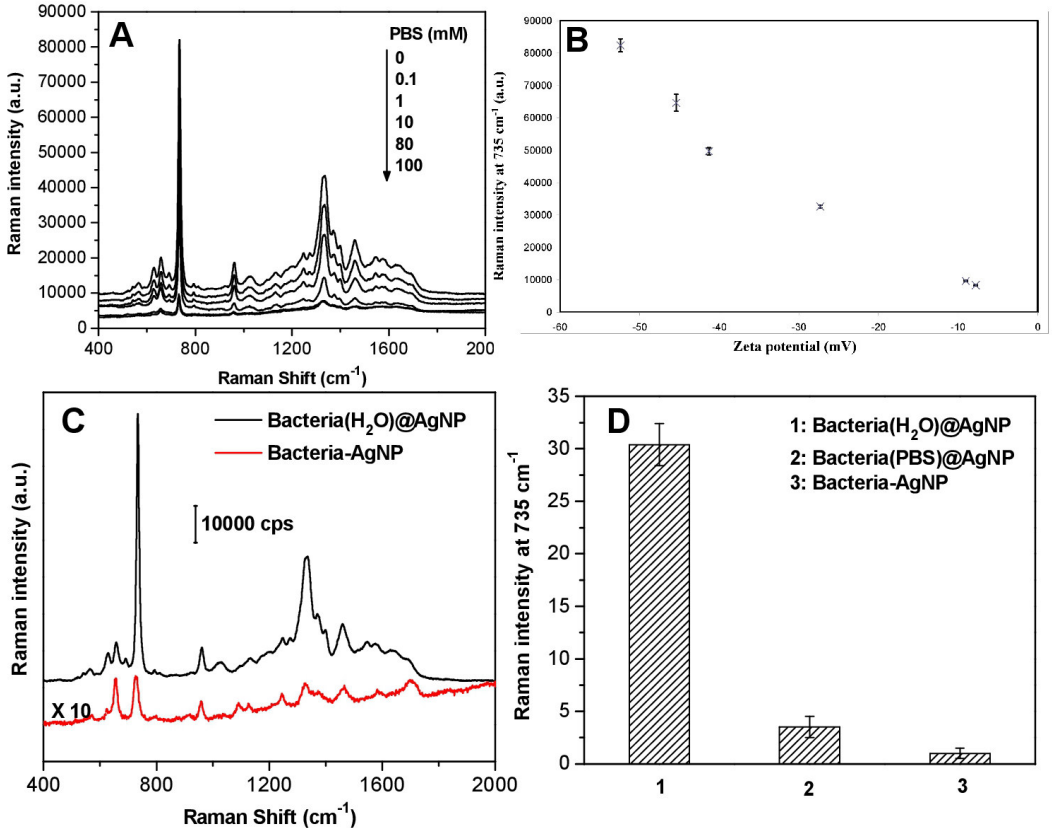


**Figure 3.5** (A) SERS spectra $1 \times 10^8$ cell/mL *E. coli DSM 1116* Bacteria(PBS)@AgNPs, washed with different concentrations of PBS. The concentrations of PBS are 0, 0.1, 1.0, 10, 80, and 100 mM, respectively. (B) Raman intensity at 735 $cm^{-1}$ vs zeta potential of the bacteria washed with different concentrations of PBS. (C) SERS spectra of bacteria obtained by two different methods. (D) Raman intensity at 735 $cm^{-1}$ for Bacteria($H_2O$)@AgNPs (0 mM PBS), Bacteria(PBS)@AgNPs (80 mM PBS), and Bacteria-AgNPs. Each sample was measured three times.

For example, the zeta potential of living *E. coli DSM 1116* ($1 \times 10^8$ cell/mL) in water (-52.4 mV) is about 6 times higher than the one in 80 mM PBS (-9.03 mV) (Figure 3.4 and Figure 3.5B). Correspondingly, the enhancement by Bacteria($H_2O$)@AgNPs (0 mM PBS) is 9±1 times higher than the one of Bacteria(PBS)@AgNPs (80 mM PBS), as assessed by the strongest vibrational band at 735 $cm^{-1}$ (Figure 3.5D). The surface charge of the bacteria in water is more negative than in PBS, which means that the surface of bacteria in water can adsorb more positive silver ions. Thus, more AgNPs will be synthesized on the surface of bacteria in aqueous suspension (see Figure 3.8D and 3.8E) and higher SERS signals of bacteria are acquired. The enhancement effects of the Bacteria@AgNPs method were further compared with the simply mixed colloid-bacterial

suspension (Bacteria-AgNPs). As it can be seen in Figure 3.5C and 3.5D, the Bacteria($H_2O$)@AgNPs feature Raman intensities about 30±2 times higher than the one of the Bacteria-AgNPs.

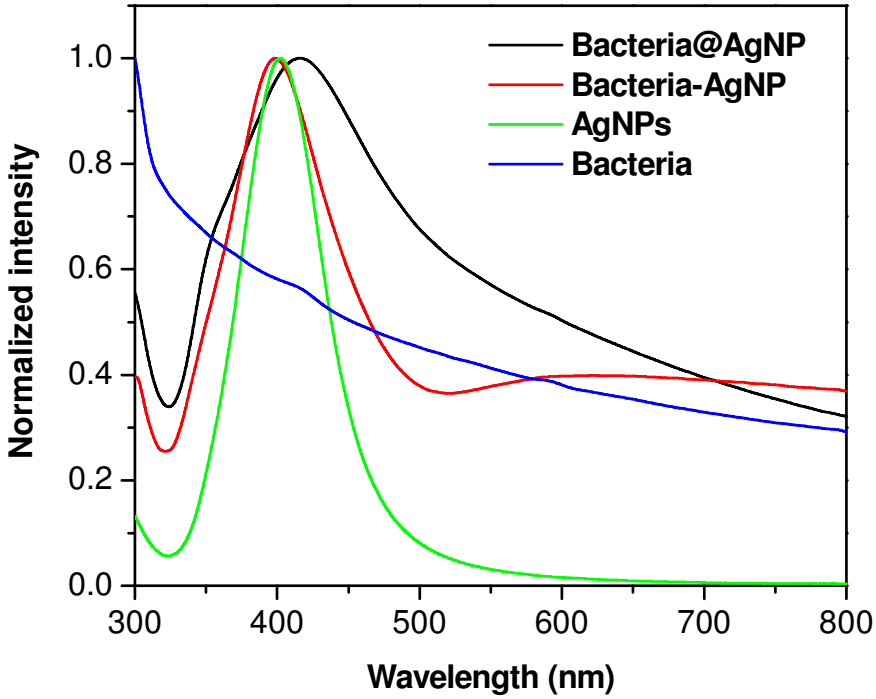


**Figure 3.6** UV-vis absorption spectra of *E. coli DSM 1116*, AgNPs, *E. coli DSM 1116* mixed with AgNPs and 0.01 M NaCl (Bacteria-AgNPs), and AgNPs coated with *E. coli DSM 1116* (water washed, Bacteria@AgNPs).

UV-vis spectroscopic characterization and TEM examination of the Bacteria@AgNPs were carried out. As shown in Figure 3.6, no distinct peaks can be observed in the UV-vis spectra of the *E. coli DSM 1116* solution. The conventional AgNPs are displayed as yellow/greenish suspension and have a narrow absorption peak at 402 nm, indicating monodisperse particles with a diameter ~30 nm (see the TEM image in Figure 3.7). The Bacteria-AgNPs display a similar main peak as the AgNPs, except that the peaks width became a little larger and a broad absorption at 600 - 700 nm shows up, which can be explained by the aggregation of AgNPs by 0.01 M NaCl. The UV-vis spectra of Bacteria@AgNPs feature a very wide absorption band at 418 nm, which is obviously red shifted compared to the one of the Bacteria-AgNPs suspension. The red shift indicates that the interparticle distance decreases and/or the size of NPs increases.

All these results indicate that the AgNPs have a different morphology and show different aggregation or assembly behavior in the Bacteria@AgNPs.

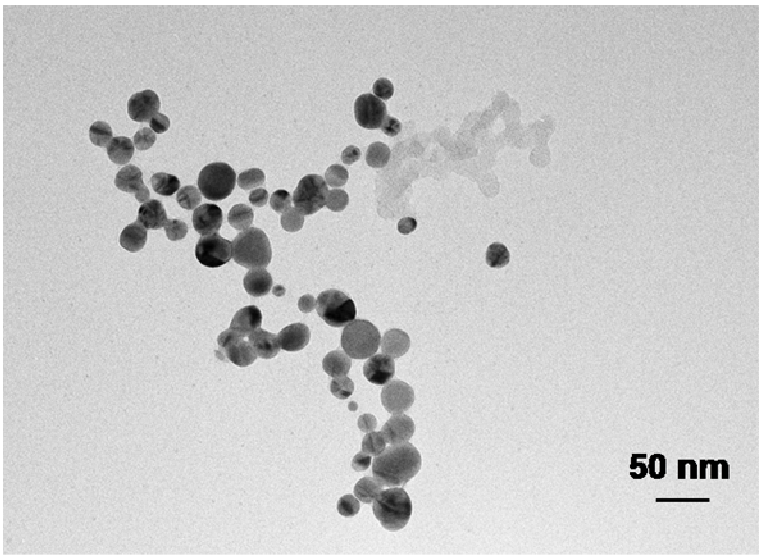


**Figure 3.7** TEM images show the size distribution of the AgNPs (mean size 30 nm).

TEM analysis was performed to further investigate the morphology of the nanostructures and the distribution of AgNPs. Figure 3.8A depicts the TEM image of $1\times10^8$ cell/mL *E. coli DSM 1116* mixed with AgNPs and 0.01 M NaCl. It can be seen that the AgNPs are randomly distributed in the solution and do not aggregate on the surface of the bacteria. Some of them are self-aggregated in the suspension owing to the aggregation reagent NaCl, but they do not adhere to the bacterial surface. The bacteria remain mostly separated. The magnified image (Figure 3.8C) reveals that the AgNPs are not intimately adhered to the cell wall of bacteria. Consequently, the cross section of the cell wall components cannot be efficiently amplified by electromagnetic field enhancement and the SERS signals of bacteria are weak. Figure 3.8B and 3.8D reveal the intimate interaction of Bacteria($H_2O$)@AgNPs with the cell walls. Most of the particles coat the bacterial surface, while only few are found unbound or clustered in the liquid phase. Figure 3.8D shows the high-magnification TEM image of Bacteria($H_2O$)@AgNPs structures. The shape of the AgNPs is irregular with a diameter of about 100 nm, which is higher than the AgNPs in "Bacteria-AgNPs"(30 nm). Some of the composites show larger, elongated structures (indicated with red arrows in Figure 3.8D), which seem to be aggregated

spontaneously, forming AgNPs cluster on the surface of the bacteria. Moreover, most of the bacteria were assembled in clusters under these conditions, generating more hot spots on the interfaces of bacteria, and consequently, stronger Raman signals. However, when bacteria were washed with 80 mM PBS, the Bacteria(PBS)@AgNPs nanostructures are very different from Bacteria($H_2O$)@AgNPs. From Figure 3.8E, we can see that there are only few relatively large AgNPs aggregates, coating only a small part of the cell wall. Most parts of the bacteria cell wall are free of AgNPs. Comparing Figure 3.8D and 3.8E, it can be seen that there are more AgNPs coating the water-washed cell than coating the PBS-washed. The formation of few relatively large AgNPs aggregates in Bacteria(PBS)@AgNPs samples can be explained by a less negative zeta potential of the cell wall in consequence of the PBS washing. Furthermore, some anions, such as $Cl^-$ (from PBS), can stimulate the formation of big AgNPs aggregated on cell wall. All these results confirm that the SERS signal intensities of the bacteria after AgNPs synthesis mainly depends on the zeta potential of cell wall.

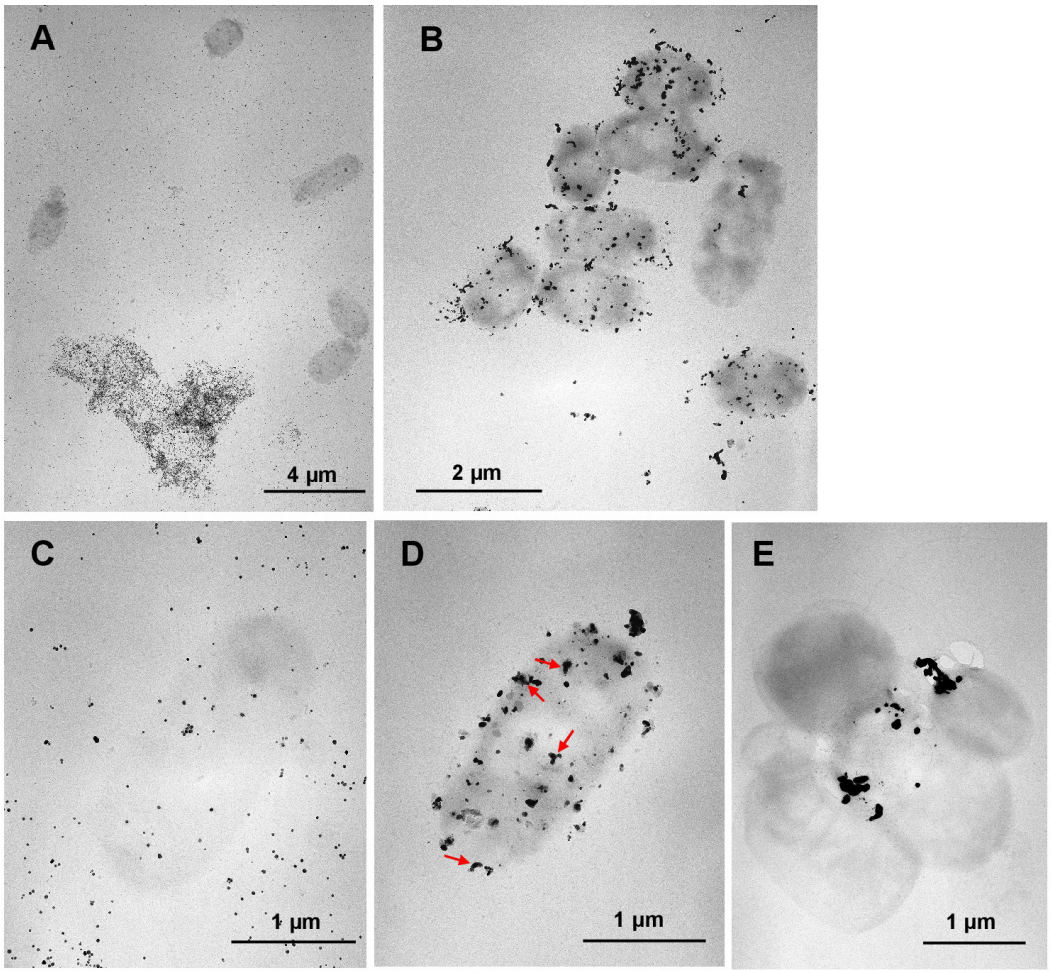


**Figure 3.8** (A) TEM image of *E. coli DSM 1116* mixed with AgNPs and 0.01 M NaCl (Bacteria-AgNPs). (B) TEM image of Bacteria($H_2O$)@AgNPs sample. (C), (D) High-magnification TEM images of (A) and (B), respectively. (E) TEM image of Bacteria(PBS)@AgNPs nanostructures (80 mM PBS).

In order to identify reasons for the strong SERS enhancement of the bacteria (the attached AgNPs on the cell surface or the free AgNPs in the suspension) and estimate the formation of AgNPs aggregated on the cell wall, the following experiment was designed:

As illustrated in Figure 3.9, firstly, a sample of 1 mL 1 × $10^8$ cell/mL Bacteria($H_2O$)@AgNPs was centrifuged with 850 g at room temperature for 5 min. Free AgNPs (diameter about 30 nm) do not sediment under such condition (such low centrifugation speed and short time), but the novel Bacteria($H_2O$)@AgNPs nanostructures can be easily precipitated, because when the bacteria are covered with some AgNPs, they become heavier. Thus, the solutions were clearly separated into two parts, the yellow supernatant and the black sediment. Subsequently, the supernatant was carefully pipetted

into another tube. In order to completely remove all free AgNPs, the sediment was washed twice by centrifugation in $H_2O$ with 850 g for 5 min (room temperature). Finally, it was filled up to 1 mL $H_2O$ for resuspension. We believe that the free AgNPs in the suspension and the Bacteria($H_2O$)@AgNPs nanostructures were successfully separated by this procedure.

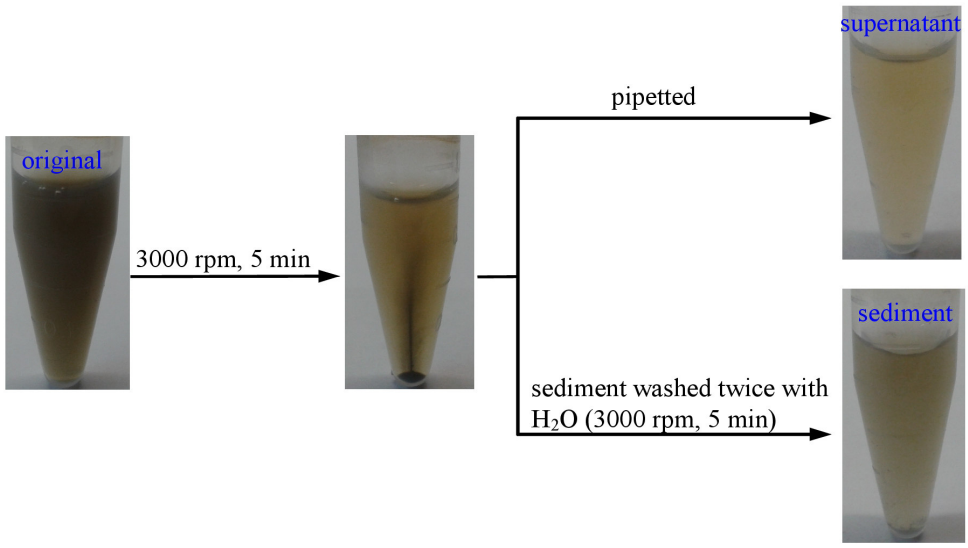


**Figure 3.9** Schematic illustration of the separation the attached AgNPs on the cell surface and the free AgNPs in the suspension.

Then we performed ICP-MS and Raman analysis of the separated materials. Table 1 shows the efficiency of $Ag^+$ reduction onto the cell wall as deduced from ICP-MS quantification. The efficiency is about 96±0.2%, which means that most of AgNPs are coating the cell wall. While the sediment makes up for only 5% (or even less) of the original volume, it contains 96% of the whole AgNPs. These results confirm that the reduction of AgNPs happens not arbitrarily, but preferentially on the cell wall.

**Table 1.** Calculation the efficiency of $Ag^+$ reduction onto the cell wall by ICP-MS

| sample | supernatant (mg/L) | sediment (mg/L) | $Ag^+$ at cell wall |
|---|---|---|---|
| 1 | 45.78 | 1280.47 | 96.55% |
| 2 | 45.43 | 1337.58 | 96.72% |
| 3 | 43.95 | 1192.93 | 96.45% |

A comparison of the corresponding Raman spectra of the supernatant and sediment in Figure 3.9 is shown in Figure 3.10.

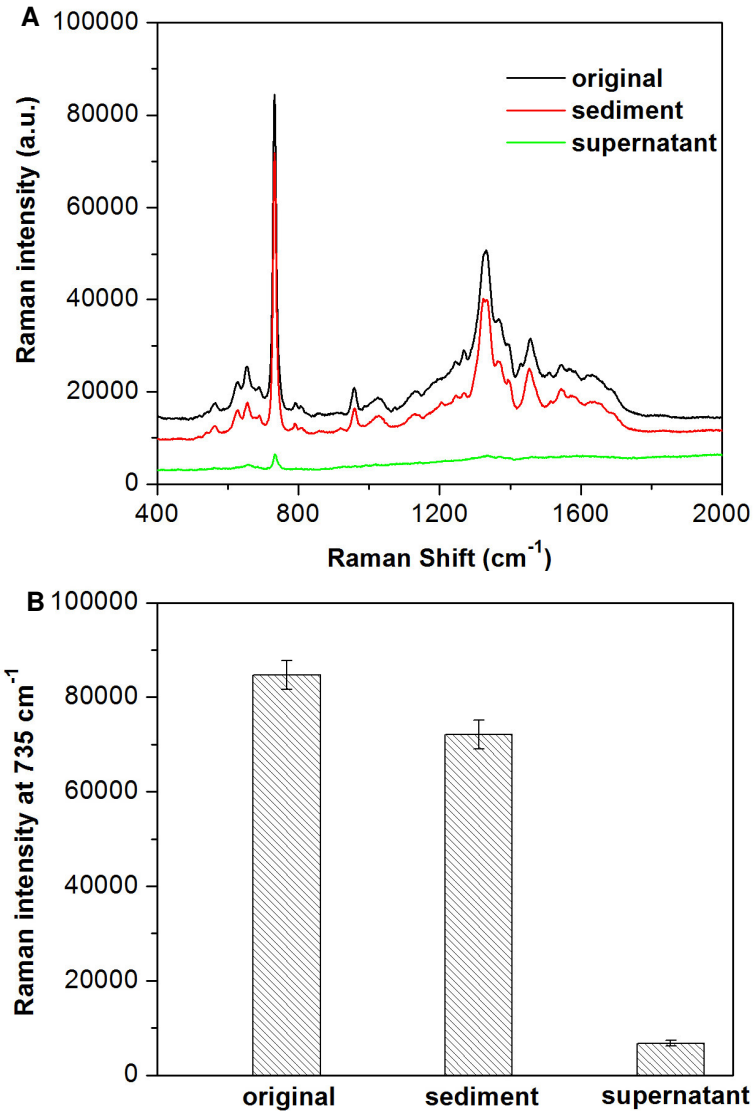


**Figure 3.10** (A) SERS spectra of original, sediment and supernatant samples in Figure 3.9. (B) Raman intensity at 735 $cm^{-1}$ of A. Each sample was measured three times.

The sediment exhibits strong SERS signals, while the supernatant exhibits only weak signals of the bacteria, which hardly rise above background. If all of bacteria were precipitated in the sediment, this SERS signals from the supernatant should disappear completely. We assume that some bacteria or bacteria fragments remain in the supernatant when we apply such low speed centrifugation. The slightly lower SERS signals of the bacteria in sediment compared to the original analysis are attributed to the

absence of free AgNPs and the likely loss of some Bacteria($H_2O$)@AgNPs nanostructures by the washing step.

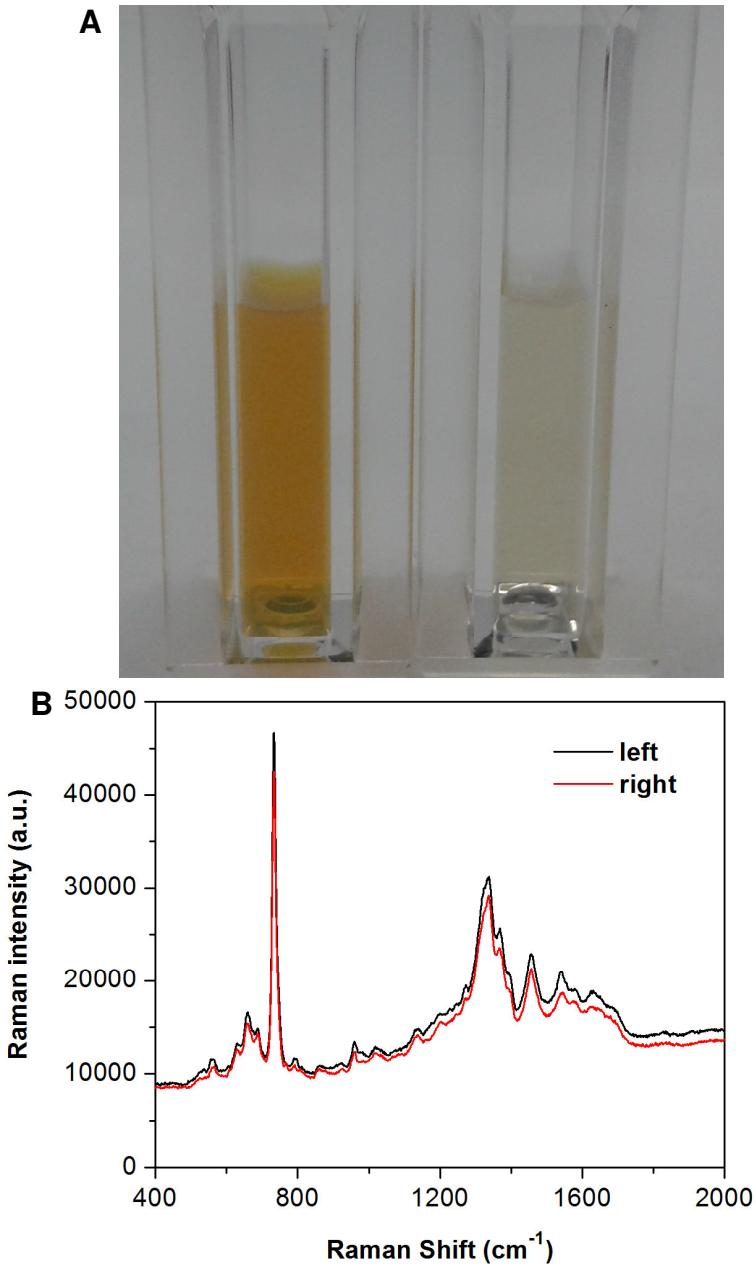


**Figure 3.11** (A) left: photo of the $1 \times 10^7$ cell/mL Bacteria($H_2O$)@AgNPs sample; right: photo of the diluted (10 times) $1 \times 10^8$ cell/mL Bacteria($H_2O$)@AgNPs solution. (B) The corresponding SERS spectra to A.

In order to further confirm that the main SERS signals of the bacteria can be ascribed to the AgNPs attached to the cell wall, we did following experiment: First, we prepared two kinds of solution. The left solution in Figure 3.11A contains $1 \times 10^7$ cell/mL Bacteria($H_2O$)@AgNPs, prepared according to the Bacteria@AgNPs. For the right

solution in Figure 3.11A, we mixed 100 μL $1 \times 10^8$ cell/mL Bacteria($H_2O$)@AgNPs sample with 900 μL water (diluted ten times), also resulting in a Bacteria($H_2O$)@AgNPs concentration of $1 \times 10^7$ cell/mL, but with a ten times lower silver concentration. Figure 3.11A illustrates the color of the solution, which may be taken as an indicator for the lower particle concentration in the right sample. Then we measured Raman for above mentioned solutions. As shown in Figure 3.11B, the SERS signal intensities are almost the same for both solutions. This observation can be explained by the consideration that the SERS signals of bacteria originate mostly from the AgNPs attached to the cell walls, while the free AgNPs in suspension just have a small effect on the overall SERS signals.

### 3.1.3 Bulk liquid bacteria detection

The Bacteria($H_2O$)@AgNPs synthesis is a highly sensitive and reproducible SERS method of bacteria detection. Figure 3.12 shows SERS spectra of different liquid phase number concentrations of *E. coli DSM 1116*, obtained by using the Bacteria($H_2O$)@AgNPs synthesis. The intensity of the SERS signals of bacteria obviously scales with the bacteria concentration ($1 \times 10^3$ to $1 \times 10^8$ cell/mL). A calibration curve is given in Figure 3.13. Down to a level of $1 \times 10^3$ cell/mL, the strongest band at 735 $cm^{-1}$ can be detected (the red circle in Figure 3.12). The Raman intensity of bacteria obviously increases with the bacteria concentrations from $1 \times 10^5$ to $1 \times 10^8$ cell/mL and exhibits a correlation coefficient R = 0.9762 (N=4). These results confirm that this strategy exhibits a huge Raman enhancement effect on the component of cell wall of *E. coli*, such as polysaccharides, amino acids, nucleic acid, lipids and proteins. The typical Raman peaks at 624, 652, 735, 955, 1330, and 1456 $cm^{-1}$ are observed (see the detailed tentative assignments of peaks in table 2).

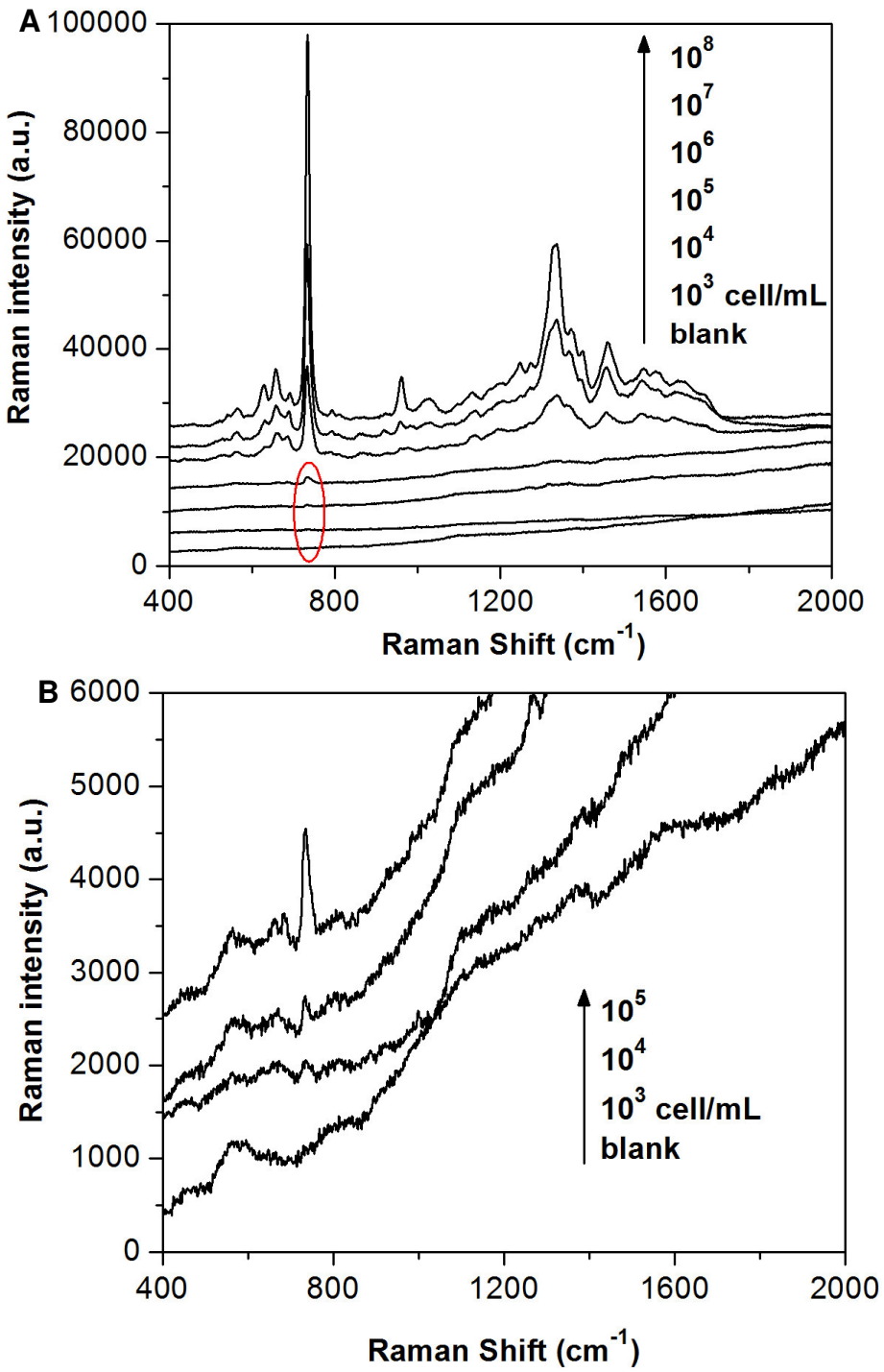


**Figure 3.12** (A) SERS spectra of different concentrations of *E. coli DSM 1116* obtained by Bacteria($H_2O$)@AgNPs synthesis. (B) SERS spectra of three low concentrations of *E. coli DSM 1116*. The concentrations are $1 \times 10^3$, $1 \times 10^4$ and $1 \times 10^5$ cell/mL, respectively. All of the Raman spectra were shifted for clarity.

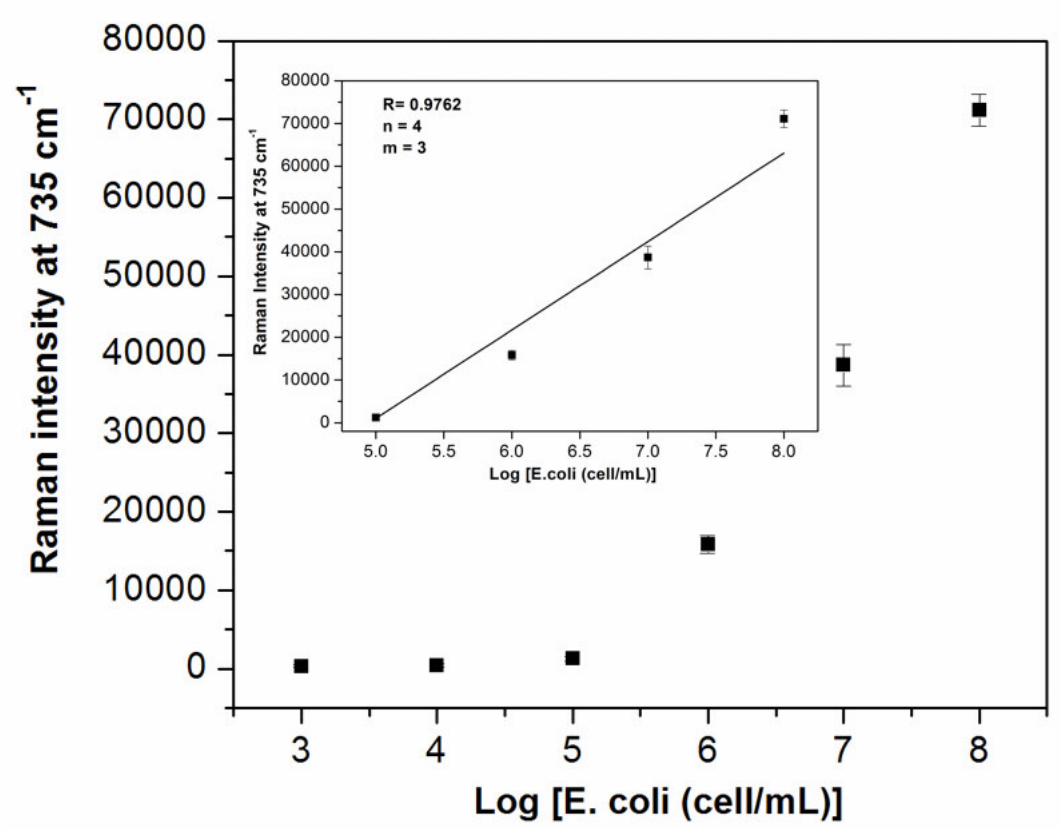


**Figure 3.13** Raman intensity of *E. coli DSM 1116* at 735 $cm^{-1}$ vs. logarithm of the corresponding *E. coli* concentration. The inset shows the correlation of the Raman intensity (at 735 $cm^{-1}$) with the logarithm of the *E. coli* concentrations in the range of $1 \times 10^5$ cell/mL to $1 \times 10^8$ cell/mL.

**Table 2.** The tentative band assignment of the SERS spectra of the *E. coli DSM 1116*.[2,86,109,110]

| **Raman Shift ($cm^{-1}$)** | **Assignment*** |
|---|---|
| 563 | carbonhydrates |
| 624 | aromatic ring skeletal |
| 652 | δ(COO-) |
| 735 | adenine, glycosidic ring mode |
| 808 | υ(CN) tyrosin, porine, valin |
| 955 | υ(CN) |
| 1128 | amide III, adenine, polyadenine and DNA |
| 1250-1310 | amide III |
| 1268 | δ($CH_2$) amide III |
| 1330 | υ($NH_2$) adenine, polyadenine, DNA |
| 1360-1440 | υ(COO-) symmetric |
| 1368 | υ(COO-) and δ(C-H) proteins |
| 1440-1460 | δ($CH_2$) saturated lipids |
| 1540-1645 | amide II, υ(CN), γ(NH) |
| 1640-1680 | amide I |

*Approximate description of the modes (υ, stretch; δ and γ, bend).

In order to investigate the potential of this strategy to discriminate between bacteria on strain level by SERS, three strains of *E. coli DSM (498/1116/5695)* and one strain of *S. epidermidis 61741* were selected as model strains. The SERS spectra in Figure 3.14A show the SERS spectra of three strains of *E. coli* and one strain of *S. epidermidis* from 60 samples batches (each strain was represented by 15 batches, samples No. 1-15 belonging to *E. coli 498*, No. 17-31: *E. coli 1116*, No. 33-47: *E. coli 5695*, No. 48-62: *S. epidermidis*). For clarity, all the SERS spectra have been normalized. The SERS spectra of the three strains of *E. coli* and *S. epidermidis* exhibit only minor differences (see Figure 3.15), because the cell walls of these *E. coli* strains and *S. epidermidis* essentially have the same components. However, we can discriminate the three strains of *E. coli* and *S. epidermidis* by hierarchy cluster analysis (HCA), which was performed in Matlab.[91] All spectra were normalized to a range from 0 to 1. A composite dendrogram derived

from HCA was used for statistical analysis. The resultant dendrogram shows clear characterization at strain level for each of the strains analyzed (Figure 3.14B).

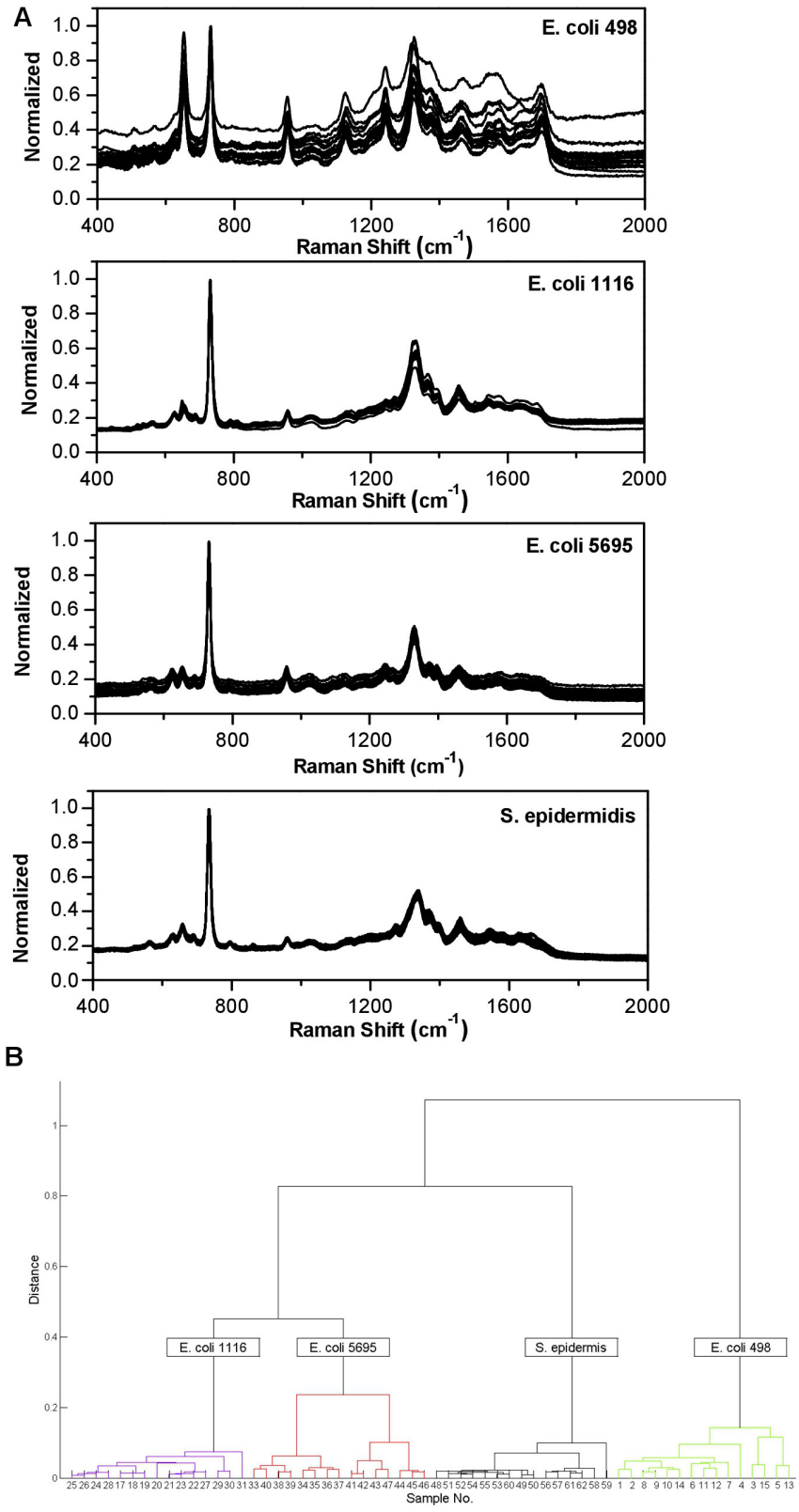


**Figure 3.14** (A) SERS spectra of three strains of *E. coli DSM (498/1116/5695)* and *S. epidermidis 61741* by using Bacteria($H_2O$)@AgNPs synthesis, each strain is represented in 15 spectra, acquired from 15 different batches of samples. (B) A composite dendrogram generated by hierarchy cluster analysis (HCA) from (A).

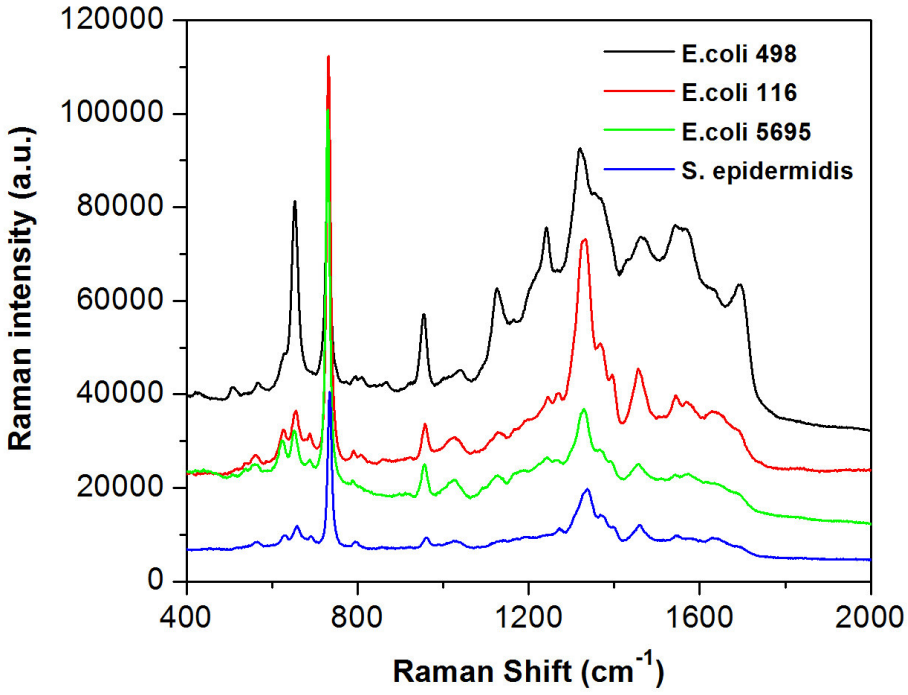


**Figure 3.15** SERS spectra of *E. coli DSM 498/1116/5695* and *S. epidermidis 61741*.

## 3.1.4 Detection of bacteria on a chip surface

We evaluated the performance of our new in situ generated SERS colloids for the detection of bacteria not only in a bulk liquid, but also on surfaces. SERS mapping experiments on Bacteria($H_2O$)@AgNPs ($1 \times 10^8$ cell/mL *E. coli DSM 1116*) were carried out on normal untreated glass slides as used in previous reports[111] and hydrophobic glass slides. One merit of a hydrophobic surface is that it substantially reduces the contact area between the droplet and the underlying surface in comparison to the hydrophilic one. Thus, the analyte present in the droplet gets higher concentrated by the liquid evaporation on the hydrophobic surface. This is known as the hydrophobic condensation effect, which further increases the SERS signals.[112] We dropped a volume (3 µL) of Bacteria($H_2O$)@AgNPs samples on normal and hydrophobic glass slides, respectively. As the images show in Figure 3.16, the droplet on the hydrophobic glass slide is much smaller; after the drying of the sample solution, again the area of sample distribution is smaller than that of on the normal glass slides, resulting in higher bacteria concentrations on the surface. The optical images in Figure 3.17 confirm this conclusion. From Figure

3.17, it can be clearly seen that the distribution of bacteria on normal glass slides is disperse; only a few bacteria are present on the selected area (40 µm × 40 µm). In contrast, there is a considerable amount of bacteria on the hydrophobic surface of the same area, and the bacteria are densely assembled to the thin bacterial film at the concentration of $1\times10^8$ cell/mL.

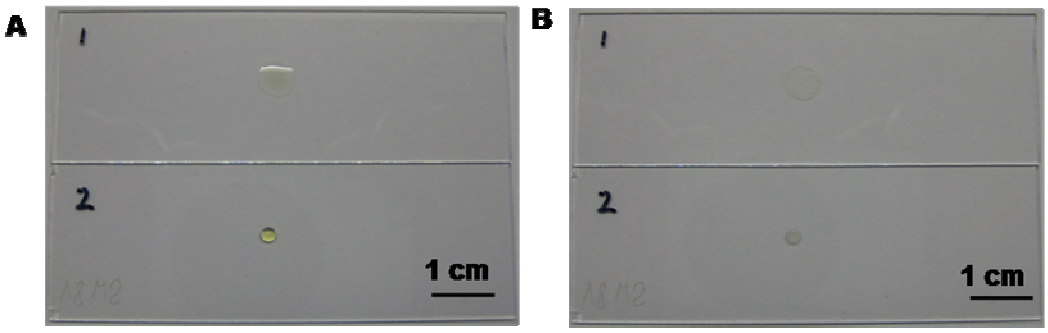


**Figure 3.16** (A) Image of a drop of 3 µL 1 × $10^8$ cell/mL Bacteria($H_2O$)@AgNPs on a normal glass slide (1-top) and on a hydrophobic glass slide (2-bottom). (B) Corresponding images of the droplets of (A) after drying.

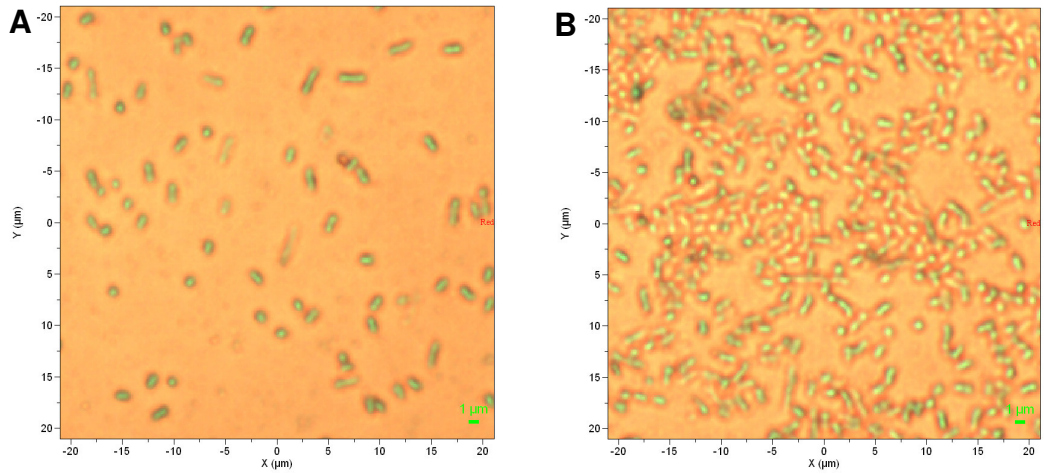


**Figure 3.17** Optical images of 1 × $10^8$ cell/mL *E. coli DSM 1116* on a normal glass slid (A) and on a hydrophobic glass slide (B), used 50× objective.

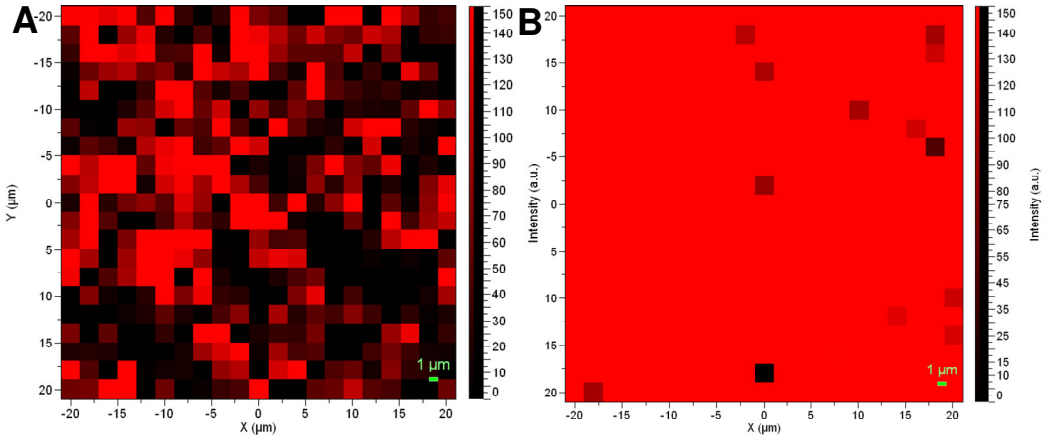


**Figure 3.18** SERS mapping images of Bacteria($H_2O$)@AgNPs ($1 \times 10^8$ cell/mL *E. coli DSM 1116*) on a normal glass slide (A) and a hydrophobic glass slide (B). The maps are based on the area of the band at 735 $cm^{-1}$.

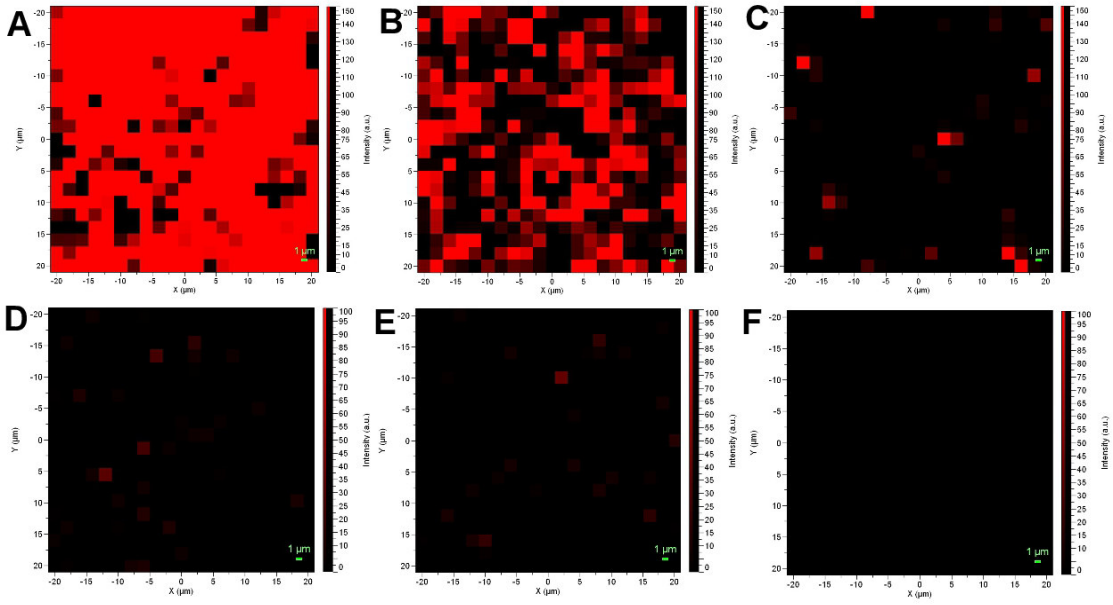


**Figure 3.19** SERS mapping of different concentrations water-washed *E. coli DSM 1116* (Bacteria($H_2O$)@AgNPs) on hydrophobic glass slides. The concentrations are $1 \times 10^7$ (A), $1 \times 10^6$ (B), $1 \times 10^5$ (C), $1 \times 10^4$ (D), $1 \times 10^3$ (E) and $1 \times 10^2$ cell/mL (F), respectively ($\lambda_{ex}$ = 633 nm, the exposure time was 1 s and the number of accumulations 5, objective 50×, step size 2 µm, mapping area: 21 × 21 = 441 points).

Finally, the homogeneity of the substrate was investigated by SERS mapping. The SERS maps shown in Figure 3.18 were obtained with 2-µm step size within an area of 40 µm × 40 µm (see the details of SERS mapping parameters in the Experimental Section). Surface coverage of the bacteria was analyzed using these maps, which was generated by using the area of the strongest peak at 735 $cm^{-1}$. Figure 3.18 shows typical SERS maps of

Bacteria($H_2O$)@AgNPs ($1 \times 10^8$ cell/mL *E. coli DSM 1116*) on two kinds of glass slides. Each red spot represents the bacteria SERS signal detected, and the black spot means that no signal of bacteria was obtained. The signals intensities vary due to the bacteria partial inhomogeneous coverage on the glass slides or the variations in the number of AgNPs around the surface of single bacterium. From Figure 3.18, it can be clearly seen that the SERS signals of bacteria distribution on hydrophobic surface are more homogenous and the number of bacteria is higher, although identical volumes and concentrations were used for both tests. Therefore, the following experiments of SERS mapping were assessed on the hydrophobic glass slides.

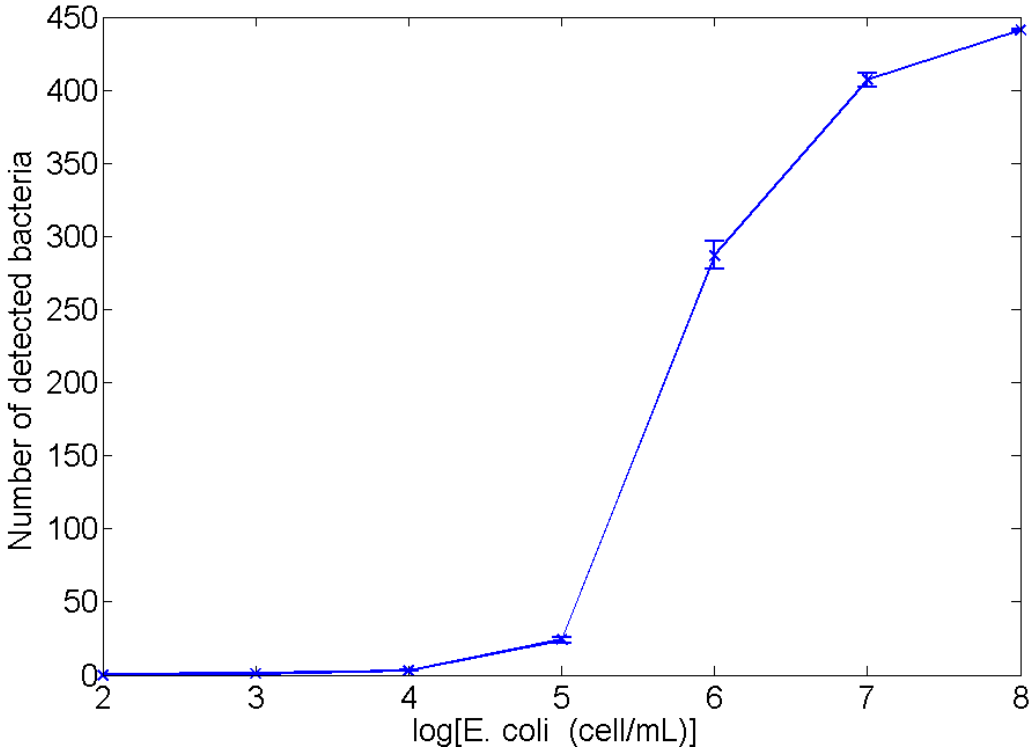


**Figure 3.20** Quantitative analysis of *E. coli DSM 1116* as derived from the map data given in Figure 3.18 and Figure 3.19. Error bars represent the standard deviation of four repetitive measurements.

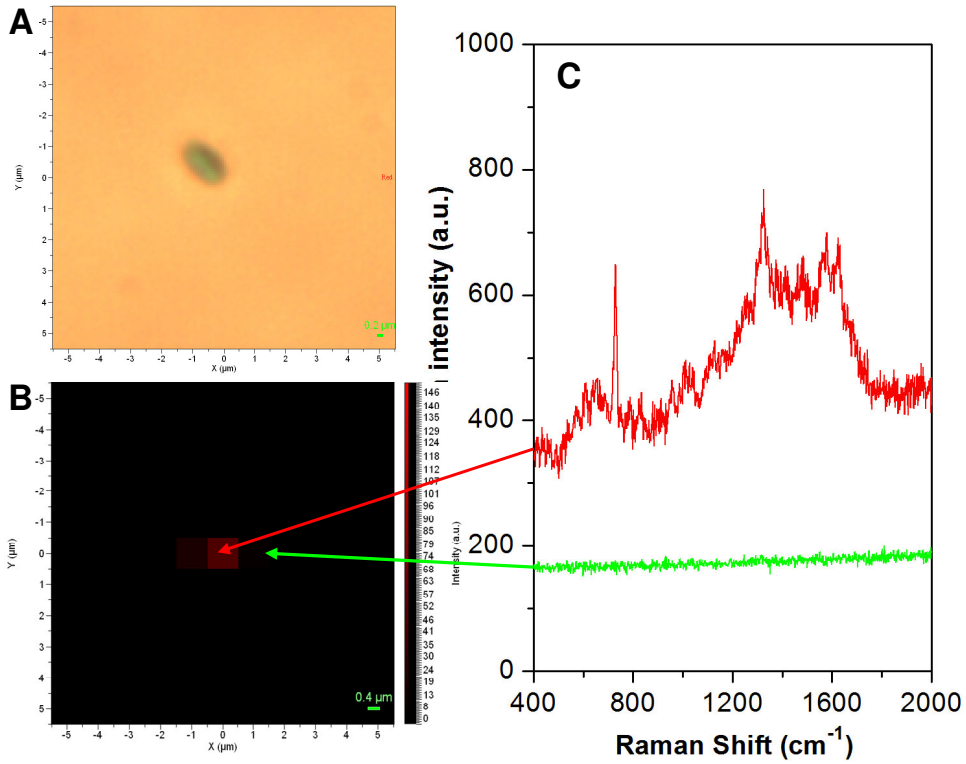


**Figure 3.21** Optical image of a single *E. coli DSM 1116* on a hydrophobic glass slide (A), corresponding SERS mapping image (B) and corresponding SERS spectra (C). ($\lambda_{ex}$ = 633 nm, the exposure time and the accumulation were 1 s and 5, objective 100×, step size 1 µm, mapping area: 11 × 11 = 121 points).

This mapping analysis of bacteria was further used to detect different concentrations of *E. coli DSM 1116* (water-washed) in drinking water. Figure 3.19 shows SERS mapping images of different concentrations of *E. coli DSM 1116* obtained by using the Bacteria($H_2O$)@AgNPs synthesis. As presented in Figure 3.20, the number of red dots, i.e. the number of bacteria bound to the surface, corresponds to the total concentration of bacteria. The approach employed for this evaluation is discussed in detail elsewhere.[113] From Figure 3.20, a LOD of 2.5 × $10^2$ cell/mL and dynamic range up to 1 × $10^8$ cell/mL can be calculated.

Our novel strategy can provide single bacterium detection by SERS mapping. Figure 3.21 shows a SERS map of a single bacterium in drinking water. Typically, the original bacteria suspension was washed by drinking water, then the Bacteria($H_2O$)@AgNPs structures were generated. Afterwards the obtained suspensions were diluted down to 1×$10^4$ cell/mL with drinking water and 3 µL of the sample suspension was pipetted on the

hydrophobic glass slides. If the bacteria are homogeneously dispersed in solution, there are statistically only 3 bacteria in 3 μL sample. SERS mapping was carried out over an area of 10 μm × 10 μm with step size of 1 μm. In order to avoid the photodegradation of the bacteria, the laser power was adjusted down to 0.14 mW. We can obviously see a red spot in Figure 3.21B, and a 1:1 compliance with the optical image in Figure 3.21A. The corresponding spectra are shown in Figure 3.21C, which illustrated that detection of single bacterium in drinking water is possible with the proposed method.

In this work, we presented an *in situ* synthesis of AgNPs on the cell wall of bacteria (Bacteria@AgNPs) for label-free SERS detection of bacteria in drinking water. Bacteria@AgNPs has been generated successfully, resulting in highly sensitive bacteria detection. It was found that the SERS signals of bacteria measured by this method mainly depends on the zeta potential of the cell wall. The enhancement effect of the SERS signal when using the Bacteria($H_2O$)@AgNPs is about 9 times higher than the one for Bacteria(PBS)@AgNPs (80 mM PBS) and about 30 times higher than the simply mixed colloid-bacterial suspension (Bacteria-AgNPs). The total assay time of the presented method is only 10 min and a total reactants volume of merely 1 mL is required in a real-world sample, when measuring in the bulk liquid. When the analysis is performed by the new, hydrophobic glass surface approach, a droplet of only 3 μL sample is necessary for each analysis. Furthermore, we can use this novel strategy to discriminate three strains of *E. coli* and one strain of *S. epidermidis* by statistical methods. This method offers many advantages, such as reduced assay time, simple handling, lower reactant volumes, a small amount of sample, and higher sensitivity and selectivity compared to previously reported label free methods, may be extended to open an avenue to develop various SERS-based biosensors.

# 3.2 SERS detection of bacteria on a microarray

## 3.2.1 Comparison of two methods

In order to assess the optimum enhancement which can be achieved with the Bacteria@AgNPs method, we compared the SERS signals of bacteria on the microarray and in solution by using three laser excitation wavelengths 532 nm, 633 nm, and 785 nm, respectively. SERS spectra were collected at the maximum respective laser power. As shown in Figure 3.22D, the strongest SERS enhancement can be observed with 633 nm excitation, lower enhancement is obtained with 532 nm excitation, while 785 nm excitation yields the lowest enhancement. We calculate the enhancement factor of the Bacteria@AgNPs method based on the intensity of the strongest vibrational band at 1388 $cm^{-1}$. It can be estimated that the enhancement factor with 633 nm excitation is about 10 times higher than the one with the 785 nm excitation (see Figure 3.23). The same phenomenon was observed in solution (see Figure 3.24).

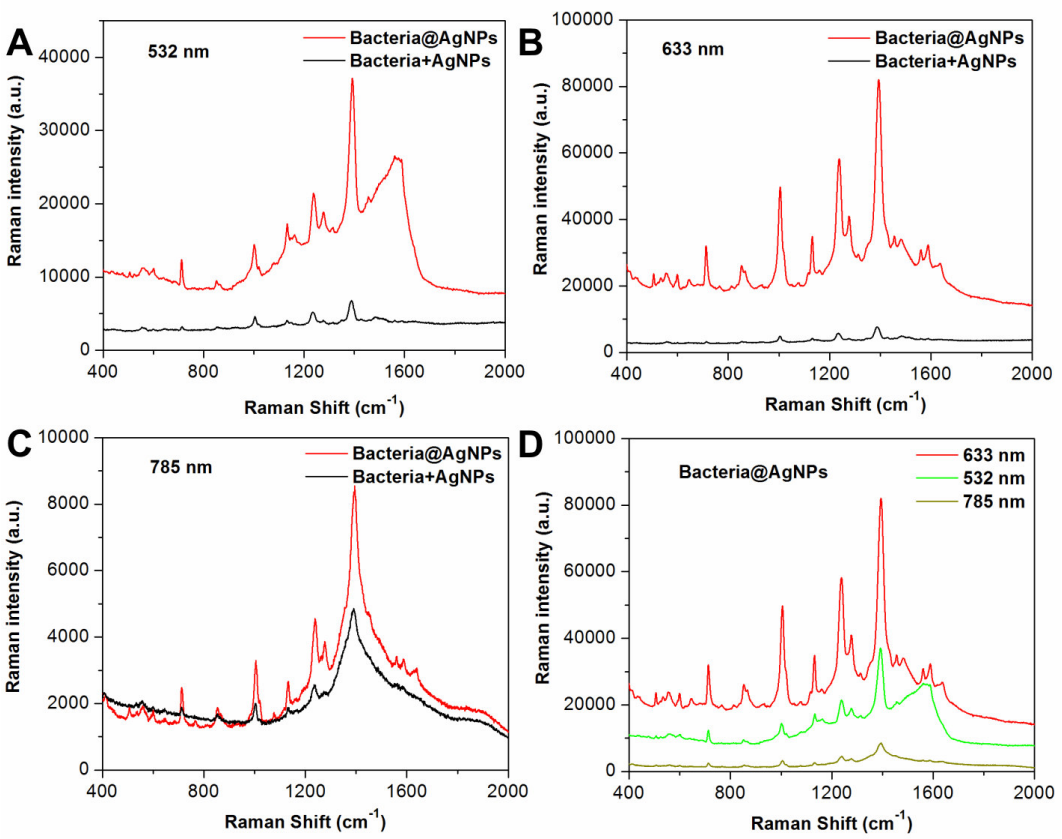


**Figure 3.22** SERS spectra of bacteria on microarray obtained by two methods, with different laser excitations: (A) 532 nm, (B) 633 nm, (C) 785 nm. (D) SERS spectra of bacteria recorded with three laser excitations by Bacteria@AgNPs method.

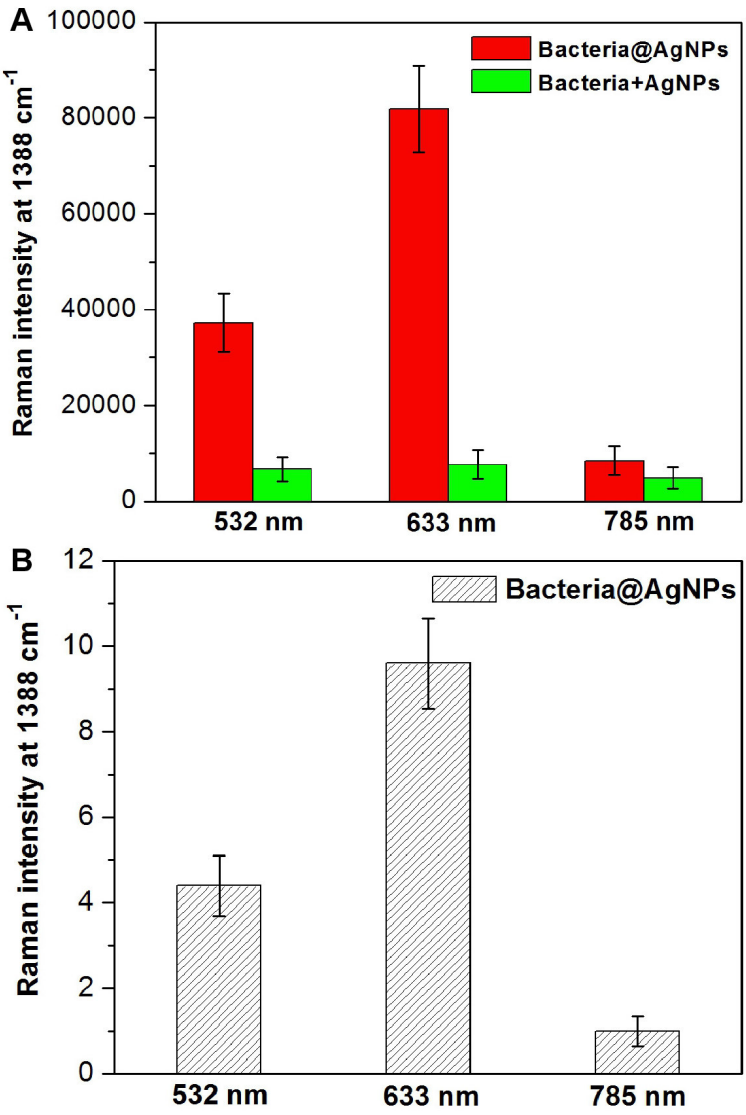


**Figure 3.23** For bacteria detection on microarray: (A) SERS intensity of bacteria (at 1388 $cm^{-1}$) obtained by Bacteria@AgNPs method and Bacteria+AgNPs method with three laser excitations. (B) The SERS enhancement factor of bacteria (1388 $cm^{-1}$) by Bacteria@AgNPs method with three laser excitations.

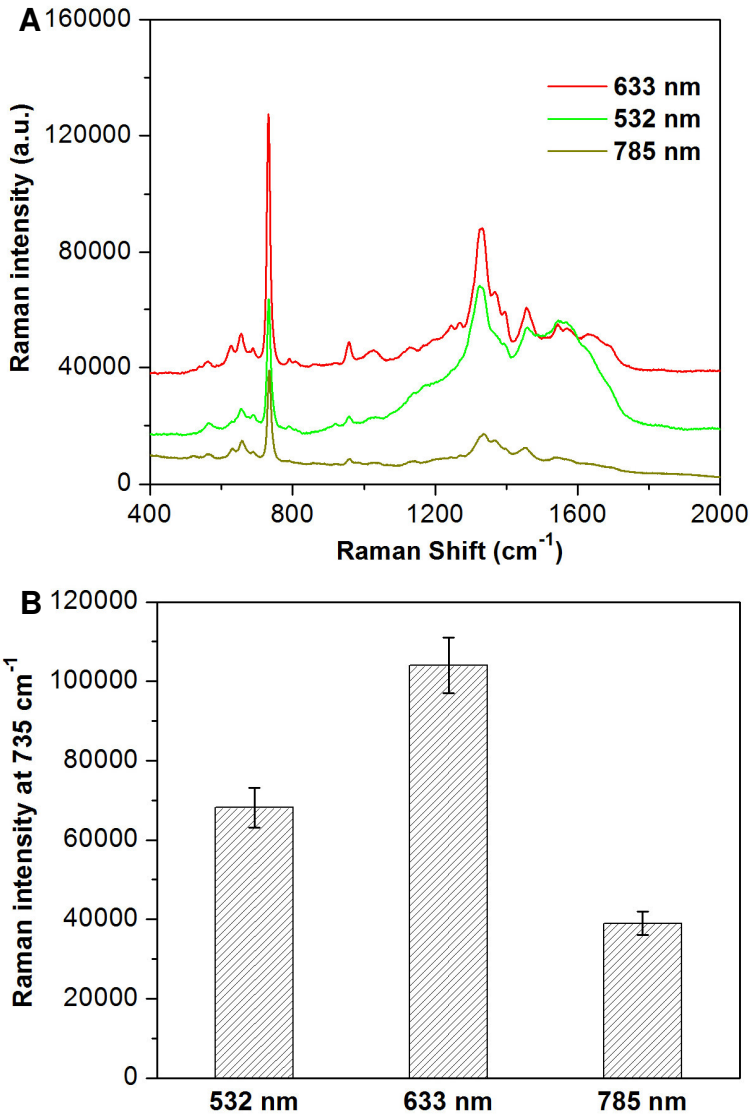


**Figure 3.24** For bacteria detection in suspension: (A) SERS intensity of bacteria obtained by Bacteria@AgNPs method with three laser excitations. (B) The SERS enhancement of bacteria (735 $cm^{-1}$) by Bacteria@AgNPs method with three laser excitations.

A similar result is observed when comparing the Bacteria@AgNPs method with the Bacteria+AgNPs method at the three different laser lines. As shown in Figure 3.22, all Raman signals of bacteria obtained by the Bacteria@AgNPs method are higher than the one obtained by the Bacteria+AgNPs method (Figure 3.22A, 3.22B and 3.22C). The enhancement factors achieved by the Bacteria@AgNPs method are about 6 times (532 nm), 11 times (633 nm), and 2 times (785 nm) higher than the one achieved by the Bacteria+AgNPs method, respectively (see Figure 3.23). In summary, the best performance with the Bacteria@AgNPs method is achieved at 633 nm, revealing one

order of magnitude enhancement than the Bacteria+AgNPs method at the same wavelength.

## 3.2.2 Best enhancement by laser line

Our previous research confirm that, by using the Bacteria@AgNPs method, the AgNPs can be directly synthesized on the surface of bacteria, induced by electrostatic force between the positive silver ions and negative bacterial cell wall.[12] Most of the AgNPs are covering the surface of bacteria[12] (see also the inset image in Figure 3.25 and Figure 3.26). Using the Bacteria+AgNPs method, the AgNPs are randomly distributed in the bacterial suspension (data were not shown). According to the SERS electromagnetic (EM) enhancement theory, the relation between the Raman intensity, $I$, and the local EM strength, $E$, is usually approximated $I \propto |E|^4$, and the relation between $E$ and the distance between nanoparticles and analytes, $D$, is described as $E \propto (1/D)^{12}$.[57] Hence, a minute reduction of $D$ leads to a significant enhancement of $I$. With the Bacteria@AgNPs method, the AgNPs are intimately attached to the cell wall, while the Bacteria+AgNPs method leads to a relatively large distance between AgNPs and bacteria.

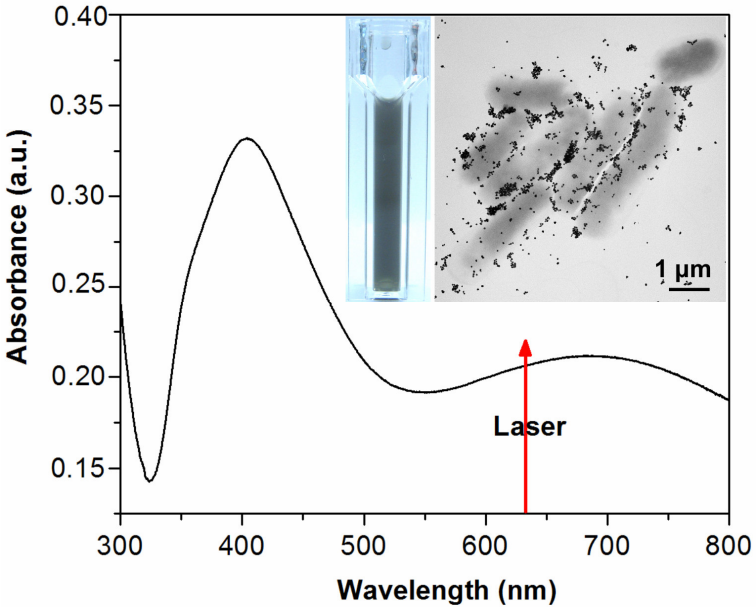


**Figure 3.25** UV-vis spectrum of Bacteria@AgNPs nanostructures in solution, stored for one week. The inset images show the color of the solution and TEM of the nanostructures.

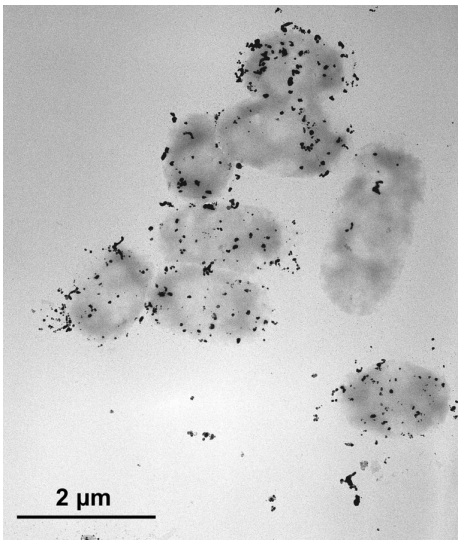


**Figure 3.26** TEM image of fresh Bacteria@AgNPs sample.

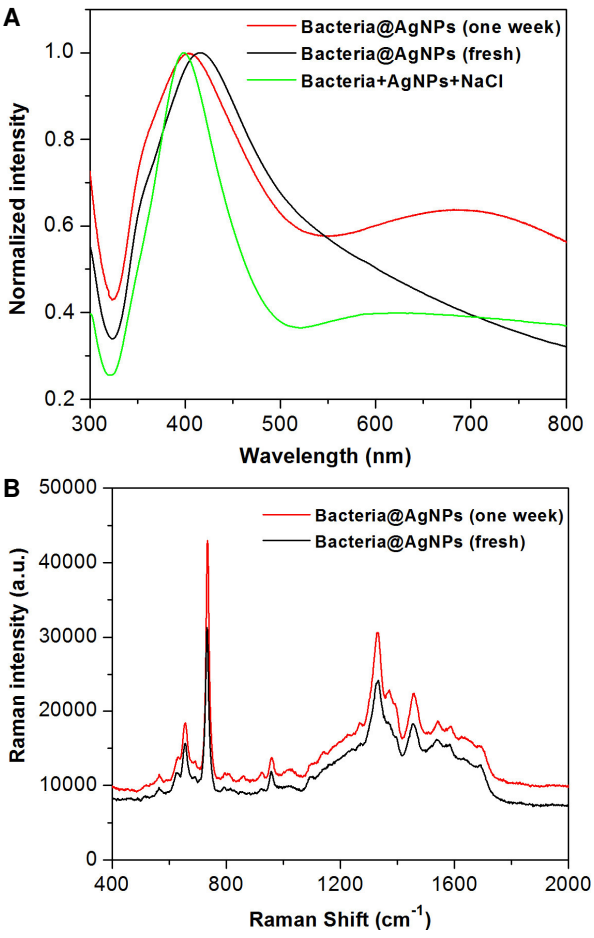


**Figure 3.27** (A) UV-vis absorption spectra *E. coli DSM 1116* mixed with AgNPs and 0.01 M NaCl (Bacteria+AgNPs+NaCl), and AgNPs coated with *E. coli DSM 1116* (Bacteria@AgNPs), including fresh one and the one of storage one week. (B) The corresponding SERS spectra in (A). The concentration of *E. coli DSM 1116* is $1 \times 10^7$ cell/mL, 633 nm laser excitation.

The wavelength dependency of the enhancement can be explained by the optical absorption these solutions. As shown in Figure 3.25, the colour of the solution is blue (see inset image in Figure 3.25). In addition to the red-shift of the absorption band of AgNPs at 410 nm (AgNPs absorption normal at 402 nm), a new broad absorption band at ~680 nm appeared. Compared to the fresh samples,[12] this band becomes significantly stronger for Bacteria@AgNPs which were stored in the refrigerator at 4 °C for one week (see Figure 3.27). The reason for this band can be found by comparing the TEM images of fresh (Figure 3.26) and aged samples (inset image of Figure 3.25): The AgNPs tend to aggregate on the cell wall, forming larger clusters. As expected, this aggregation leads to higher SERS signal of the aged (one week) Bacteria@AgNPs samples than for the fresh samples (see Figure 3.27). For a simple mixture of bacteria with AgNPs (Bacteria+AgNPs), this peak was not observed in the course of aging, not even in the presence of NaCl, which is considered an aggregation agent. As the AgNPs randomly aggregated in solution, specific aggregation on the cell wall does not take place for these particles. Hence, the appearance of the new absorption peaks at 680 nm can be attributed to the novel Bacteria@AgNPs nanostructures.

In herein, due to the novel Bacteria@AgNPs nanostructures appeared a new absorption peaks at ~680 nm, when 633-nm laser is used in SERS measurement, the Bacteria@AgNPs nanostructures absorb most of laser light and significantly amplify the scattering cross section of the bacterial cell wall components. Therefore, the strongest Raman signals of bacteria can be obtained at 633-nm laser excitation. When the 532-nm or 785-nm laser are used, the Bacteria@AgNPs nanostructures only absorbed partial laser light (due to the laser lines far away from the new absorption peaks), the scattering cross section of the bacterial cell wall components are just amplified a little. Thus the SERS signals of bacteria were significantly lower. These analyses confirm that the significant SERS enhancement when using 633-nm laser excitation mainly originates from huge EM enhancement from the novel Bacteria@AgNPs nanostructures. Thus all the following experiments were carried by using the 633-nm excitation.

### 3.2.3 Quality of antibody spots

As shown in Figure 3.28, the diameter of antibody spots is about 400 µm. The surface coverage of bacteria with AgNPs by the Bacteria@AgNPs method is higher than the one by the Bacteria+AgNPs. In the case of the Bacteria@AgNPs method (Figure 3.28A and 3.28C), the spots are regular; bacteria are homogeneously distributed on the spots, while with the Bacteria+AgNPs method (Figure 3.28B and 3.28D), the spots are irregular, the bacteria are inhomogeneously distributed, and the surface coverage of the spots is lower. These observations are consisted with our previous reported results,[12] the bacteria coverage is poorer than with the Bacteria@AgNPs method. We believed that the binding force between antibodies and bacteria is significantly reduced by the NaCl, which is required with the Bacteria+AgNPs method as aggregation reagent. The addition of the NaCl may lead to desorption of the bacteria which are flushed away during the washing step.

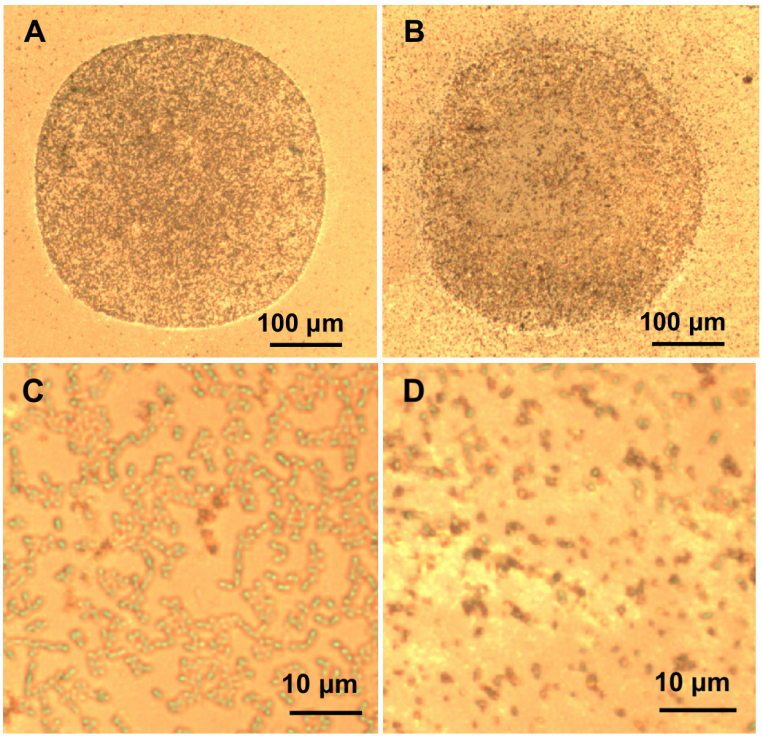


**Figure 3.28** Microscopic images of 1 × $10^8$ cell/mL *E. coli* DSM 1116 on microarray by the Bacteria@AgNPs method (A) and the Bacteria+AgNPs method (B). (C), (D) Zoom-in images of (A) and (B).

## 3.2.4 Detection of bacteria on a microarray

### Reproducibility

The novel SERS strategy for bacteria detection on microarray has a good reproducibility. As shown in Figure 3.29, serial SERS spectra of $1 \times 10^8$ cell/mL *E. coli DSM 1116* on microarray from 5 different samples display the same SERS spectra and intensity, indicating that this method can be used for quantitative bacteria detection.

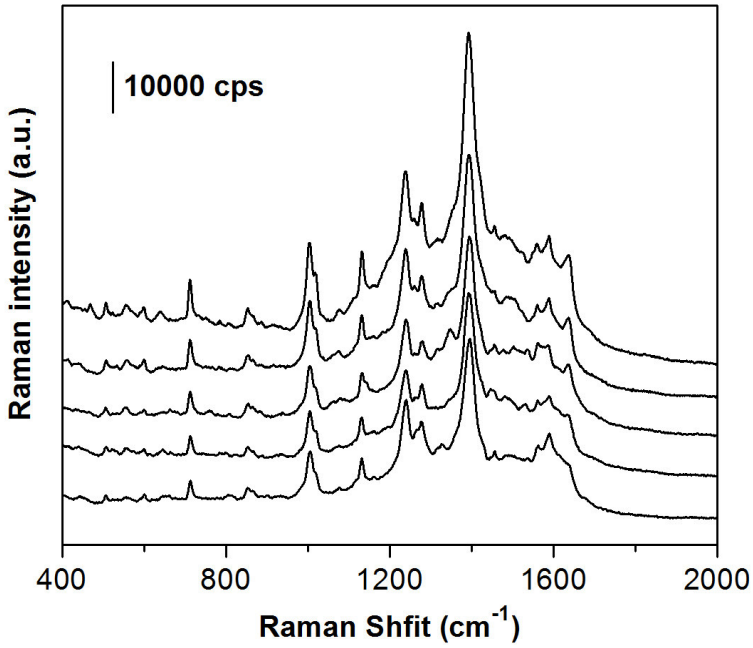


**Figure 3.29** A serial SERS spectra of $1 \times 10^8$ cell/mL *E. coli DSM 1116* on microarray from 5 different samples based on Bacteria@AgNPs method.

### Different concentrations of bacteria

Figure 3.30 shows SERS spectra of different concentrations of *E. coli DSM 1116* on microarray. The intensity of the SERS signals of bacteria obviously rises with the increase of the bacteria concentration from $1 \times 10^3$ cell/mL to $1 \times 10^8$ cell/mL. Even at $1 \times 10^3$ cell/mL level, the band at 1388 $cm^{-1}$ can be clearly observed. Furthermore, we can see that the SERS intensity of bacteria is almost the same, when the bacteria concentrations are $1 \times 10^3$, $1 \times 10^4$, and $1 \times 10^5$ cell/mL, respectively. That is because only one bacterium was detected at these concentrations. As we know, the laser spot size

is about 4 $\mu m^2$, when using 10× objectives. The laser spot can cover just single bacteria on microarray when the concentrations of bacteria are too low. However, the number of the detected bacteria will be higher with the increase of bacterial concentrations (see Figure 3.31). Thus, the SERS signals of bacteria were obviously increased, when the concentrations of bacteria changed from $1 \times 10^6$ cell/mL to $1 \times 10^8$ cell/mL. These results confirm that this strategy exhibits a huge SERS enhancement effect on the components of cell wall of *E. coli*, such as polysaccharides, amino acids, nucleic acid, lipids and proteins. The typical Raman peaks including 556, 710, 1000, 1130, 1234, 1275, and 1388 $cm^{-1}$ can be detected (see the detailed tentative assignments of peaks in table 3).

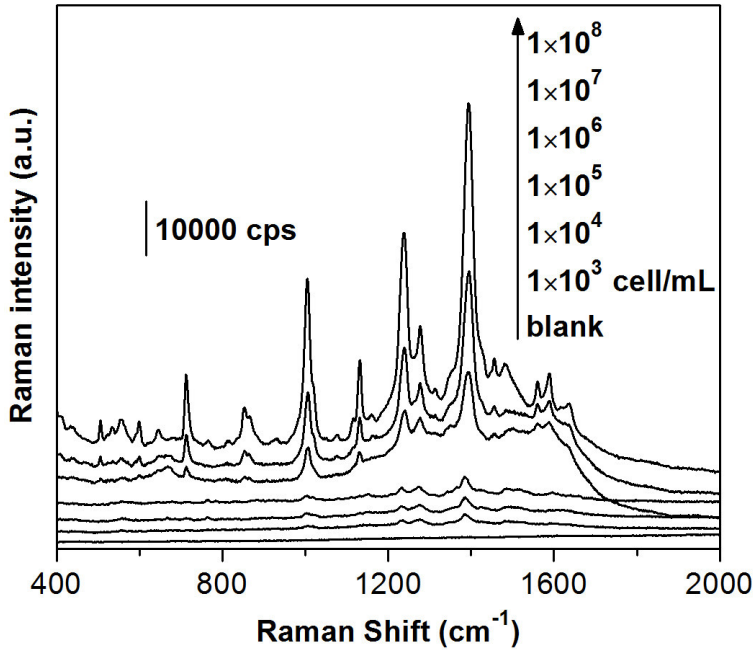


**Figure 3.30** SERS spectra of different concentrations of *E. coli DSM 1116* on microarray obtained by Bacteria@AgNPs method. The concentrations are $1 \times 10^3$, $1 \times 10^4$, $1 \times 10^5$, $1 \times 10^6$, $1 \times 10^7$ and $1 \times 10^8$ cell/mL, respectively.

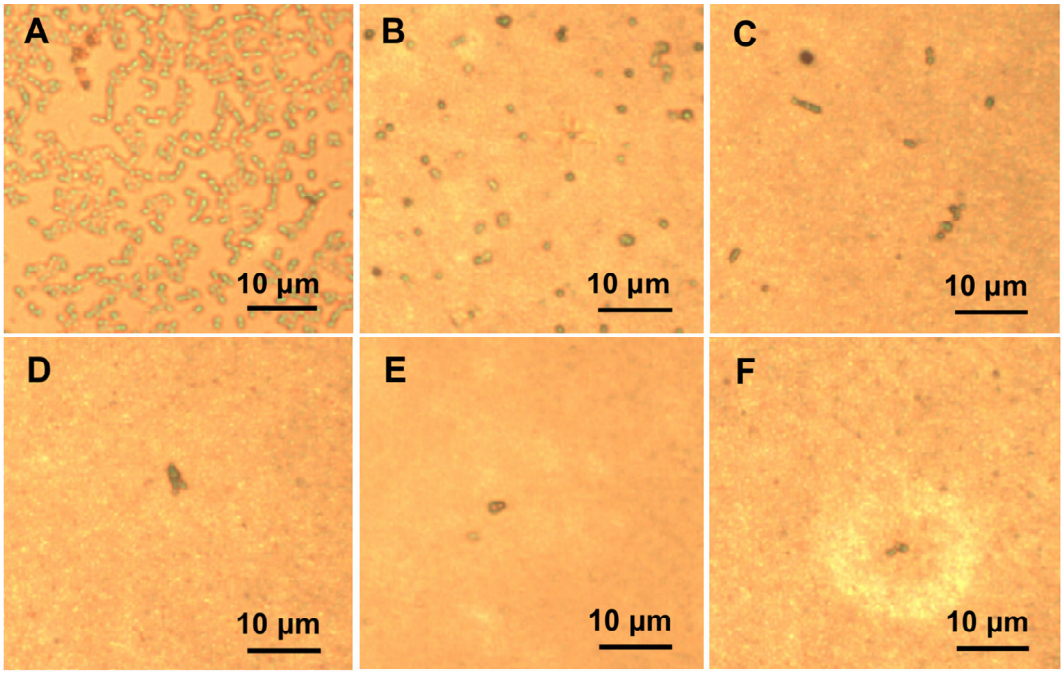


**Figure 3.31** Microscopic images of different concentrations of *E. coli DSM 1116* on microarray by Bacteria@AgNPs method. The concentrations are $1 \times 10^8$ (A), $1 \times 10^7$ (B), $1 \times 10^6$ (C), $1 \times 10^5$ (D), $1 \times 10^4$ (E) and $1 \times 10^3$ (F) cell/mL, respectively.

**Table 3.** The tentative band assignment of the SERS spectra of the *E. coli DSM 1116*.[110,113,114]

| **Raman Shift ($cm^{-1}$)** | **Assignment*** |
|---|---|
| 556 | carbohydrates |
| 710 | adenine |
| 850 | different C-N stretch |
| 1000 | C=C deformation |
| 1074 | carbohydrates, C-C, C-O, -C-OH |
| 1130 | amide III, adenine, polyadenine and DNA |
| 1234 | aromatic amino acids in proteins |
| 1275 | $CH_2$ deformation, amide III |
| 1330 | =CH in plane (lipid) or amide III (protein) |
| 1388 | adenine, guanine (protein) COO- stretching sym |
| 1455 | $CH_2$ deformation |
| 1558 | COO- stretching antisym |
| 1636 | amide I |

## Single cell measurements

It should be noted that a single bacterium can be detected by significant EM enhancement mechanism upon the formation of the Bacteria@AgNPs nanostructures on the microarray. As shown in Figure 3.32, the SERS signals were obviously observed from one single bacterium and there are no signals recorded outside of the bacterium. Furthermore, the SERS signals of a single bacterium has a good reproducibility. As shown in Figure 3.33, serial SERS spectra of a single *E. coli DSM 1116* on microarray from four different samples display the same SERS spectra and intensity, indicating that most of bacteria were covered with AgNPs, and the cover efficiency is very high. Thus, it is illustrated that detection of single bacteria on a microarray is possible with the proposed strategy.

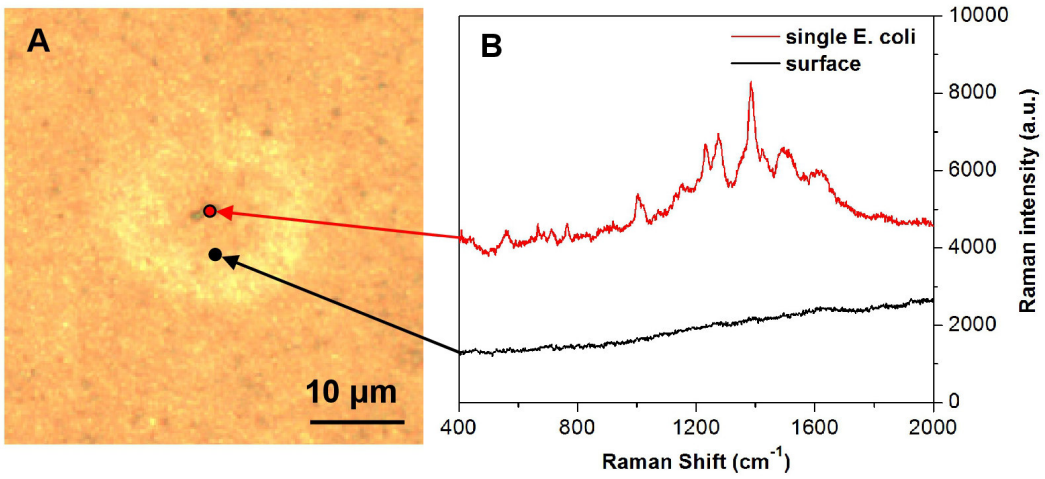


**Figure 3.32** Microscopic images of single *E. coli DSM 1116* on a microarray (A) and the corresponding SERS spectra (B).

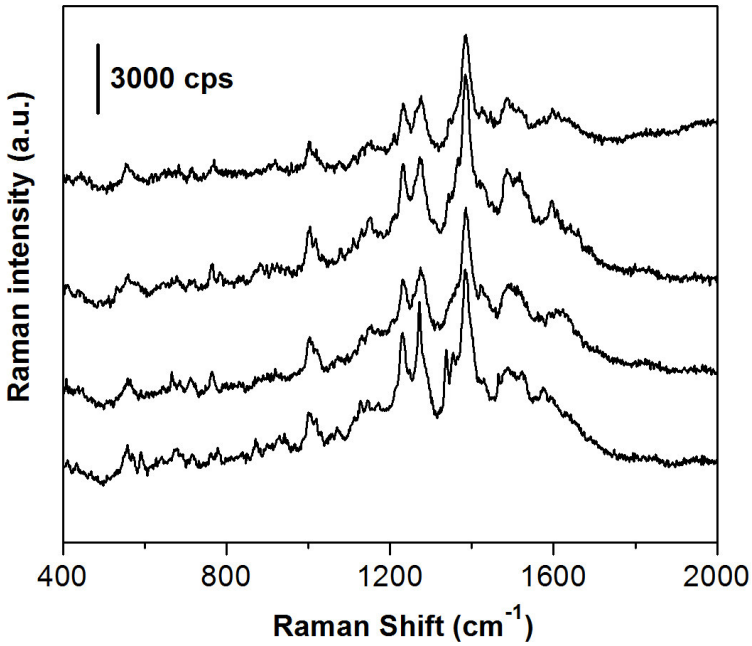


**Figure 3.33** Serial SERS spectra of single *E. coli DSM 1116* from a microarray and from four different samples based on the Bacteria@AgNPs method. The used bacteria concentration is $1 \times 10^3$ cell/mL, one pot contained 3 µL.

Employing directly synthesized AgNPs on the surface of bacteria (Bacteria@AgNPs) is a simple and highly efficient strategy for the sensitive detection of bacteria on a microarray platform. While the approach does not require more preparation time than conventional mixing of pregenerated $AgNP_S$ with bacteria, it reveals a ten times higher signal, thus allowing for more reliable identification of individual bacteria, collected on a microarray surface. It has been demonstrated that such Bacteria@AgNPs nanostructures reveal the highest enhancement at an excitation wavelength of 633 nm laser line, which can be explained by the plasmon interaction of the AgNPs aggregating on the bacteria surface. The simplicity and sensitivity may help to establish SERS a routine tool in bacteria microarray readout. Future work will be devoted to real multicomponent analysis on microarrays, comprising different receptors on one chip.

## 3.3 Counting live and dead bacteria by SERS mapping

As we mentioned in the theory section, it remains a challenge to achieve rapid and accurate identification live and dead bacteria. Up to now, many methods, such as flow cytometry, enzyme-linked immunosorbent assay (ELISA), and polymerase chain reaction (PCR), have been developed for rapid identification of low concentrations bacteria, none of these methodologies can distinguish between live and dead bacteria. This is, because the live and dead bacteria have the same signal output by such methodologies. Thus, great efforts have recently been stimulated for developing a novel method for rapid and sensitive identification of live and dead bacteria.

The current methods for distinguishing live and dead bacteria are commonly time-consuming and involve complex instrumentation such as plate counting, atomic force microscopy (AFM),[116] fourier transform infrared microspectroscopy,[117] fluorescent techniques combined with PCR or flow cytometry,[118-122] which require enrichment procedures, frequent instrument calibration, and sophisticated samples preparation. These costly instrument-based techniques are not applicable for most of the in situ rapid enumeration techniques of live and dead bacteria in aqueous environment. Thus, a novel detection principle has trended toward in situ, rapid, visual, and operating ease of sensitive techniques such as chemosensors and biosensors. Due to the fact that the same strains of live and dead bacteria almost have the same components and the strong interfering background from water in aqueous environment and biological samples, thus, the in situ rapid discrimination of live and dead bacteria in aqueous phase is still a challenging task, even simple counting them. The surface-enhanced Raman scattering (SERS) mapping reported herein is promising to meet this challenge, which employs our silver nanoparticles coating bacteria structure (Bacteria@AgNPs) as the recognition element and SERS mapping as visual signal output for rapid enumeration of live and dead bacteria.

SERS mapping possesses advantages in terms of working in the field of biology and biomedical research, primarily because of its capability of providing spectral information of molecular species (its structure and its environment) with high spatial resolution at the submicron range. However, the development of SERS mapping methods is limited by the design of SERS nanostructures which should be sensitive and specific to analytes. In this section, Bacteria@AgNPs nanostructures were prepared in live and dead bacteria suspensions by our in situ synthesis method, respectively. We found that only the live Bacteria@AgNPs give strong SERS signals of bacteria, on the contrary, the dead Bacteria@AgNPs almost have no SERS signals (Figure 3.34). We designed detailed experiments to confirm this phenomenon and it could be explained by the membrane charge of the bacteria. We further successfully demonstrate the utility of SERS for calculating different percentage of dead bacteria in aqueous environment. Finally, we successfully counted live and dead bacteria with such method by SERS mapping. The preliminary results are shown below.

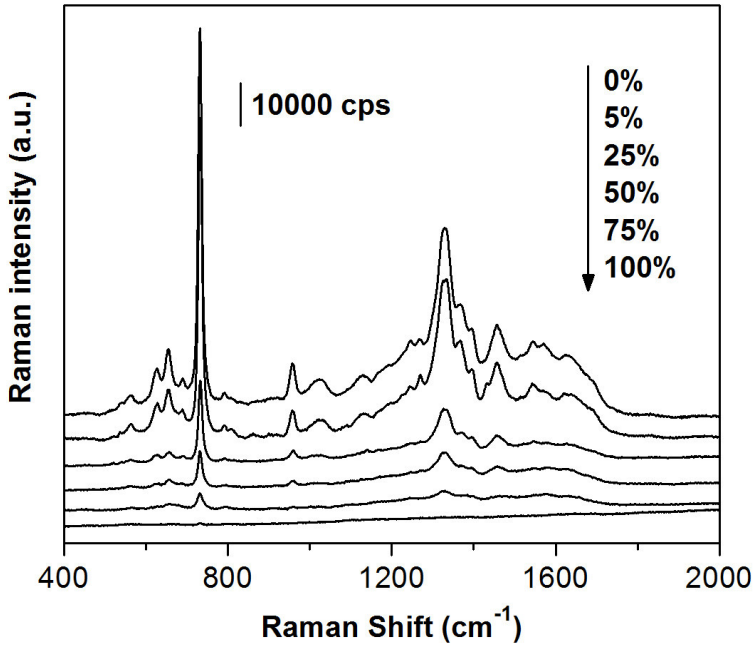


**Figure 3.34** SERS spectra of different percentage of dead *E. coli DSM 1116*. The concentrations of *E. coli* are $1 \times 10^8$ cell/mL.

As shown in Figure 3.34, we can see that the more E. coli dead, the lower SERS signals were obtained. There is almost no signal when the bacteria are 100% dead.

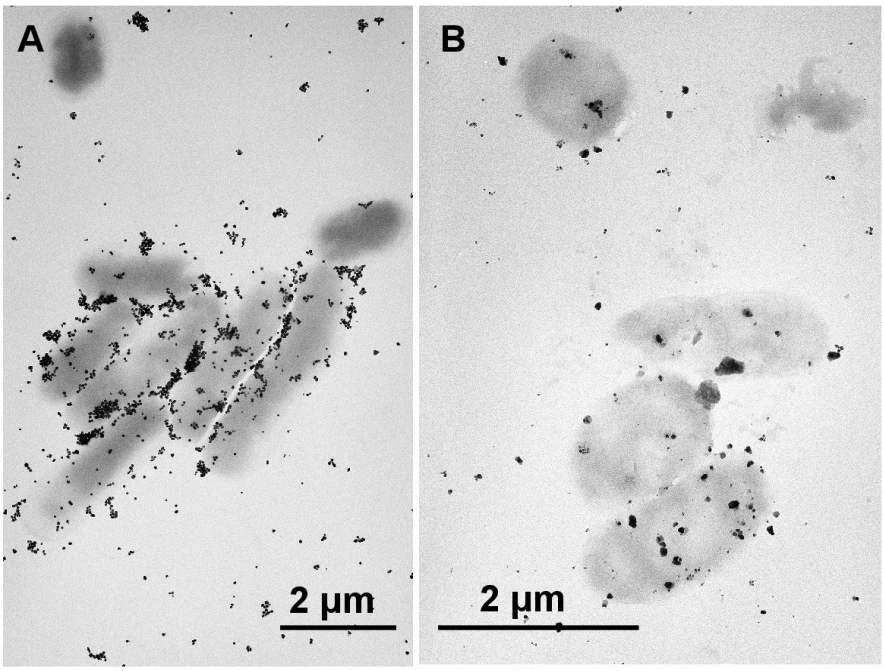


**Figure 3.35** The TEM images of 0% dead (A) and 100% dead (B) Bacteria@AgNPs. Bacteria are E. coli.

As shown in Figure 3.35, we can clearly see that most of AgNPs coat the live bacterial surfaces, and the AgNPs spontaneous aggregate as cluster, whereas only a few of AgNPs coat the dead bacterial surfaces.

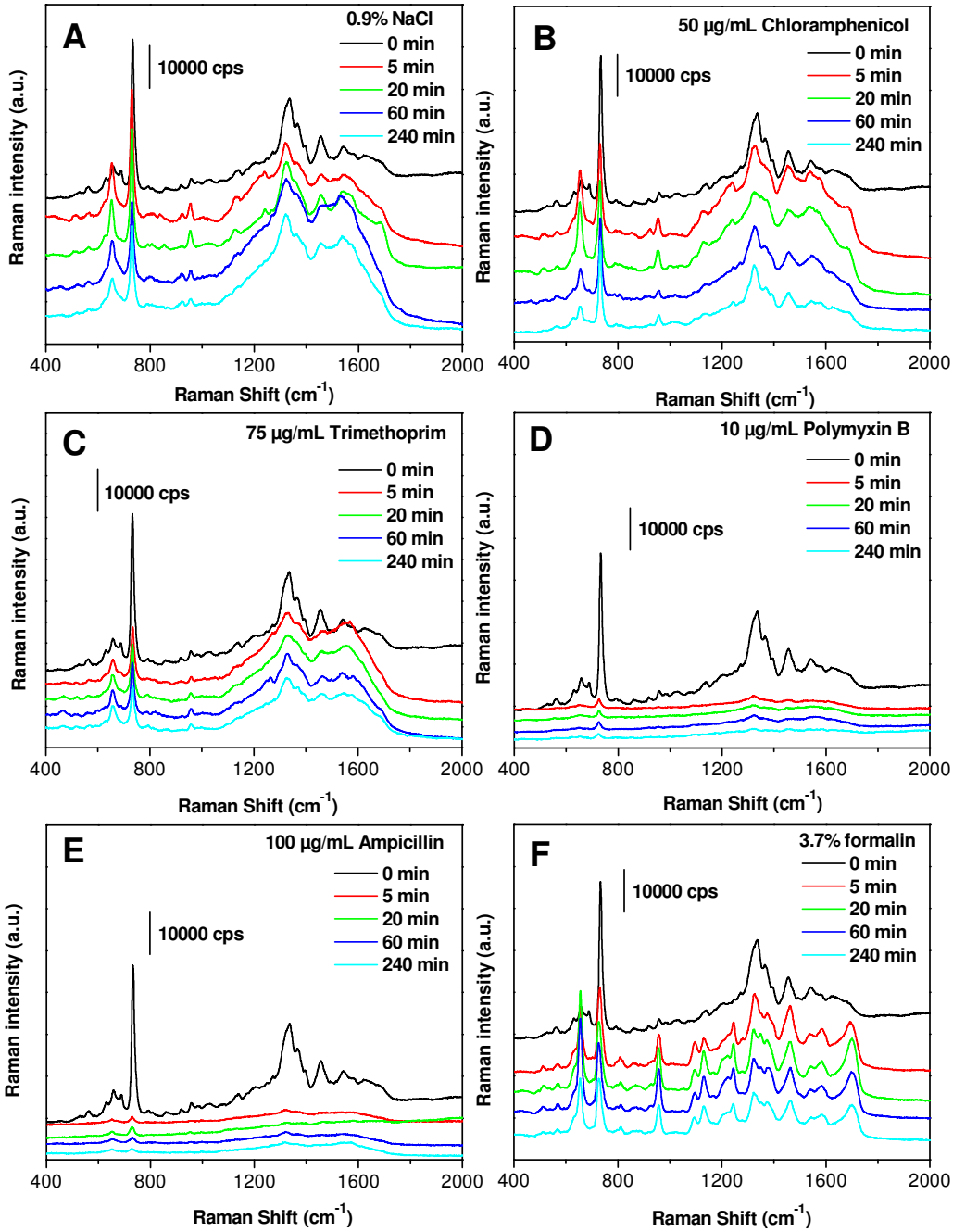


**Figure 3.36** The SERS spectra of bacteria ($1 \times 10^7$ cell/mL *E. coli DSM 1116*) killed by different antibiotics concentrations at 0, 5, 20, 60, and 240 min. The antibiotics are 0.9% NaCl plus no antibiotics (A), 50 µg/mL chloramphenicol (B), 75 µg/mL trimethoprim (C), 10 µg/mL polymyxin B (D), 100 µg/mL ampicillin (E), and 3.7% formalin (F), respectively.

As shown in Figure 3.36, we can observe that the bacteria almost have no Raman signals when killed by polymyxin B and ampicillin. However, the Raman signals of bacteria only decrease a little when killed by other antibiotics. These results are due to different way of antibiotics to kill bacteria. For polymyxin B and ampicillin, both of them can rupture the cell wall of bacteria within 5 min. For other antibiotics, they killed bacteria either through blocking new protein synthesis or through cross-linking of the proteins. The cell wall of bacteria is still intact, not destroyed. All of these results are confirmed that the SERS signals of bacteria are mainly depended on the cell wall, when using our in situ coating AgNPs strategy. All of the concentrations of bacteria are $1 \times 10^7$ cell/mL *E. coli DSM 1116*.

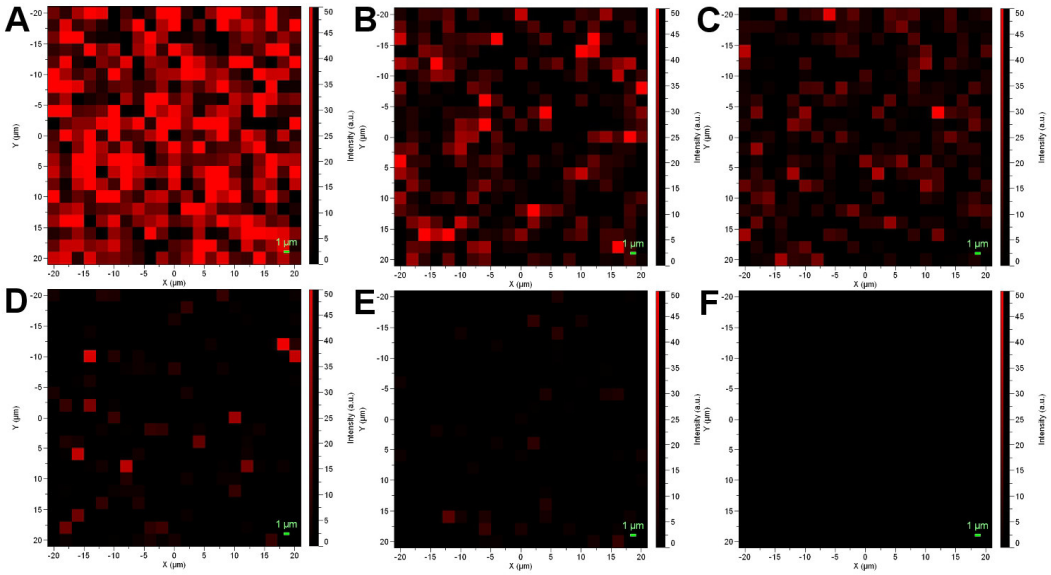


**Figure 3.37** SERS mapping of different percentage of dead bacteria on hydrophobic glass slides. The percentages of dead bacteria are 0% (A), 5% (B), 25% (C), 50% (D), 75% (E) and 100% (F), respectively.

As shown in Figure 3.37, we can clearly see that the more bacteria dead, a fewer number of red spots on the SERS images is seen, which means a lower SERS signals of bacteria is obtained. The concentration of bacteria is $1 \times 10^8$ cell/mL *E. coli DSM 1116*.

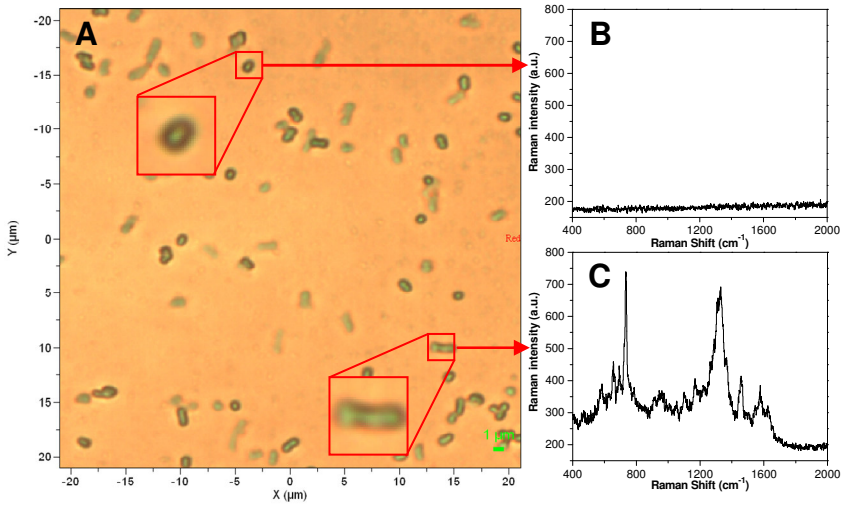


**Figure 3.38** Discrimination of single live and dead bacteria. (A) Optical images of 50% dead bacteria on hydrophobic glass slides, the area are 40 μm × 40 μm. The red squares are the original and enlarged single bacterium. (B) SERS spectrum of a single dead bacterium. (C) SERS spectrum of a single live bacterium. The concentration of E. coli is $1 \times 10^6$ cell/mL, used is a 100× objective.

As shown in Figure 3.38, these results confirm that we can discriminate between live and dead bacteria at single cell level by our in situ AgNPs coating strategy.

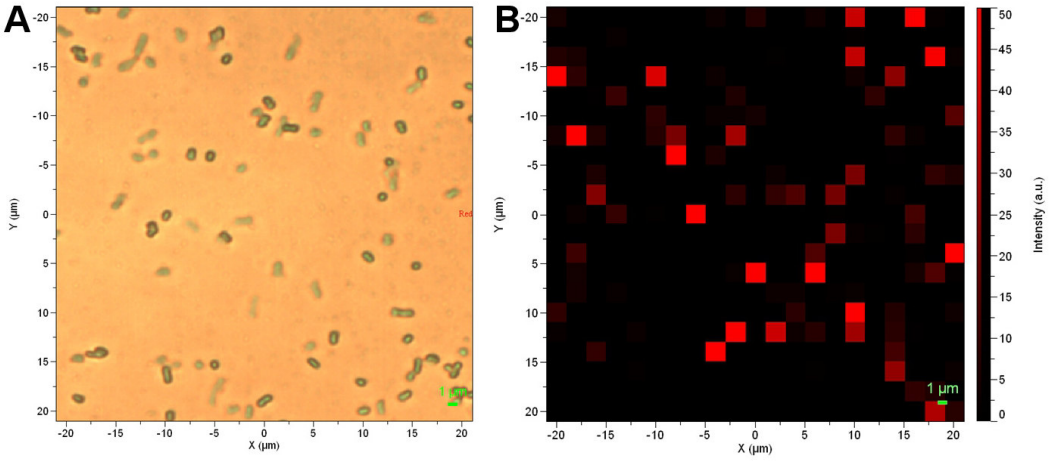


**Figure 3.39** Counting live and dead bacteria through SERS mapping on the hydrophobic glass slides. (A) Optical images of 50% dead bacteria on normal glass slides, the areas are 40 μm × 40 μm. (B) The corresponding SERS image from A. The SERS mapping was constructed using the strongest peak at 735 $cm^{-1}$. The concentration of E. coli is $1 \times 10^6$ cell/mL, used is a 100× objective.

As shown in Figure 3.39, we can calculate that there are 90 cells in the optical area, and there are 46 red spots in SERS mapping images. In here, owing to the bacteria are well dispersed on hydrophilic glass slides and the mapping step sizes is 2 μm, one red spot (4 $\mu m^2$) only covers one bacterium (the dimension of E. coli is 2 μm × 1.5 μm). Then

we can calculate that the percentage of live bacteria is 46/90 = 51.1%, which is almost equal to the expected value (50%). All these results confirmed that our in situ coating AgNPs on the cell wall can be used to determine live and dead bacteria through SERS mapping.

# 4 Summary and Outlook

# 4.1 Research summary

In the first part of this thesis, we reported an in situ synthesis of AgNPs-coating on the cell wall of bacteria for SERS-based label-free detection of bacteria in drinking water. It is a more efficient way to achieve intimate contact between NPs and the bacteria cell in comparison to previous methods. We firstly soaked bacteria in silver nitrate solution, and then used hydroxylamine hydrochloride as reducing agent. Finally, a "colloid deposit" was formed on the cell wall of bacteria, which is addressed in the following as Bacteria@AgNPs. It was found that the SERS signals of bacteria measured by this method mainly depends on the zeta potential of the cell wall. The enhancement effect of the SERS signal when using the Bacteria($H_2O$)@AgNPs is about 9 times higher than the one for Bacteria(PBS)@AgNPs (80 mM PBS) and about 30 times higher than the simply mixed colloid-bacterial suspension (Bacteria-AgNPs). The total assay time of the presented method is only 10 min and a total reactant volume of merely 1 mL is required in a real-world sample, when measuring in the bulk liquid. When the analysis is performed by the hydrophobic glass surface approach, a droplet of only 3 μL volume is necessary for each analysis. Furthermore, we can use this strategy to discriminate three strains of *E. coli* and one strain of *S. epidermidis* by statistical methods (Hierarchy Cluster Analysis). This method offers many advantages, such as reduced assay time, simple handling, lower reactant volumes, a small amount of sample, and higher sensitivity and selectivity compared to previously reported label-free methods.

In the second part, microarray technology represented a high-potential tool for solving multianalyte problems in the analytical and bioanalytical field.[23] In addition, the immunoassay technique applied on the microarray system offers the possibility to selectively capture specific antigens, such as bacteria and viruses.[22] Thus, a highly sensitive, selective, multianalysis, and high-throughput bacteria assay is highly demanded. In this part, we report on the application of the novel in situ synthesis of Bacteria@AgNPs nanostructures as readout tool for a label-free microarray SERS

detection of bacteria we presented earlier.[86,115] With the optimum enhancement laser line (633 nm), the SERS signals of bacteria on a microarray surface is increased 11 times as compared to the previously reported simply mixed (Bacteria+AgNPs) microarray system. This result is due to: (1) a more efficient way to achieve intimate contact between NPs and the bacterial cell in comparison to previous methods, (2) more efficient coverage of bacteria with AgNPs by the Bacteria@AgNPs method than achieved by Bacteria+AgNPs. The total assay time is 2 h and the total sample volume needed in order to analyze bacteria is only 1 mL. The sensitivity and simplicity needed for the detection and identification of a single bacterium on a microarray is achieved. To further investigate this microarray SERS sensor, the selectivity and multianalysis of the sensor with different antigens and antibodies will be carried out in the future.

In the third part, we prepared live and dead bacteria Bacteria@AgNPs nanostructures by our in situ synthesis method. We found that only the live Bacteria@AgNPs give strong SERS signals of bacteria, however, the dead Bacteria@AgNPs almost have no SERS signals. We designed detailed experiments to confirm this phenomenon was ascribed to the membrane charge of the bacteria. We further successfully demonstrate the utility of SERS for calculating the percentage of dead bacteria in an aqueous sample. Finally, we successfully counted live and dead bacteria with such method by SERS mapping.

## 4.2 Future research work

In future work, we plan to real-time detect bacteria in microfluidic cells. Until to now, we have successfully fabricated two kinds of microfluidic cells (Figure 4.1), and we found that the solution in the right side device can be mixed better than left side, thus we will use the right side device in future experiments.

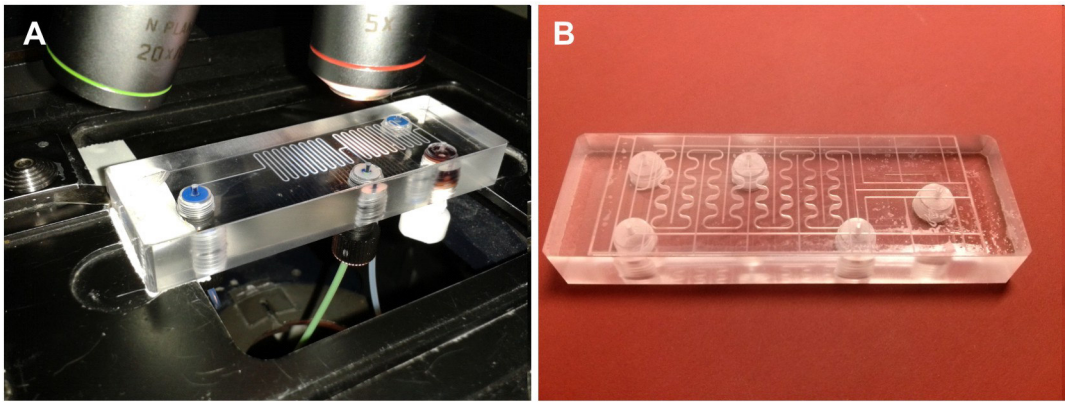


**Figure 4.1** Photos of microfluidic cells.

1) Optimizing the parameters by detection of Rhodamine 6G (R6G), such as the flow rate, detection position, and so on.

2) Detection of bacteria by using pre-synthesis AgNPs using the optimal parameters.

3) Detection of bacteria by using our novel in situ synthesis AgNPs in the microfluidic cell, and comparison the SERS signals of bacteria with two synthesis AgNPs methods.

4) Capture the bacteria at the detection point through modifying the channel with cationic polymer, such as polybrene.

5) Detection of bacteria with the above mentioned capture method and under two different synthesis AgNPs strategies.

6) Discrimination of live and dead bacteria in a microfluidic cell by our in situ AgNPs synthesis method.

# 5 Abbreviations

| | |
|---|---|
| 3D | Three-dimensional |
| AgNPs | Silver nanoparticles |
| AuNPs | Gold nanoparticles |
| AFM | Atomic force microscopy |
| a.u. | Arbitrary unit |
| breath | Breathing |
| CaDPA | Calcium dipicolinate |
| C. diphtheriae | *Corynebacterium diphtheriae* |
| CCD | Charge coupled device |
| C. glutamicum | *Corynebacterium glutamicum* |
| C. pseudotuberculosis | *Corynebacterium pseudotuberculosis* |
| CSLM | Confocal scanning laser microscopy |
| CTAB | Cetyltrimethylammonium bromide |
| DAPI | 4',6-diamidino-2-phenylindole |
| CV | Crystal violet |
| CT | Charge transfer |
| DMAP | 4-Dimethylaminopyridine |
| DMF | Dimethylformamide |
| DNA | Deoxyribonucleic acid |
| DSC | N,N´-Disuccinimidyl carbonate |
| E. coli | *Escherichia coli* |
| ELISA | Enzyme-linked immunosorbent assay |
| EM | Electromagnetic enhancement |
| GFP | Green fluorescent protein |
| GOPTS | 3-Glycidyloxypropyltrimethoxysilane |
| HCA | Hierarchy cluster analysis |
| HOMO | Highest occupied molecular orbital |
| HRP | Horseradish peroxidase |
| ICP/MS | Inductively coupled plasma/mass spectrometry |
| IR | Infrared spectroscopy |
| IWC | Institute of Hydrochemistry |
| LbL | Layer by layer |
| LOD | Limit of detection |

| | |
|---|---|
| LPS | Lipopolysaccharides |
| LSPR | Localized surface plasmon resonance |
| LUMO | Lowest unoccupied molecular orbital |
| NHS | N-Hydroxysuccinimid |
| NPs | Nanoparticles |
| NR | Normal Raman |
| PABT | p-aminobenzenethiol |
| PAH | Poly (allylamine hydrochloride) |
| PBS | Phosphate buffered saline |
| PCR | Polymerase chain reaction |
| PEG | Polyethylene glycol |
| RM | Raman microscopy |
| RNA | Ribonucleic acid |
| RS | Raman spectroscopy |
| S. aureus | *Staphylococcus aureus* |
| S. epidermidis | *Staphylococcus epidermidis* |
| S. typhimurium | *Salmonella typhimurium* |
| SEM | Scanning electron microscopy |
| SERS | Surface-enhanced Raman scattering |
| SERRS | Surface-enhanced resonance Raman scattering |
| SPR | Surface plasmon resonance |
| TEM | Transmission electron microscopy |
| TNT | Trinitrotoluene |
| UV | Ultra violet |
| Vis | Visible |
| $\delta$ | Deformation |
| $\nu$ | Stretching |
| $\rho$ | Rocking |

# 6 References

(1) Fan, C.; Hu, Z. Q.; Mustapha, A.; Lin, M. S., Rapid detection of food- and waterborne bacteria using surface-enhanced Raman spectroscopy coupled with silver nanosubstrates. *Appl. Microbiol. Biot.* **2011**, *92*, 1053-1061.
(2) Walter, A.; Marz, A.; Schumacher, W.; Rosch, P.; Popp, J., Towards a fast, high specific and reliable discrimination of bacteria on strain level by means of SERS in a microfluidic device. *Lab Chip* **2011**, *11*, 1013-1021.
(3) Mead, P. S.; Slutsker, L.; Griffin, P. M.; Tauxe, R. V., Food-related illness and death in the United States - Reply. *Emerg. Infect. Dis.* **1999**, *5*, 841-842.
(4) Civil liability for agroterrorism: in House Bill 98. **2008**.
(5) Magni, M. V. *Detection of bacteria, viruses, parasites and fungi-bioterrorism prevention*; Springer: Dordrecht, 2008.
(6) Madigan, M.; Martinko, J. *Brock biology of microorganisms*; Prentice-Hall Inc.: New Jersey, 2005.
(7) Gram, H. C., Über die isolierte Färbung der Schizomyceten in Schnitt - und Trockenpräparaten. *Fortschritte der Medizin* **1884**, *2*, 185-189.
(8) http://en.wikipedia.org/wiki/Gram_staining#mediaviewer/File:Gram_stain_01.jpg.
(9) http://en.wikipedia.org/wiki/Bacterial_cell_structure#mediaviewer/File:Average_prokaryote_cell-_en.svg.
(10) Zhang, X. Y.; Young, M. A.; Lyandres, O.; Van Duyne, R. P., Rapid detection of an anthrax biomarker by surface-enhanced Raman spectroscopy. *J. Am. Chem. Soc.* **2005**, *127*, 4484-4489.
(11) Osborn, M. J., Studies on gram-negative cell wall, I. evidence for role of 2-keto-3-deoxyoctonate in lipopolysaccharide of salmonella typhimurium. *Proc. Natl. Acad. Sci. USA* **1963**, *50*, 499-506.
(12) Zhou, H.; Yang, D.; Ivleva, N. P.; Mircescu, N. E.; Niessner, R.; Haisch, C., SERS detection of bacteria in water by in situ coating with Ag nanoparticles. *Anal. Chem.* **2014**, *86*, 1525-1533.
(13) Gray, N. F., Drinking water quality, problems and solutions. *Cambridge University Press: Cambridge* **2008**.
(14) Hugo, W. B.; Russell, A. D., Pharmaceutical microbiology. *Blackwell, Oxford, 6th edn.,* **1998**.
(15) http://www.biolog.com/.
(16) Dittrich, W.; Göhde, W., Flow-through chamber for photometers to measure and count particles in a dispersion medium. *DE 1815352* **1968**.
(17) Clarke, R. G.; Pinder, A. C., Improved detection of bacteria by flow cytometry using a combination of antibody and viability markers. *J. Appl. Microbiol.* **1998**, *84*, 577-584.
(18) Davey, H. M.; Kell, D. B., Flow cytometry and cell sorting of heterogeneous microbial populations: The importance of single-cell analyses. *Microbiological Reviews* **1996**, *60*, 641-&.
(19) Seidel, M.; Niessner, R., Automated analytical microarrays: a critical review. *Anal. Bioanal. Chem.* **2008**, *391*, 1521-1544.
(20) Fodor, S. P. A.; Read, J. L.; Pirrung, M. C.; Stryer, L.; Lu, A. T.; Solas, D., Light-directed, spatially addressable parallel chemical synthesis. *Science* **1991**, *251*, 767-773.
(21) Wolter, A.; Niessner, R.; Seidel, M., Preparation and characterization of functional poly(ethylene glycol) surfaces for the use of antibody microarrays. *Anal. Chem.* **2007**, *79*, 4529-4537.
(22) Wolter, A.; Niessner, R.; Seidel, M., Detection of Escherichia coli O157 : H7, Salmonella typhimurium, and Legionella pneumophila in water using a flow-through chemiluminescence microarray readout system. *Anal. Chem.* **2008**, *80*, 5854-5863.

(23) Jona, G.; Snyder, M., Recent developments in analytical and functional protein microarrays. *Curr. Opin. Mol. Ther.* **2003**, *5*, 271-277.
(24) Ivleva, N. P.; Wagner, M.; Horn, H.; Niessner, R.; Haisch, C., In situ surface-enhanced Raman scattering analysis of biofilm. *Anal. Chem.* **2008**, *80*, 8538-8544.
(25) Schuster, K. C.; Reese, I.; Urlaub, E.; Gapes, J. R.; Lendl, B., Multidimensional information on the chemical composition of single bacterial cells by confocal Raman microspectroscopy. *Anal. Chem.* **2000**, *72*, 5529-5534.
(26) Efrima, S.; Zeiri, L., Understanding SERS of bacteria. *J. Raman. Spectrosc.* **2009**, *40*, 277-288.
(27) Fleischm.M; Hendra, P. J.; McQuilla.Aj, Raman-spectra of pyridine adsorbed at a silver electrode. *Chem. Phys. Lett.* **1974**, *26*, 163-166.
(28) Jeanmaire, D. L.; Vanduyne, R. P., Surface raman spectroelectrochemistry. I. heterocyclic, aromatic, and aliphatic-amines adsorbed on anodized silver electrode. *J. Electroanal. Chem.* **1977**, *84*, 1-20.
(29) Albrecht, M. G.; Creighton, J. A., Anomalously intense Raman-spectra of pyridine at a silver electrode. *J. Am. Chem. Soc.* **1977**, *99*, 5215-5217.
(30) Zhou, H. B.; Zhang, Z. P.; Jiang, C. L.; Guan, G. J.; Zhang, K.; Mei, Q. S.; Liu, R. Y.; Wang, S. H., Trinitrotoluene explosive lights up ultrahigh Raman scattering of nonresonant molecule on a top-closed silver nanotube array. *Anal. Chem.* **2011**, *83*, 6913-6917.
(31) Schlucker, S., SERS microscopy: nanoparticle probes and biomedical applications. *Chemphyschem* **2009**, *10*, 1344-1354.
(32) Preciado-Flores, S.; Wheeler, D. A.; Tran, T. M.; Tanaka, Z.; Jiang, C. Y.; Barboza-Flores, M.; Qian, F.; Li, Y.; Chen, B.; Zhang, J. Z., SERS spectroscopy and SERS imaging of Shewanella oneidensis using silver nanoparticles and nanowires. *Chem. Commun.* **2011**, *47*, 4129-4131.
(33) Willets, K. A., Surface-enhanced Raman scattering (SERS) for probing internal cellular structure and dynamics. *Anal. Bioanal. Chem.* **2009**, *394*, 85-94.
(34) Sun, L.; Sung, K. B.; Dentinger, C.; Lutz, B.; Nguyen, L.; Zhang, J. W.; Qin, H. Y.; Yamakawa, M.; Cao, M. Q.; Lu, Y.; Chmura, A. J.; Zhu, J.; Su, X.; Berlin, A. A.; Chan, S.; Knudsen, B., Composite organic-inorganic nanoparticles as Raman labels for tissue analysis. *Nano Lett.* **2007**, *7*, 351-356.
(35) Qian, X. M.; Peng, X. H.; Ansari, D. O.; Yin-Goen, Q.; Chen, G. Z.; Shin, D. M.; Yang, L.; Young, A. N.; Wang, M. D.; Nie, S. M., In vivo tumor targeting and spectroscopic detection with surface-enhanced Raman nanoparticle tags. *Nat. Biotechnol.* **2008**, *26*, 83-90.
(36) Kahraman, M.; Zamaleeva, A. I.; Fakhrullin, R. F.; Culha, M., Layer-by-layer coating of bacteria with noble metal nanoparticles for surface-enhanced Raman scattering. *Anal. Bioanal. Chem.* **2009**, *395*, 2559-2567.
(37) Jarvis, R. M.; Law, N.; Shadi, L. T.; O'Brien, P.; Lloyd, J. R.; Goodacre, R., Surface-enhanced Raman scattering from intracellular and extracellular bacterial locations. *Anal. Chem.* **2008**, *80*, 6741-6746.
(38) Bell, S. E. J.; Sirimuthu, N. M. S., Surface-enhanced Raman spectroscopy (SERS) for sub-micromolar detection of DNA/RNA mononucleotides. *J. Am. Chem. Soc.* **2006**, *128*, 15580-15581.
(39) Liu, H. L.; Yang, Z. L.; Meng, L. Y.; Sun, Y. D.; Wang, J.; Yang, L. B.; Liu, J. H.; Tian, Z. Q., Three-dimensional and time-ordered surface-enhanced Raman scattering hotspot matrix. *J. Am. Chem. Soc.* **2014**, *136*, 5332-5341.

(40) Xia, Y. Y.; Xiao, H. P., Au nanoplate/polypyrrole nanofiber composite film: preparation, characterization and application as SERS substrate. *J. Raman. Spectrosc.* **2012**, *43*, 469-473.
(41) Singh, A. K.; Senapati, D.; Wang, S. G.; Griffin, J.; Neely, A.; Candice, P.; Naylor, K. M.; Varisli, B.; Kalluri, J. R.; Ray, P. C., Gold nanorod based selective identification of Escherichia coli bacteria using two-photon Rayleigh scattering spectroscopy. *ACS Nano* **2009**, *3*, 1906-1912.
(42) Gomez-Grana, S.; Perez-Juste, J.; Alvarez-Puebla, R. A.; Guerrero-Martinez, A.; Liz-Marzan, L. M., Self-assembly of Au@Ag nanorods mediated by gemini surfactants for highly efficient SERS-active supercrystals. *Adv. Opt. Mater.* **2013**, *1*, 477-481.
(43) Khlebtsov, B. N.; Khanadeev, V. A.; Tsvetkov, M. Y.; Bagratashvili, V. N.; Khlebtsov, N. G., Surface-enhanced Raman scattering substrates based on self-assembled pegylated gold and gold-silver core-shell nanorods. *J. Phys. Chem. C* **2013**, *117*, 23162-23171.
(44) Xu, J. Y.; Wang, J.; Kong, L. T.; Zheng, G. C.; Guo, Z.; Liu, J. H., SERS detection of explosive agent by macrocyclic compound functionalized triangular gold nanoprisms. *J. Raman. Spectrosc.* **2011**, *42*, 1728-1735.
(45) Yuan, H. K.; Liu, Y.; Fales, A. M.; Li, Y. L.; Liu, J.; Vo-Dinh, T., Quantitative surface-enhanced resonant Raman scattering multiplexing of biocompatible gold nanostars for in vitro and ex vivo detection. *Anal. Chem.* **2013**, *85*, 208-212.
(46) Osinkina, L.; Lohmuller, T.; Jackel, F.; Feldmann, J., Synthesis of gold nanostar arrays as reliable, large-scale, homogeneous substrates for surface-enhanced Raman scattering imaging and spectroscopy. *J. Phys. Chem. C* **2013**, *117*, 22198-22202.
(47) Lim, D. K.; Jeon, K. S.; Kim, H. M.; Nam, J. M.; Suh, Y. D., Nanogap-engineerable Raman-active nanodumbbells for single-molecule detection. *Nat. Mater.* **2010**, *9*, 60-67.
(48) Sawai, Y.; Takimoto, B.; Nabika, H.; Ajito, K.; Murakoshi, K., Observation of a small number of molecules at a metal nanogap arrayed on a solid surface using surface-enhanced Raman scattering. *J. Am. Chem. Soc.* **2007**, *129*, 1658-1662.
(49) Li, S. Z.; Pedano, M. L.; Chang, S. H.; Mirkin, C. A.; Schatz, G. C., Gap structure effects on surface-enhanced Raman scattering intensities for gold gapped rods. *Nano Lett.* **2010**, *10*, 1722-1727.
(50) Lee, S. J.; Morrill, A. R.; Moskovits, M., Hot spots in silver nanowire bundles for surface-enhanced Raman spectroscopy. *J. Am. Chem. Soc.* **2006**, *128*, 2200-2201.
(51) Hu, M.; Ou, F. S.; Wu, W.; Naumov, I.; Li, X. M.; Bratkovsky, A. M.; Williams, R. S.; Li, Z. Y., Gold nanofingers for molecule trapping and detection. *J. Am. Chem. Soc.* **2010**, *132*, 12820-12822.
(52) Fang, Y.; Seong, N. H.; Dlott, D. D., Measurement of the distribution of site enhancements in surface-enhanced Raman scattering. *Science* **2008**, *321*, 388-392.
(53) Stuart, D. A.; Yonzon, C. R.; Zhang, X. Y.; Lyandres, O.; Shah, N. C.; Glucksberg, M. R.; Walsh, J. T.; Van Duyne, R. P., Glucose sensing using near-infrared surface-enhanced Raman spectroscopy: Gold surfaces, 10-day stability, and improved accuracy. *Anal. Chem.* **2005**, *77*, 4013-4019.
(54) Nie, S. M.; Emery, S. R., Probing single molecules and single nanoparticles by surface-enhanced Raman scattering. *Science* **1997**, *275*, 1102-1106.
(55) Kneipp, K.; Wang, Y.; Kneipp, H.; Perelman, L. T.; Itzkan, I.; Dasari, R.; Feld, M. S., Single molecule detection using surface-enhanced Raman scattering (SERS). *Phys. Rev. Lett.* **1997**, *78*, 1667-1670.
(56) Lombardi, J. R.; Birke, R. L., A unified view of surface-enhanced Raman scattering. *Acc. Chem. Res.* **2009**, *42*, 734-742.

(57) Kneipp, K.; Kneipp, H.; Itzkan, I.; Dasari, R. R.; Feld, M. S., Surface-enhanced Raman scattering and biophysics. *J. Phys-condens. Mat.* **2002**, *14*, R597-R624.
(58) Schatz, G. C., Theoretical-studies of surface enhanced Raman-scattering. *Acc. Chem. Res.* **1984**, *17*, 370-376.
(59) Moskovits, M., Surface-enhanced spectroscopy. *Rev. Mod. Phys.* **1985**, *57*, 783-826.
(60) Otto, A.; Mrozek, I.; Grabhorn, H.; Akemann, W., Surface-enhanced Raman-scattering. *J. Phys-condens. Mat.* **1992**, *4*, 1143-1212.
(61) Willets, K. A.; Van Duyne, R. P., Localized surface plasmon resonance spectroscopy and sensing. *Annu. Rev. Phys. Chem.* 2007; Vol. 58, p 267-297.
(62) Pieczonka, N. P. W.; Aroca, R. F., Single molecule analysis by surfaced-enhanced Raman scattering. *Chem. Soc. Rev.* **2008**, *37*, 946-954.
(63) Witlicki, E. H.; Andersen, S. S.; Hansen, S. W.; Jeppesen, J. O.; Wong, E. W.; Jensen, L.; Flood, A. H., Turning on resonant SERS using the chromophore-plasmon coupling created by host-guest complexation at a plasmonic nanoarray. *J. Am. Chem. Soc.* **2010**, *132*, 6099-6107.
(64) Campion, A.; Kambhampati, P., Surface-enhanced Raman scattering. *Chem. Soc. Rev.* **1998**, *27*, 241-250.
(65) Kim, N. H.; Lee, S. J.; Moskovits, M., Aptamer-mediated surface-enhanced Raman spectroscopy intensity amplification. *Nano Lett.* **2010**, *10*, 4181-4185.
(66) Wu, H.; Lin, D. D.; Pan, W., High performance surface-enhanced Raman scattering substrate combining low dimensional and hierarchical nanostructures. *Langmuir.* **2010**, *26*, 6865-6868.
(67) Yang, K. H.; Liu, Y. C.; Yu, C. C., Simple strategy to improve surface-enhanced Raman scattering based on electrochemically prepared roughened silver substrates. *Langmuir.* **2010**, *26*, 11512-11517.
(68) Stamplecoskie, K. G.; Scaiano, J. C.; Tiwari, V. S.; Anis, H., Optimal size of silver nanoparticles for surface-enhanced Raman spectroscopy. *J. Phys. Chem. C* **2011**, *115*, 1403-1409.
(69) Zeng, J.; Zheng, Y. Q.; Rycenga, M.; Tao, J.; Li, Z. Y.; Zhang, Q. A.; Zhu, Y. M.; Xia, Y. N., Controlling the shapes of silver nanocrystals with different capping agents. *J. Am. Chem. Soc.* **2010**, *132*, 8552-8553.
(70) Duan, G. T.; Cai, W. P.; Luo, Y. Y.; Li, Y.; Lei, Y., Hierarchical surface rough ordered Au particle arrays and their surface enhanced Raman scattering. *Appl. Phys. Lett.* **2006**, *89*.
(71) Guerrini, L.; Aliaga, A. E.; Carcamo, J.; Gomez-Jeria, J. S.; Sanchez-Cortes, S.; Campos-Vallette, M. M.; Garcia-Ramos, J. V., Functionalization of Ag nanoparticles with the bis-acridinium lucigenin as a chemical assembler in the detection of persistent organic pollutants by surface-enhanced Raman scattering. *Anal. Chim. Acta* **2008**, *624*, 286-293.
(72) Canamares, M. V.; Chenal, C.; Birke, R. L.; Lombardi, J. R., DFT, SERS, and single-molecule SERS of crystal violet. *J. Phys. Chem. C* **2008**, *112*, 20295-20300.
(73) Myers, A. B., Resonance Raman intensities and charge-transfer reorganization energies. *Chem. Rev.* **1996**, *96*, 911-926.
(74) Doering, W. E.; Nie, S. M., Spectroscopic tags using dye-embedded nanoparticles and surface-enhanced Raman scattering. *Anal. Chem.* **2003**, *75*, 6171-6176.
(75) dos Santos, D. P.; Temperini, M. L. A.; Brolo, A. G., Mapping the energy distribution of SERRS hot spots from anti-stokes to stokes intensity ratios. *J. Am. Chem. Soc.* **2012**, *134*, 13492-13500.
(76) Hirakawa, A. Y.; Tsuboi, M., Molecular geometry in an excited electronic state and a preresonance Raman effect. *Science* **1975**, *188*, 359-361.

(77) McHugh, C. J.; Keir, R.; Graham, D.; Smith, W. E., Selective functionalisation of TNT for sensitive detection by SERRS. *Chem. Commun.* **2002**, 580-581.
(78) McHugh, C. J.; Smith, W. E.; Lacey, R.; Graham, D., The first controlled reduction of the high explosive RDX. *Chem. Commun.* **2002**, 2514-2515.
(79) Ingram, A.; Byers, L.; Faulds, K.; Moore, B. D.; Graham, D., SERRS-based enzymatic probes for the detection of protease activity. *J. Am. Chem. Soc.* **2008**, *130*, 11846-11847.
(80) Graham, D.; Faulds, K., Quantitative SERRS for DNA sequence analysis. *Chem. Soc. Rev.* **2008**, *37*, 1042-1051.
(81) Stevenson, R.; Ingram, A.; Leung, H.; McMillan, D. C.; Graham, D., Quantitative SERRS immunoassay for the detection of human PSA. *Analyst.* **2009**, *134*, 842-844.
(82) McKenzie, F.; Graham, D., Controlled assembly of SERRS active oligonucleotide-nanoparticle conjugates. *Chem. Commun.* **2009**, 5757-5759.
(83) Laing, S.; Hernandez-Santana, A.; Sassmannshausen, J.; Asquith, D. L.; McInnes, I. B.; Faulds, K.; Graham, D., Quantitative detection of human tumor necrosis factor alpha by a resonance Raman enzyme-linked immunosorbent assay. *Anal. Chem.* **2011**, *83*, 297-302.
(84) Liu, X. J.; Knauer, M.; Ivleva, N. P.; Niessner, R.; Haisch, C., Synthesis of core-shell surface-enhanced Raman tags for bioimaging. *Anal. Chem.* **2010**, *82*, 441-446.
(85) Doering, W. E.; Piotti, M. E.; Natan, M. J.; Freeman, R. G., SERS as a foundation for nanoscale, optically detected biological labels. *Adv. Mater.* **2007**, *19*, 3100-3108.
(86) Knauer, M.; Ivleva, N. P.; Liu, X. J.; Niessner, R.; Haisch, C., Surface-enhanced Raman scattering-based label-free microarray readout for the detection of microorganisms. *Anal. Chem.* **2010**, *82*, 2766-2772.
(87) Abell, J. L.; Garren, J. M.; Driskell, J. D.; Tripp, R. A.; Zhao, Y. P., Label-free detection of micro-RNA hybridization using surface-enhanced Raman spectroscopy and least-squares analysis. *J. Am. Chem. Soc.* **2012**, *134*, 12889-12892.
(88) Drummond, T. G.; Hill, M. G.; Barton, J. K., Electrochemical DNA sensors. *Nat. Biotechnol.* **2003**, *21*, 1192-1199.
(89) Golightly, R. S.; Doering, W. E.; Natan, M. J., Surface-enhanced Raman spectroscopy and homeland security: a perfect match? *ACS Nano* **2009**, *3*, 2859-2869.
(90) Kahraman, M.; Keseroglu, K.; Culha, M., On sample preparation for surface-enhanced Raman scattering (SERS) of bacteria and the source of spectral features of the spectra. *Appl. Spectrosc.* **2011**, *65*, 500-506.
(91) Jarvis, R. M.; Goodacre, R., Discrimination of bacteria using surface-enhanced Raman spectroscopy. *Anal. Chem.* **2004**, *76*, 40-47.
(92) Prucek, R.; Ranc, V.; Kvitek, L.; Panacek, A.; Zboril, R.; Kolar, M., Reproducible discrimination between Gram-positive and Gram-negative bacteria using surface enhanced Raman spectroscopy with infrared excitation. *Analyst.* **2012**, *137*, 2866-2870.
(93) Zeiri, L.; Bronk, B. V.; Shabtai, Y.; Eichler, J.; Efrima, S., Surface-enhanced Raman spectroscopy as a tool for probing specific biochemical components in bacteria. *Appl. Spectrosc.* **2004**, *58*, 33-40.
(94) Sztainbuch, I. W., The effects of Au aggregate morphology on surface-enhanced Raman scattering enhancement. *J. Chem. Phys.* **2006**, *125*.
(95) Kahraman, M.; Yazici, M. M.; Sahin, F.; Bayrak, O. F.; Culha, M., Reproducible surface-enhanced Raman scattering spectra of bacteria on aggregated silver nanoparticles. *Appl. Spectrosc.* **2007**, *61*, 479-485.
(96) Kahraman, M.; Yazici, M. M.; Sahin, F.; Culha, M., Convective assembly of bacteria for surface-enhanced Raman scattering. *Langmuir.* **2008**, *24*, 894-901.

(97) Berry, V.; Gole, A.; Kundu, S.; Murphy, C. J.; Saraf, R. F., Deposition of CTAB-terminated nanorods on bacteria to form highly conducting hybrid systems. *J. Am. Chem. Soc.* **2005**, *127*, 17600-17601.
(98) Berry, V.; Saraf, R. F., Self-assembly of nanoparticles on live bacterium: An avenue to fabricate electronic devices. *Angew. Chem. Int. Ed.* **2005**, *44*, 6668-6673.
(99) Wilson, W. W.; Wade, M. M.; Holman, S. C.; Champlin, F. R., Status of methods for assessing bacterial cell surface charge properties based on zeta potential measurements. *J. Microbiol. Meth.* **2001**, *43*, 153-164.
(100) Efrima, S.; Bronk, B. V., Silver colloids impregnating or coating bacteria. *J. Phys. Chem. B* **1998**, *102*, 5947-5950.
(101) Zeiri, L.; Bronk, B. V.; Shabtai, Y.; Czege, J.; Efrima, S., Silver metal induced surface enhanced Raman of bacteria. *Colloid Surface. A* **2002**, *208*, 357-362.
(102) Yang, L. B.; Liu, H. L.; Wang, J.; Zhou, F.; Tian, Z. Q.; Liu, J. H., Metastable state nanoparticle-enhanced Raman spectroscopy for highly sensitive detection. *Chem. Commun.* **2011**, *47*, 3583-3585.
(103) Qian, K.; Yang, L. B.; Li, Z. Y.; Liu, J. H., A new-type dynamic SERS method for ultrasensitive detection. *J. Raman. Spectrosc.* **2013**, *44*, 21-28.
(104) Li, J.; McLandsborough, L. A., The effects of the surface charge and hydrophobicity of Escherichia coli on its adhesion to beef muscle. *Int. J. Food Microbiol* **1999**, *53*, 185-193.
(105) Walczak, J. J.; Wang, L. X.; Bardy, S. L.; Feriancikova, L.; Li, J.; Xu, S. P., The effects of starvation on the transport of Escherichia coli in saturated porous media are dependent on pH and ionic strength. *Colloid Surface. B* **2012**, *90*, 129-136.
(106) Kim, H. N.; Bradford, S. A.; Walker, S. L., Escherichia coli O157:H7 transport in saturated porous media: role of solution chemistry and surface macromolecules. *Environ. Sci. Technol.* **2009**, *43*, 4340-4347.
(107) Schwegmann, H.; Feitz, A. J.; Frimmel, F. H., Influence of the zeta potential on the sorption and toxicity of iron oxide nanoparticles on S. cerevisiae and E. coli. *J. Colloid Interf. Sci* **2010**, *347*, 43-48.
(108) Burks, G. A.; Velegol, S. B.; Paramonova, E.; Lindenmuth, B. E.; Feick, J. D.; Logan, B. E., Macroscopic and nanoscale measurements of the adhesion of bacteria with varying outer layer surface composition. *Langmuir.* **2003**, *19*, 2366-2371.
(109) Sengupta, A.; Brar, N.; Davis, E. J., Bioaerosol detection and characterization by surface-enhanced Raman spectroscopy. *J. Colloid Interf. Sci* **2007**, *309*, 36-43.
(110) Ivleva, N. P.; Wagner, M.; Szkola, A.; Horn, H.; Niessner, R.; Haisch, C., Label-free in situ SERS imaging of biofilms. *J. Phys. Chem. B* **2010**, *114*, 10184-10194.
(111) Gao, D. M.; Wang, Z. Y.; Liu, B. H.; Ni, L.; Wu, M. H.; Zhang, Z. P., Resonance energy transfer-amplifying fluorescence quenching at the surface of silica nanoparticles toward ultrasensitive detection of TNT. *Anal. Chem.* **2008**, *80*, 8545-8553.
(112) Xu, F. G.; Zhang, Y.; Sun, Y. J.; Shi, Y.; Wen, Z. W.; Li, Z., Silver nanoparticles coated zinc oxide nanorods array as superhydrophobic substrate for the amplified SERS effect. *J. Phys. Chem. C* **2011**, *115*, 9977-9983.
(113) Schwarzmeier, K.; Knauer, M.; Ivleva, N. P.; Niessner, R.; Haisch, C., Bioaerosol analysis based on a label-free microarray readout method using surface-enhanced Raman scattering. *Anal. Bioanal. Chem.* **2013**, *405*, 5387-5392.
(114) Wang, Y. L.; Lee, K.; Irudayaraj, J., Silver nanosphere SERS probes for sensitive identification of pathogens. *J. Phys. Chem. C* **2010**, *114*, 16122-16128.
(115) Knauer, M.; Ivleva, N. P.; Niessner, R.; Haisch, C., A flow-through microarray cell for the online SERS detection of antibody-captured E. coli bacteria. *Anal. Bioanal. Chem.* **2012**, *402*, 2663-2667.

(116) Cerf, A.; Cau, J. C.; Vieu, C.; Dague, E., Nanomechanical properties of dead or alive single-patterned bacteria. *Langmuir.* **2009**, *25*, 5731-5736.
(117) Notingher, I.; Jones, J. R.; Verrier, S.; Bisson, I.; Embanga, P.; Edwards, P.; Polak, J. M.; Hench, L. L., Application of FTIR and Raman spectroscopy to characterisation of bioactive materials and living cells. *Spectrosc-int. J.* **2003**, *17*, 275-288.
(118) Kramer, M.; Obermajer, N.; Matijasic, B. B.; Rogelj, I.; Kmetec, V., Quantification of live and dead probiotic bacteria in lyophilised product by real-time PCR and by flow cytometry. *Appl. Microbiol. Biot.* **2009**, *84*, 1137-1147.
(119) Masakiyo, Y.; Yoshida, A.; Takahashi, Y.; Shintani, Y.; Awano, S.; Ansai, T.; Sawayama, S.; Shimakita, T.; Takehara, T., Rapid LED-based fluorescence microscopy distinguishes between live and dead bacteria in oral clinical samples. *Biomed. Res-tokyo.* **2010**, *31*, 21-26.
(120) Rudi, K.; Moen, B.; Dromtorp, S. M.; Holck, A. L., Use of ethidium monoazide and PCR in combination for quantification of viable and dead cells in complex samples. *Appl. Environ. Microb.* **2005**, *71*, 1018-1024.
(121) Lee, J. L.; Levin, R. E., Quantification of total viable bacteria on fish fillets by using ethidium bromide monoazide real-time polymerase chain reaction. *Int. J. Food Microbiol* **2007**, *118*, 312-317.
(122) Wang, S. S.; Levin, R. E., Discrimination of viable Vibrio vulnificus cells from dead cells in real-time PCR. *J. Microbiol. Meth.* **2006**, *64*, 1-8.
(123) Leopold, N.; Lendl, B., A new method for fast preparation of highly surface-enhanced Raman scattering (SERS) active silver colloids at room temperature by reduction of silver nitrate with hydroxylamine hydrochloride. *J. Phys. Chem. B* **2003**, *107*, 5723-5727.
(124) Knauer, M.; Ivleva, N. P.; Niessner, R.; Haisch, C., Optimized surface-enhanced Raman scattering (SERS) colloids for the characterization of microorganisms. *Anal. Sci.* **2010**, *26*, 761-766.